



Norwegian University of
Science and Technology

Conceptual Structural Design of High- Rise Buildings with Wind Alterations

Elise Hverven

Civil and Environmental Engineering

Submission date: June 2017

Supervisor: Anders Rönquist, KT

Norwegian University of Science and Technology
Department of Structural Engineering



ACCESSIBILITY
OPEN


Department of Structural Engineering
Faculty of Engineering Science and Technology
NTNU- Norwegian University of Science and Technology

MASTER THESIS 2017

SUBJECT AREA: Structural Design	DATE: June 8 th 2017	NO. OF PAGES: 96+60
------------------------------------	------------------------------------	------------------------

TITLE:
Conceptual Structural Design of High-Rise Buildings with Wind Alterations
Konseptuelt design av høyhus med tilpasninger for vind

BY:
Elise Myhre Hverven



SUMMARY:
The aim of this thesis is to develop a conceptual structural design for a tall building located in Oslo, Norway. For a structural engineering student, it is vital to reflect on how the structural system can enhance the architectural expression of the building. When a skyscraper is situated in Oslo, the governing load is wind. When adding alterations to a basic configuration, the building can be optimized structurally to withstand wind induced pressure, this also adds a unique architectonic expression of the building. Basic geometrical shapes, both with and without alterations, have been analyzed in computer software wind tunnel testing. As a result, the plan geometry and modifications over the vertical height are optimized for uniform wind loads. Due to the results from the wind tunnel testing, the hexagonal and octagonal models were further analyzed in the computer program ETABS. All together there were six models; the basic geometries, models with twisting over the vertical height, and models with tapering and twisting over the vertical height. In ETABS the models were exposed to earthquake and wind loads according to given National Standards. Consequently, the stiffness and flexibility of the structures under these loads was evaluated. Results from the computational program and further manually calculated results, have been compared to Norwegian thresholds within serviceability of structures. From the analysis results, it is possible to conclude that the additional examined alterations will enhance the buildings performance under wind loads. The displacements are reduced, as well as the over-all volume of the load-resisting structure. The acceleration of the structures under wind loads are roughly equivalent for all the models. Consequently, twisting and tapering over the vertical height, as well as a reduced volume of the load-bearing structure, does not reduce the global stiffness of the structures.

RESPONSIBLE TEACHER: Prof. Nils Erik Anders Rønnequist
SUPERVISOR: Prof. Nils Erik Anders Rønnequist
CARRIED OUT AT: Department of Structural Engineering (NTNU)

ABSTRACT

Throughout the past seventy years, the skyscraper's evolution has evolved due to the close relationship and cooperation between architects, engineers, and technology. This partnership has led to a field where the architectural expression is directly linked to the structural performance and structural design of high-rise buildings.

The aim of this thesis is to develop a conceptual structural design for a tall building located in Oslo, Norway. For a structural engineering student, it is therefore vital to reflect on how the structural system can enhance the architectural expression of the building. When a skyscraper is situated in Oslo, the governing load is wind. When adding alterations to a basic configuration, the building can be optimized structurally to withstand wind induced pressure, this also adds a unique architectonic expression of the building.

Basic geometrical shapes, both with and without alterations, have been analyzed in computer software wind tunnel testing. As a result, the plan geometry and modifications over the vertical height are optimized for uniform wind loads. Due to the results from the wind tunnel testing, the hexagonal and octagonal models were further analyzed in the computer program ETABS. All together there were six models; the basic geometries, models with twisting over the vertical height, and models with tapering and twisting over the vertical height. In ETABS the models were exposed to earthquake and wind loads according to given National Standards. Consequently, the stiffness and flexibility of the structures under these loads was evaluated. Results from the computational program and further manually calculated results, have been compared to Norwegian thresholds within serviceability of structures.

From the analysis results, it is possible to conclude that the additional examined alterations will enhance the buildings performance under wind loads. The displacements due to wind and seismic loads are reduced, as well as the over-all volume of the load-resisting structure. The acceleration of the structures under wind loads are roughly equivalent for all the models. Consequently, twisting and tapering over the vertical height, as well as a reduced volume of the load-bearing structure, do not reduce the global stiffness of the structures.

Skyskraperne har gjennomgått en rivende utvikling de siste sytti årene grunnet det tette samarbeidet mellom arkitekter, ingeniører og ny teknologi. Dette har ledet til at det arkitektoniske designet er nå direkte koblet til den strukturelle konstruksjonen av bygget.

Formålet med denne masteroppgaven er å utvikle et konseptuelt designet høyhus i Oslo, Norge. For en student med spesialisering innenfor konstruksjonsteknologi er det derfor viktig å fokusere på hvordan konstruksjonen kan optimaliseres til å motstå lastene, men samtidig oppnå et unikt arkitektonisk uttrykk. Når en skyskraper er lokalisert i Oslo, er vind den dominerende lasten. Ved å modifisere bygget over den vertikale høyden, kan konstruksjonen optimaliseres med tanke på vindlast. Dette vil igjen ha en positiv innvirkning på det arkitektoniske designet.

Grunnleggende geometriske former, både med og uten modifikasjoner, har blitt analysert i programvare-genererte vindtunneler. Disse resultatene danner grunnlaget for valg og optimalisering av modellene. De som fikk best resultater fra vindtunnel-testen hadde heksagonale og oktagonale grunnformer. Formene ble videre analysert i modelleringsprogrammet ETABS. Alt i alt var det seks modeller; de to basis geometriene, modeller med rotasjon over den vertikale høyden, og modeller med rotasjon og avtrapping over den vertikale høyden. I programmet ETABS ble modellene eksponert for jordskjelvs- og vindlast i henhold til de norske standardene. Resultatene fra programmet og videre manuelle kalkulasjoner ble kontrollert opp mot nasjonale bruksgrenser.

Resultatene viser at modifikasjoner over den vertikale høyden forbedrer bygningenes evne til å tåle vind. De horisontale forskyvningene fra vind- og jordskjelvslast er redusert, på tross av at volumet av den lastbærende konstruksjonen er minsket. Akselerasjonene under ekstreme vindforhold er sammenlignbare for alle modellene. Konklusjonen er at rotasjon og avtrapping over den vertikale høyden, samt redusert volum av den lastbærende konstruksjonen, ikke fører til en redusert stivhet av konstruksjonene.

ACKNOWLEDGMENT

This is a Master thesis belonging to the Department of Structural Engineering at The Norwegian University of Science and Technology, NTNU. The thesis is within Structural Design and Engineering Architecture, with the aim to reflect and study both of these fields. The topic and context is designed by the student with the help of Prof. Nils Erik Anders Rønnquist; the main supervisor, to be able to create an unconventional topic of investigation.

Articles, books, National Standards and technical reports have been used as guidelines and supporting literature for the decision making process and analysis results. The calculations are mainly calculated by following the Norwegian restrictions; found in the Eurocodes, supporting National Annex, and ISO-standards. For the conceptual design portion of the thesis, supporting literature has been used to obtain the desired structural and architectonic design.

ETABS, Autodesk Revit, Autodesk Flow Design, and Rhinoceros with the plugin Ladybug, are the supporting software programs that have been used to achieve the model designs and results for wind and seismic design analysis of the structure.

The student had the unique opportunity to spend two semesters abroad at Nanyang Technological University, NTU, in Singapore. Singapore's skyline is filled with prominent skyscrapers, and they have some of the most exceptional designs. The Student's participation in the course CV6108: Analysis and Design of Tall Buildings at NTU, led to an interest and basic knowledge within the field of skyscrapers. This paved the way for the topic of the thesis.

I would like to direct thank my supervisor, Prof. Nils Erik Anders Rønnquist. Guidance, humor, and a critical eye from Prof. Rønnquist was highly necessary throughout these past months. The co-workers at EDRMedeso have also been a tremendous help, with being able to grant the student with a license for ETABS.

Trondheim, June 8th 2017



Elise Myhre Hverven

Contents

Summary	VII
Contents	VII
List of Figures	XIII
List of Tables	XVII
1 Introduction	1
2 The Evolution of the High-Rise	3
2.1 The Change in Civil Construction After World War II	3
2.2 Le Corbusier and His Modernistic Approach	4
2.2.1 Le Corbusier's Take on the Skyscraper	5
2.3 Mies von de Rohe	6
2.3.1 The Mies Columns	6
2.4 The Contribution from SOM	7
2.4.1 Myron Goldsmith and Fazular Kahn	8
3 21st Century Skyscraper's	11
3.1 Sustainable Design	11
3.1.1 Materials	13
3.2 Designing Sufficiently Against Wind	15
3.2.1 Solutions That Benefit in Oslo, Norway	17
3.3 Existing Skyscrapers and the Publics Feedback	20
3.3.1 Oslo and the Publics View on High-Rise	20
3.3.2 Other Examples in Europe	21
4 The Governing Structural Aspects	25
4.1 Load-Bearing Structure	26
4.1.1 Height Considerations	27
4.2 Introduction to Wind Loads	27
4.2.1 Method of Calculating Wind Response	28
4.2.2 Building Drift, Lateral Deflection and Displacements	29
4.2.3 Acceleration of Buildings	30
4.3 Torsional Moment	31

4.4	Seismic Considerations	32
4.4.1	Fundamental Modes and Fundamental Frequencies	33
4.4.2	Response Spectrum and Time History Analysis	33
4.4.3	Inter-Story Drift	34
4.4.4	Overturning Moment	35
5	Site Location and Geometric Parameters	37
5.1	Property Location	37
5.2	Shading Considerations for Buildings Location	40
5.3	Options for the Shape and Plan Geometry	40
5.3.1	Drag Coefficients and Drag Forces for Different Geometries	41
5.3.2	Deciding on the H/B-Ratio	42
5.4	Results from Autodesk Flow Design	42
6	Determining the Geometry	47
6.1	Governing Wind Directions	47
6.1.1	Influence on the Geometry	49
6.2	Additional Changes to the Geometry	50
6.3	Plan Section and Structural Bearing	52
7	Implementation of the Structural Aspects	53
7.1	Achieving a Suitable Load-Bearing Structure	53
7.2	Wind Loads on the Structure	53
7.2.1	Torsional Moment	54
7.3	Determining the Service Cores	56
7.3.1	Calculations of the Torsional Stresses in the Service Cores	56
7.3.2	Additional the Walls with Openings	59
7.4	Seismic Loading and Natural Frequencies	60
7.4.1	Elastic Response Spectrum	60
8	Designing the Structures in BIM	63
8.1	Deciding on the Most Efficient Building Software Program	63
8.1.1	ETABS	64
8.2	Basic Steps to Generate the Models	64
8.3	Limitations to ETABS	64
8.3.1	Composite Columns	65
8.3.2	Glue Laminated Timber	65
8.3.3	Hollow Concrete Slabs	66
8.4	Modeling the Plan Section	67
8.5	Static Load Cases	68
8.5.1	Wind Loading	68
8.6	Earthquake Loads	69
8.6.1	ETABS Implementation of Seismic Load Pattern	71
8.7	Load Combinations	72
8.8	Changes Due to Results from Analysis	72

9	Structural Results	75
9.1	Main components	76
9.2	Results from ETABS for Wind Analysis	77
9.2.1	Load combinations	78
9.2.2	Displacement and drift	78
9.2.3	Wind Acceleration and Modal Results	79
9.2.4	Calculations for ISO 10137	80
9.2.5	Calculations for ISO 2631-1 and ISO 2631-2	82
9.2.6	Overturning Moment	82
9.3	Results from ETABS for Seismic Loads	83
9.3.1	Displacement and drift	85
9.3.2	Acceleration and Modal Results	85
9.4	Amount of Concrete and Steel	86
9.5	Glue Laminated Timber Elements	87
9.5.1	Axial Force Design of Columns	87
9.5.2	Cross Sectional Dimensions	89
9.6	Final Model in Revit	89
10	Conclusion	93
	Bibliography	95
A		ii
A.1	Mean Wind Calculations	ii
A.1.1	Basic Wind Velocity	ii
A.1.2	Mean Wind Speed	iii
A.2	Peak Velocity Pressure	v
A.2.1	Wind Turbulence	v
A.2.2	Peak Velocity Pressure	vi
A.3	Wind Actions	vi
A.3.1	Wind Pressure on External Surfaces	vi
A.3.2	Calculation of $c_s c_d$	vii
A.3.3	Wind Force Calculations Using Method 1	ix
A.3.4	Wind Force Calculations Using Method 2	xi
A.4	Wake Buffeting	xii
A.5	Vortex Shedding	xii
B		xiv
B.1	Wind Acceleration Calculations	xiv
B.1.1	Calculation of the Standard Deviation	xv
B.1.2	Results of the Acceleration	xviii
C		xx
C.1	Calculations of the Glue Laminated Elements	xxi
C.1.1	Material Property for GL32c	xxi
C.1.2	Combined Tension and Bending Equation	xxii

C.1.3	Buckling in Compression	xxiii
C.1.4	Second Order Effects	xxiii
C.1.5	Slenderness of the Columns	xxiv
C.1.6	Combined Compression and Bending Equation	xxiv
C.1.7	Shear Equation	xxv
D		xxvi
D.1	Results from ETABS for Plain Octagon Model	xxvi
D.1.1	Plan and 3D View of the Structure	xxvi
D.1.2	Utilization of Composite Columns	xxvii
D.1.3	Displacements	xxviii
D.1.4	Drift Ratio	xxix
D.1.5	Overturning Moments	xxx
D.1.6	Shell Stresses in Shear Walls	xxxi
E		xxxii
E.1	Results from ETABS for Twisted Octagon Model	xxxii
E.1.1	Plan and 3D View of the Structure	xxxii
E.1.2	Utilization of Composite Columns	xxxiii
E.1.3	Displacements	xxxiv
E.1.4	Drift Ratio	xxxv
E.1.5	Overturning Moments	xxxvi
E.1.6	Shell Stresses in Shear Walls	xxxvii
F		xxxviii
F.1	Results from ETABS for Twisted and Tapered Octagon Model	xxxviii
F.1.1	Plan and 3D View of the Structure	xxxviii
F.1.2	Utilization of Composite Columns	xxxix
F.1.3	Displacements	xl
F.1.4	Drift Ratio	xli
F.1.5	Overturning Moments	xlii
F.1.6	Shell Stresses in Shear Walls	xliii
G		xliv
G.1	Results from ETABS for Plain Hexagon Model	xliv
G.1.1	Plan and 3D View of the Structure	xliv
G.1.2	Utilization of Composite Columns	xlv
G.1.3	Displacements	xlvi
G.1.4	Drift Ratio	xlvii
G.1.5	Overturning Moments	xlviii
G.1.6	Shell Stresses in Shear Walls	xliv
H		l
H.1	Results from ETABS for Twisted Hexagon Model	l
H.1.1	Plan and 3D View of the Structure	l
H.1.2	Utilization of Composite Columns	li

H.1.3	Displacements	lii
H.1.4	Drift Ratio	liii
H.1.5	Overturning Moment	liv
H.1.6	Shell Stresses in Shear Walls	lv
I		lvi
I.1	Results from ETABS for Twisted and Tapered Hexagon Model . . .	lvi
I.1.1	Plan and 3D View of the Structure	lvi
I.1.2	Utilization of Composite Columns	lvii
I.1.3	Displacements	lviii
I.1.4	Drift Ratio	lix
I.1.5	Overturning Moments	lx
I.1.6	Shell Stresses in Shear Walls	lxi

List of Figures

2.1	Image of Le Corbusier's <i>Dom-ino</i> (Ábalos and Herreros, 2003)	4
2.2	Image of Mies van de Rohe's expressive columns (Hverven, 2017) . .	6
2.3	The evolution of Mies columns (Ábalos and Herreros, 2003)	7
2.4	Image of John Hancock Center in Chicago (Hverven, 2017)	9
3.1	Shanghai center on a regular day (Hverven, 2016)	12
3.2	Västerbroplan in Stockholm; exterior (Møller, 2015)	14
3.3	Västerbroplan in Stockholm; plan view (Møller, 2015)	14
3.4	Variety of alterations to the plan geometry (Amin and Ahuja, 2010)	16
3.5	Green atrium at Emporia. Photo by Tord-Rikard Söderström	20
3.6	The Triangle by Herzog de Meuron (Herzog de Meuron, 2016)	22
3.7	The Turning Torso in Malmø by Santiago Calatrava (Architecture Magazine, 2015)	23
5.1	Overview of the development in Bjørvika (Plan- og bygningsetaten, 2016)	38
5.2	Overview of the desired property (Kartverket, 2017)	39
6.1	The solar path over the year in Oslo	47
6.2	The wind rose for Oslo when temperature is over 16 degrees and wind speed is larger than 1 m/s	48
6.3	The wind rose for Oslo when temperature is under 0 degrees and wind speed is larger than 1 m/s	49
6.4	The 10-year mean wind profile for hourly wind speed over the height, in Oslo	51
7.1	Mean wind speed, $v_m(z)$	54
7.2	Wind force to calculate torsional moment, from CEN (Figure 7.1, 2005)	55
7.3	Overturning moment due to turbulence	55
7.4	Illustration of the service core	56
7.5	Illustration of the service core, with additional walls	59
7.6	Figure of elastic response spectrum from (Figure NA.3(903), CEN, 2009)	61

8.1	The specified material properties for GL32c	66
8.2	The plan view and 3D view of octagon with twisting and tapering alterations	67
8.3	Implementing the wind loading in ETABS	69
8.4	Seismic: NS-EN 1998-1 implementation	70
8.5	Response spectrum	70
8.6	Time history analysis in frequency domain	71
8.7	Time history in time domain	71
8.8	The truss system in each model. Stresses shown in the service core as well	73
9.1	Utilization degree for composite columns at elevation 7	76
9.2	Illustration of the plan section, shown by octagon tapered and twisted in Revit	77
9.3	Limiting acceleration from ISO (Figure D.1, 2007)	81
9.4	Overview of moment, M33, in shear walls	83
9.5	Axial force distribution in the exterior glue laminated timber columns	87
9.6	Axial force distribution in the exterior glue laminated timber columns with displacements	88
9.7	Cross sections for the glue laminated columns	89
9.8	Octagon tapered and twisted model in Revit	90
9.9	Octagon tapered and twisted model in Revit, section view	90
9.10	Octagon tapered and twisted model in Revit, ground perspective	91
A.1	Mean wind speed, $v_m(z)$	iv
A.2	Wind turbulence over the height, $I_v(z)$	v
A.3	Peak velocity pressure over the height, $q_p(z)$	vi
A.4	Wind profile over the height (CEN, 2005)	vii
A.5	Wind profile over the height for surface D	ix
A.6	Wind profile over the height for surface A	x
A.7	Wind profile over the height for surface B	x
A.8	Wind profile over the height for surface E	x
A.9	Wind profile over the height for hexagon	xi
A.10	Wind profile over the height for octagon	xii
C.1	Elements that were calculated	xx
D.1	Plan section and 3D view of octagon plain model	xxvi
D.2	Utilization degree for composite columns at elevation G for ULS wind loads	xxvii
D.3	Utilization degree for composite columns at elevation 7 for ULS wind loads	xxvii
D.4	Displacement due to serviceability wind loads	xxviii
D.5	Displacement due to serviceability seismic loads	xxviii
D.6	Drift ratio due to serviceability wind loads	xxix
D.7	Drift ratio due to serviceability seismic loads	xxix

D.8	Overturning moment due to serviceability wind loads	xxx
D.9	Overturning moment due to serviceability seismic loads	xxx
D.10	Stress S11 at elevation X=17.15 m due to ULS wind loads	xxxi
D.11	Stress S22 at elevation X=17.15 m due to ULS wind loads	xxxi
E.1	Plan section and 3D view for octagon twisting modelxxxii
E.2	Utilization degree for composite columns at elevation G for ULS wind loads	xxxiii
E.3	Utilization degree for composite columns at elevation 7 for ULS wind loads	xxxiii
E.4	Displacement due to serviceability wind loads	xxxiv
E.5	Displacement due to serviceability seismic loads	xxxiv
E.6	Drift ratio due to serviceability wind loadsxxxv
E.7	Drift ratio due to serviceability seismic loadsxxxv
E.8	Overturning moment due to serviceability wind loads	xxxvi
E.9	Overturning moment due to serviceability seismic loads	xxxvi
E.10	Stress S11 in service core at elevation X=17,15 m due to ULS wind loads	xxxvii
E.11	Stress S22 in service core at elevation X=17,15 m due to ULS wind loads	xxxvii
F.1	Plan section and 3D view of octagon twisting and tapered model	xxxviii
F.2	utilization degree for composite columns at elevation G due to ULS wind loads	xxxix
F.3	utilization degree for composite columns at elevation G due to ULS wind loads	xxxix
F.4	Displacements due to serviceability wind loads	xl
F.5	Displacements due to serviceability seismic loads	xl
F.6	Drift ratio due to serviceability wind loads	xli
F.7	Drift ratio due to serviceability seismic loads	xli
F.8	Overturning moment due to serviceability wind loads	xlii
F.9	Overturning moment due to serviceability seismic loads	xlii
F.10	Stress S11 at service core at elevation X=11.65 m due to ULS wind loads	xliii
F.11	Stress S22 at service core at elevation X=11.65 m due to ULS wind loads	xliii
G.1	Plan section and 3D view of hexagon plain	xliv
G.2	Utilization degree for composite columns in elevation G due to ULS wind loads	xlv
G.3	Utilization degree for composite columns in elevation 7 due to ULS wind loads	xlv
G.4	Displacement due to serviceability wind loads	xlvi
G.5	Displacement due to serviceability seismic loads	xlvi
G.6	Drift ratio due to serviceability wind loads	xlvii
G.7	Drift ratio due to serviceability seismic loads	xlvii

G.8	Overturning moment due to serviceability wind loads	xlvi
G.9	Overturning moment due to serviceability seismic loads	xlvi
G.10	Stress S11 in service core at elevation X=11.65 m due to ULS wind loads	xlvi
G.11	Stress S22 in service core at elevation X=11.65 m due to ULS wind loads	xlvi
H.1	Elevation view and 3D view of hexagon twisting model	1
H.2	Utilization degree at elevation G due to ULS wind loads	li
H.3	Utilization degree at elevation 7 due to ULS wind loads	li
H.4	Displacement due to serviceability wind loads	lii
H.5	Displacement due to serviceability seismic loads	lii
H.6	Drift ratio due to serviceability wind loads	liii
H.7	Drift ratio due to serviceability seismic loads	liii
H.8	Overturning moment due to serviceability wind loads	liv
H.9	Overturning moment due to serviceability seismic loads	liv
H.10	Stress S11 at elevation X=17.15 m due to ULS wind loads	lv
H.11	Stress S22 at elevation X=17.15 m due to ULS wind loads	lv
I.1	Plan section and 3D view of hexagonal twisting and tapered	lvi
I.2	Utilization degree at elevation G for ULS wind loads	lvii
I.3	Utilization degree at elevation 7 for ULS wind loads	lvii
I.4	Displacement due to serviceability wind loads	lviii
I.5	Displacement due to serviceability seismic loads	lviii
I.6	Drift ratio due to serviceability wind loads	lix
I.7	Drift ratio due to serviceability seismic loads	lix
I.8	Overturning moment due to serviceability wind loads	lx
I.9	Overturning moment due to serviceability seismic loads	lx
I.10	Stress S11 at elevation X=17.15 m due to ULS wind loads	lxi
I.11	Stress S22 at elevation X=17.15 m due to ULS wind loads	lxi

List of Tables

2.1	Le Corbusier's ' <i>Five Points of Architecture</i> '	5
4.1	Recommended values for maximum deflection from doctoral dissertation (Honfi, 2013)	30
4.2	Critical inter-story drift values for SLS	35
5.1	Results from Autodesk Flow Design for various shapes, part 1	43
5.2	Results from Autodesk Flow Design for various shapes, part 2	44
6.1	Results From Autodesk Flow Design for Geometrical Alterations, part 1	50
7.1	Equations and parameters used to calculate the stress due to torsion	57
7.2	Equations and parameters used to calculate the stress due to torsion	57
7.3	Equations and parameters used to calculate the stress due to torsion	58
7.4	Results for overturning moment	58
7.5	Inputting values for elastic response spectrum	60
8.1	Loading on the structures	68
8.2	Governing load combinations in ETABS	72
9.1	Results from ETABS for wind displacement, drift ratio and overturning moment	78
9.2	Results from ETABS for modal periods and frequencies	79
9.3	Results from manual calculations for acceleration	80
9.4	Results from manual calculation for acceleration according to ISO 10137	80
9.5	Comparing the results for the seismic loads in octagon tapered and twisted model	84
9.6	Results from ETABS for seismic displacement	85
9.7	Results from ETABS for acceleration and mode shapes	85
9.8	Results from ETABS for mass	86
A.1	Site factors that alter the basic wind speed	iii
A.2	Site factors that alter the mean wind speed	iv
A.3	Parameters used to calculate $c_s c_d$	viii

A.4 Parameters used to calculate w_e ix

B.1 Values form NS-EN 1991-1-4 xvi

B.2 Values to determine R^2 xviii

B.3 Results for acceleration calculation xviii

C.1 Strength parameters for GL32c xxii

C.2 Design parameters for GL32c xxii

SYMBOLS AND ABBREVIATIONS

Latin Letters

Symbol	Description
A_{Ed}	design value of seismic action
A_{ref}	reference area
B^2	background response part
I_v	turbulence intensity
M_{Ed}	design bending moment from analysis
M_{Rd}	design bending moment resistance
N_{Ed}	design axial force from analysis
N_{Rd}	design axial resistance
N_{SPT}	Standard Penetrative Test blow-count
P_{NCR}	reference probability of exceedance in 50 years of the reference seismic action
S_L	non-dimensional power spectral density function
$S_e(T)$	elastic horizontal ground acceleration response spectrum
T_1	fundamental period of vibration for building
T_C	corner period at the upper limit of the constant acceleration region
T_s	duration of the stationary part of seismic action
V_{Ed}	design shear force from analysis
V_{Rd}	design shear resistance
a_g	design ground acceleration for type A ground
a_{vg}	design ground acceleration in the vertical direction
c_{alt}	altitude factor
c_d	dynamic factor
c_{dir}	directional factor
c_f	force coefficient
c_p	pressure coefficient
c_{prob}	probability factor
c_{season}	seasonal factor
f_L	non-dimensional frequency
f_{cd}	design value of concrete compressive strength
f_{ctm}	mean value of the tensile strength of concrete
f_{yd}	design value of yield strength of steel
k_{cirt}	factor for buckling
k_{mod}	modification factor for loading of timber

k_p	peak factor
k_r	terrain factor; reduction factor
m_1	equivalent mass per unit length
n_1	fundamental frequency
n_i	natural frequency of the structure of the mode i
v_b	basic wind speed
$v_{b,0}$	fundamental value of the basic wind velocity
v_{crit}	critical wind velocity of vortex shedding
v_m	mean wind velocity
z_0	roughness length
z_e	reference height for external wind action
z_{max}	maximum height
z_{min}	minimum height
z_s	reference height for determining the structural factor
A	area
B	width of the structure
D	depth of the structure
E	Young's modulus
H	height
K	mode shape factor; effective stiffness
S	soil factor
Sc	Scruton number
T	vibration period of linear single degree of freedom system
g	acceleration of gravity
k	equivalent roughness
m	mass per unit length
n	number of stories
q	behavior factor
r	radius
t	time
w	wind pressure
z	height above ground

Greek Letters

Symbol	Description
σ	stress; standard deviation
δ	logarithmic decrement of damping
η	variable
λ	slenderness ratio
σ_v	standard deviation of the turbulence
$\sigma_{a,x}$	standard deviation of along-wind acceleration
ρ	air density
ϵ_0	bandwidth factor
ϵ_1	frequency factor
ν	up-crossing frequency; Poisson ratio; kinematic viscosity
Ψ	reduction factor
ζ	exponent of mode shape
γ_M	partial material factor

Abbreviations

Abbreviation	Description
A.C.	After Christ
BIM	Building Information Modeling
CEN	Comité Européen de Normalisation
CO ₂	Carbon Dioxide
DCL	Ductility Class Low
ETABS	Extended Three-Dimensional Analysis of Building Structures
H/B-Ratio	Height - to - Width Ratio
HCS	Hollow Core Slabs
IIT	Illinois Institute of Technology
ISO	International Organization for Standardization
LEED	Leadership in Energy and Environmental Design
NA	National Annex
NS-EN	National Standard - European Norm
SDOF	Single Degree Of Freedom
SLS	Service Limit State
SOM	Company Skidmore, Owings and Merrills
SRSS	Suare Root of Sum of Squares
ULS	Ultimate Limit State
WWII	World War II

CHAPTER 1

INTRODUCTION

High-rise buildings are today iconic structures that have a purpose beyond housing people and offices. They often form the skyline and thus also function as an image of the city itself. They are symbols of power and economic prosperity, as well as innovation. New advances in structural engineering has made it possible to adapt the architectural design to the local culture and expression.

You employ stone, wood, and concrete, and with these materials you build a house and palaces. That is construction. Ingenuity is at work. But suddenly you touch my heart, you do me good, I am happy and I say: "This is beautiful." This is Architecture. Art enters in. -Le Corbusier (1989)

The aim of this thesis is to design a unique skyscraper for Oslo, considering both the structural and architectural aspects. Oslo is the capital of Norway, a city that is currently undergoing a steep increase in population (Høydahl, 2010). When a city is going through this type of change, there are only two possible options; one is to increase the area of the city center by building horizontally; the other is to build in height vertically. Proximity to work places, infrastructure, leisure activities, and environmental footprint are great arguments for a vertical expansion of the city, as stated by Al-Chalabi (2015). The aim of this thesis is to create a signature high-rise building that can enhance the architectural expression of Oslo's skyline with a modernized structural design.

Since this is a conceptual design study, the thesis covers the selection process of a structure that is designed within the fields of architecture and structural engineering. The architectural study covers the evolution of the skyscraper, including how the pioneers contributed to the current high-rise buildings. This includes the influential architects choice of materials, geometries, sustainable features, and statement elements; and how these contributed to well-functioning conceptual design.

Buildings are often loved or hated purely on the basis of their looks, and despite the sophisticated technical input that goes into their realization, without some spiritual interaction between the structure and its city and people, it can only be regarded as a failure -Hijjas Kasturi (1988)

There is a connection between sustainable building materials and old Norwegian building traditions. The goal is to design a building that clearly recites the Scandinavian landscape and traditions. Recent development in structural engineering has made it possible to combine new structural solutions with these architectural aspects.

When a high-rise is situated in Oslo, Norway, the governing load is wind. Some of the most stunning skyscrapers today, from an architectural standpoint, have geometries that have been implemented in response to structural resistance for wind loads (Dupré, 2013). Thus, the aim is to minimize these wind forces by various alterations to basic geometries. Concluding, the building design can be optimized against loads while also following the 21st century architectural norm of the skyscraper; to be a unique high-rise that is as light as possible.

By determining the governing load pattern and load combinations for the building, it is possible to alter the shapes to increase the structural resistance. In Norway, building requirements and limits are defined by International Standards and Eurocodes. By using computational programs, it is possible to design the structure, use site specific loads, and analyze how alterations effect the behavior of the building.

The thesis is divided into three main parts. The first part discusses the architectural and technical history of skyscrapers and how these elements can be implemented in the conceptual design in the most efficient way. For a structural engineering student, it is important to understand the history and evolution of skyscrapers and why the pioneers chose to express the high-rise buildings in these certain ways. The building's location for my thesis is selected, and software program is used to see how the geometrical shape is influenced by local climate conditions.

Secondly, the thesis covers the structural theories related to structural design of a high-rise. Documented wind tunnel experiments of high-rise structures and alterations efficiency is evaluated, such as the results from Kwok et al. (2015). The site specific loads are determined from Eurocodes, and thresholds are implemented and discussed.

Finally, the most beneficial structural shapes are modeled in Building Information Modeling, BIM. Loads are applied, and results for the seismic and wind load combinations are analyzed. The beneficial effect of the chosen wind induced alterations are discussed, and the resulting increase in structural resistance is shown.

CHAPTER 2

THE EVOLUTION OF THE HIGH-RISE

Architecture can be seen as a combination of earlier architectural époques and a reaction to these eras. In the world of high-rise buildings, the evolution is mainly concentrated to the last 70 years. Therefore, to be able to understand how the skyscraper is constructed today, it is necessary to have a brief overview of the evolution over the past 70 years. Leaps of new technology have been the main factor for changes in the construction methods. Due to the advance structural knowledge and techniques needed to build a high-rise, these buildings are distinct in the architectural world compared to other constructions. The evolution of the skyscraper is mainly due to innovative technical solutions created by structural engineers, and not architects as other constructions.

Technology is part of civilization and being anti-technology would be like declaring war on architecture and civilization itself... The best architecture comes from a synthesis of all the elements that separately compromise a building -Sir Norman Foster (1999)

2.1 The Change in Civil Construction After World War II

After the Second World War, WWII, the basic principles in building construction changed. The earlier positive and utopian way of building was now exchanged for realism. This resulted in more practical buildings. However, during WWII, new technology had sprung in the manufacturing sector, and this was now implemented into the civil engineering field (Ábalos and Herreros, 2003).

Due to a change in the industry, the commercial companies now required larger buildings for their manufacturing and distribution. The office building had an even more dominant role in the cities than earlier. Consequently, the office building evolved into new and larger constructions, due to the changed demand. The result is later known as the contemporary city, lead by Le Corbusier. The office buildings and the high-rise buildings were products of industrialization and the technology that had evolved from the mechanical engineering sector. The style of the buildings were mainly modernistic.

The evolution of the 21st century high-rise is due to a combination of change in construction methods and groundbreaking architectural development. The architectural and structural engineering evolution of the high-rise can be seen as a gradual development with main contributions by a handful of individuals.

2.2 Le Corbusier and His Modernistic Approach

Le Corbusier was a pioneer in understanding the potential of the skyscrapers. Through his works, these ideas evolved into cities where the urban plan was not only focused around the skyscraper itself, but also on the effects of solar radiation, social development, and transportation access. His work is however highly debated, and many believed that his ideas were unpromising and even damaging. The skeptics believed that Le Corbusier's take on the urban city could be considered as the death of the largest cities. An aspect that Jacobs (1961) discussed in '*The Death and Life of Great American Cities*'.

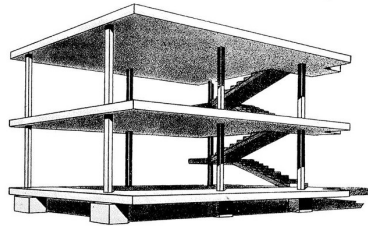


Figure 2.1: Image of Le Corbusier's *Dom-ino* (Ábalos and Herreros, 2003)

Le Corbusier is most known for his take on the modernistic approach of architecture, and is without doubt considered as one of the pioneers within the field. His most famous contributions to the modernistic architecture can be seen in his works '*Villa Savoye*', and '*Dom-ino*' that is shown in Figure 2.1. The latter was a pavilion finished in 1914 that illustrated his five pillars in modern architecture. These five main aspects, shown in Table 2.1, also influenced his take on the evolution of the skyscraper and the contemporary city (Ábalos and Herreros, 2003).

Pillars	Description
One	Pilotis. Replacing the supporting walls such that each level is only supported by a grid system of reinforced concrete columns.
Two	Free facade. Creating an open facade that releases the exterior from the structural system.
Three	The horizontal window. Connecting the outside to the inside. Horizontal bands of windows that light all the interior rooms.
Four	Free ground plan. With only columns in the free plan, it was desired to create open plans with as few separating walls as possible.
Five	Roof gardens. Giving back to nature the area that was taken by the building, as well as for domestic purpose.

Table 2.1: Le Corbusier's *'Five Points of Architecture'*

2.2.1 Le Corbusier's Take on the Skyscraper

Le Corbusier got his education at the well-known Le Beaux Art in Paris. This school taught mainly in traditional neoclassicistic architectural style. Even so, the school was influenced by the structural system that had evolved in Paris. The grid system of the urban planning and the easy commute in the center, were aspects that formed Le Corbusier's take on the skyscraper.

During the 1920s Le Corbusier evolved his view on the modern development of American cities. He believed that it was necessary to centralize the city around the business district, where the skyscraper was essential to achieve the desired outcome and density. By maintaining his wish for *'The Five Points in Architecture'* as universal pillars, the skyscrapers evolved as symmetric and repetitive stories. This repetition of levels vertically was seen as the ultimate manifestation of the pact between geometry and mechanics (Ábalos and Herreros, 2003). The high-rise buildings consisted of load-bearing columns, glass curtain walls and a roof garden; all aspects from *'The Five Points of Architecture'*.

In the following years, Le Corbusier incremented new factors into his take on high-rise. When considering the effect of solar radiation, the skyscraper evolved to a structure that was able to achieve desirable sunlight angles. Consequently, the structure was in a higher degree fixed to the surrounding topography. Le Corbusier also substituted the earlier glass curtain wall with a non-load carrying system that had shading options for the direct sun conditions. Le Corbusier's original idea of an urban system of uniform structures, had now evolved into a topological varying structures. He had now built a bridge between his earlier separation between industry, technology, surrounding topography and building forms (Ábalos and Herreros, 2003).

2.3 Mies von de Rohe

When enjoying the Chicago's skyline to this current day, one can study Mies von de Rohe's contributions to the field. Mies von de Rohe revolutionized the tall building industry by being the first person to build a building for multi-purpose use. The Seagram Building, 1958, located in New York is the first of its kind, by combining residential floors with hotel, offices and a soft-story for public use.

2.3.1 The Mies Columns

One of the main aspects Mies von de Rohe is known for, is his unique and expressive columns. The first projects include the characteristic L-profile columns. Each column consisted of four steel L-profiles that were covered with coated galvanized steel. The effect was mirror-like columns that reflected the external surrounds; bringing the external environment inside. The columns also had the unusual cross-like shape, which created a unique expression for his time.

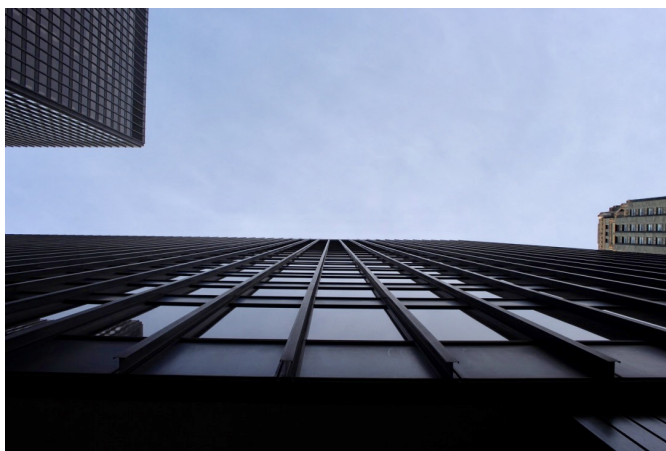


Figure 2.2: Image of Mies van de Rohe's expressive columns (Hverven, 2017)

Later, when Mies started constructing the skyscrapers, the columns remained as a main architectonic expression, shown in Figure 2.2. One of the first tall building that Mies constructed was the Lake Shore Apartments located next to The Michigan River in Chicago. The classical mirror glass facade was replaced with segmental vertical glass between I-profile steel columns. These columns were located on the exterior of the facade. By doing this, Mies used the well-known structural element, the I-profile, as the main architectonic element on the facade, shown in Figure 2.2.

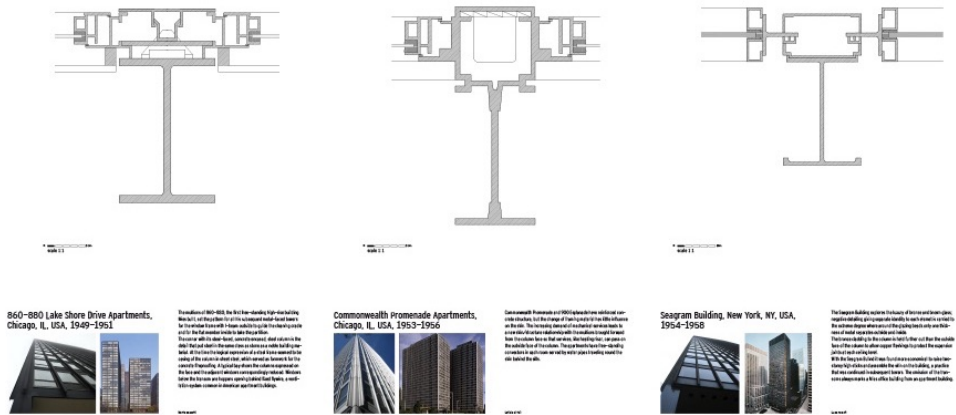


Figure 2.3: The evolution of Mies columns (Ábalos and Herreros, 2003)

In the later works by Mies von de Rohe, the simple yet expressive statement of the Lake Shore Apartments was from an architectural standpoint satisfied in a larger extent. This can be illustrated by the Seagram Building located in New York. A similar I-profile was used on this facade, however there is an increased architectonic unity between the columns and the rest of the facade. When one studies the details of the overlap between the columns and the glass segments, one can study the evolution of Mies' technique. In Figure 2.3, it is clear that for the Lake Shore Apartments, furthest to the left, the two parts have a separated structural finish. Like two separate items being placed together. In the Seagram Building, furthest to the right in Figure 2.3, the central axis of both components are aligned. The connection is simple and in an higher degree architectonically pure (Ábalos and Herreros, 2003). This implementation of architectural design to the load-bearing components was an advancement in high-rise structures.

2.4 The Contribution from SOM

During the late twentieth century, the evolution of the skyscraper was mainly due to the company Skidmore, Owings and Merrils; SOM. The structural system of the skyscraper changed dramatically during the years 1960s to 1990s. The buildings went from a symmetric steel-grid supported by a reinforced concrete facade, to individually specialized 3D-analyzed frames. The development led to a more beneficial structure for resisting the external load.

2.4.1 Myron Goldsmith and Fazular Kahn

In Goldsmith's Master thesis, it is clear that Goldsmith had a unique take on the combination of architecture and structural engineering. "*The Effects of Scale*", by Goldsmith (1953), focused on replacing the fixed connections in tall buildings with flexible tie bars and joints. Goldsmith analyzed structures with a rigid load-bearing exterior frame that absorbed all the horizontal wind forces, while the light structure inside supported only the gravitational loads. The thesis concluded that with a sufficient envelope, it was possible to build up to 80 stories, without increasing the volume of the load-bearing system substantially. The result was in some way the opposite of Le Corbusier's accepted view on the Platonic idea of forms, and how each object has an optimal size and shape (Ábalos and Herreros, 2003).

In the late 1950s, Goldsmith started to collaborate with Fazular Kahn, a collaboration that lasted for many years. Both were professors at Illinois Institute of Technology, IIT, while also being partners at SOM. When one is considering the individual contributions in physics, Einstein is seen as the most influential person within the field. In high-rise structural systems, Fazular Kahn is this individual. One can say that his theories and achievements are the main reason we have the variety of possibilities today in load-bearing systems for a high-rise. Kahn gave form to the ideas that Goldsmith had established in his thesis, but was unable to construct (Ábalos and Herreros, 2003).

"I strive for structural simplicity... The technical man must not be lost in his own technology". -Fazlur Kahn (1982)

Kahn was an analytical engineer who evolved the methods of detailed analysis. This led the industry away from the accepted earlier manually calculated solutions. His studies resulted in structures that pushed the ultimate limit design of high-rise structures. By doing this, he gave materials a new spatial concept. Computer software that was developed by the 1960s led to new systems. This, combined with the development of high-grade steel made it possible for Kahn to create structures that could resist the horizontal wind forces and downward pull from gravity more efficiently. The forces were now absorbed in three dimensions. By analyzing the wind as not only loads that lead to deflection and shear, but as an aerodynamic mass, Kahn was able to look at the vibrations and fatigue that the wind inflicted on the structure. Through his work, new and more efficient load-bearing structures were invented (Ábalos and Herreros, 2003).

When considering high-rise buildings, wind energy is a governing issue compared to earthquakes, due to the buildings low natural frequency. It is highly necessary for a building to be able to prevent an increase in the sway by implementing natural or additional dampers in the structural system. Dampers will contribute to minimize the response under earthquake loads, while rigidity in the load-bearing system will minimize the wind induced response. However, the combination of wind and earthquake leads to an optimal structure being flexible as possible for earthquake

forces, and as rigid as possible to prevent sway due to wind forces.

The collaboration between Goldsmith and Kahn led first to the *'tube-in-tube'* structural element. Here, one has combined the envelope evolved by Goldsmith in his thesis, with a central service core. As a result, structures were designed with floors of equal thickness over the vertical height, since they were not influenced by the overturning moment, as a result of the additional service core. The plan structure is optimized such that the shear walls in the service core interact with the envelope. This leads to an increase in the efficiency by decreasing the deflection and sway. Column free space was achieved in the stories, an optimal and groundbreaking solution for office buildings.



Figure 2.4: Image of John Hancock Center in Chicago (Hverven, 2017)

In Goldsmith's thesis he discussed that an optimal reticulated frame would be one consisting of diagonals on the exterior facade (Goldsmith, 1953). He argues that this shortens the distance of load transfer, by the loads being transferred to the corner columns more efficiently. This became a reality in Kahn's John Hancock Center built in Chicago, 1969. The first diagonal tube was created. It was considered as an optimal structure where the triangular grid resisted the wind loads in an efficient way. The diagonal cross-bracing, as shown in Figure 2.4, is continuous from face to face. The bracing is connected to the columns, allowing the loads to be transferred. The 100-story building could achieve greater heights, becoming the tallest building in The United States at the time. However, the owner wanted a building that was optimal and not only seen as a project to reach fame. The diagonal bracing absorbed half of the skyscraper's actual loading, even under extreme wind conditions. As a result, it became possible to decrease the amount of

co-existing load-bearing steel. The new technology had large economical and mass advantages.

Fazlur Kahn, together with Bruce J. Graham, continued his innovative take on the structural system of high-rise structures. This can be seen in Willis Tower, previously known as Sears Tower. The new product was the bundled tube. Willis Tower was constructed using nine connected tubes, each with an envelope structure with a large influence from Goldsmith. The nine parts are varying in height. This efficiently increases the stability of the building by lowering the center of gravity. The loading is dissipated downwards into the major mass of the building by each tube. Consequently, each tube acts independently, receiving only a portion of the stresses. The tubes intersect with one another, and by doing this release the exterior columns from loads, creating rigid diaphragms. Compared to the John Hancock Center, the bundled tubes used for the Willis Tower can in a larger degree be adaptable to multiple structures (Dupré, 2013).

"Through the search to conquer new heights, initiated by Goldsmith and developed by Kahn - as a reconsideration of the relationship between scale and typology codified by Le Corbusier in his Five Points and by Mies in his isotopic structures - in just fifteen years the skyscraper underwent a complete revision" - Ábalos and Herreros (2003).

Today's skyscrapers can be seen as a combination of the structural and architectural solutions invented and evolved by Le Corbusier, Mies von de Rohe, Goldsmith and Kahn. Consequently, these key personnel's results in the world of high-rise structures are highly significant today.

CHAPTER 3

21ST CENTURY SKYSCRAPER'S

During the last decade, the amount of skyscrapers in the world has dramatically increased. After the tragic terrorist attack of The World Trade Center in New York, known as 9/11, the construction of super-tall structures went to a halt. Lower high-rise buildings were a priority due to safety considerations. After the economical recession in 2008 the construction of super-tall structures, and the race to achieve the tallest building in the world, boomed yet again. As of 2013, there were over 500 buildings under construction or built, that were over 200 meters tall (Dupré, 2013).

Currently the world's tallest building is Burj Khalifa in the United Arab Emirates of 828 meters and 162 floors. Nonetheless, The Kingdom Tower, in Saudi Arabia, is under construction and is planned to be open to the public in 2018. The actual height is unknown, but if rumors are correct, it is going to be over 1000 meters tall, breaking all previous records and limits. Thus, as Dupré (2013) concludes, today it is possible to build buildings that are over a kilometer in height, with a height-to-width ratio that one never thought was possible in Kahn and Goldsmith's time. Imagination is the only limit when constructing skyscrapers. This is largely due to the efficient collaboration between architects and engineers in the evolution of skyscrapers.

3.1 Sustainable Design

It is predicted that the world's population will be 9 billion by 2050 and that 70 percent of that population will be living in the cities. Today, buildings are the reason for approximately one third of the greenhouse gas emissions (Al-Chalabi, 2015). The beneficial green aspects of skyscrapers compared to other buildings are; the reduction in ground floor footprint, increased available area for green zones, the wind that impacts the structures can be used to produce energy or to reduce ventilation costs, and the deep foundations for the stability lead to it being possible to harness the geothermal energy. Other aspects that favor the skyscraper is that they have lower life-cycle costs, are more marketable and deliver social benefits in the form of enhanced employee productivity and health (Dupré, 2013). When considering this with the combination of increased urbanization in cities, it is a growing understanding that the correct way of building is upwards, and doing this in a sustainable way.

Today, there are certifications that categorize skyscrapers based on their environmental performance. These are the universal LEED-certificate, and stricter custom certifications for a few of the leading countries within the field. Due to new technology, it is possible to decrease the energy requirement for a high-rise by 50 percent. By using smart solutions for ventilation, heating, light and materials, it is possible to achieve buildings that have in sum positive effect on the environment, compared to lower buildings. When implementing green gardens and natural water reservoirs in the structure, it will lead to a sustainable and aesthetically beautiful building.



Figure 3.1: Shanghai center on a regular day (Hverven, 2016)

The focus on sustainability in building construction has dramatically increased in the last decades. This is mainly due to the increasing awareness and acceptance of the climate change the planet is undergoing, based on human made global warming. Some of the most industrial cities are daily experiencing unhealthy levels of smog and polluted air. One of these cities is Shanghai in China, where the level of pollution is announced as weather reports. Here, some of the tallest structures are situated; Shanghai Tower, Shanghai World Financial Center, Jin Mao Tower and Oriental Pearl Tower. Due to the high levels of smog, the uppermost parts of the buildings cannot be seen from ground level, as shown in Figure 3.1. The Shanghai Tower is the last to be completed, and is a recipe of the future skyscrapers by having a main focus on sustainable solutions. Its design meets the requirements for LEED Gold certification and a China Green Building Three Star rating (Dupré, 2013). The building can be seen as a vertical city by having a twisting prismatic form with gardens wrapped around the exterior of the core. Glass facades are placed on both the envelope and outside the building core. This creates a buffer zone leading to less heating and cooling requirements. The plan geometry is optimized to maintain a controlled amount of solar light reaching the office space (Dupré, 2013).

3.1.1 Materials

A Concrete and Steel

Classical high-rise structures have the main load-bearing system consisting of steel columns supported by concrete slabs. Technology has led to high-strength steel that can withstand greater forces; both in compression and tension. The concrete has also evolved by researches on the strength effect of changing the aggregates and adding different fiber solutions into the concrete mixture.

Concrete is a material with great compressional strength but very limited tensional strength. Consequently, the common practice is to use pure concrete in the compressional segment and add steel reinforcement in the tensional part. Today, composite systems are in the frontier of achieving long span bearing systems. A composite system is constructed from a steel profile enclosed in concrete or concrete filled steel tubes. Strength is gained by the combination of these two materials, with additional rebars where it is needed.

When considering which materials are most efficient, it is usually desired to take into account; cost, carbon dioxide emissions, weight and inter-story drift. Numerical analysis is the best method to achieve the most optimal structure and use of materials. Composite structures are popular due to the low cost, easy fireproofing, quick construction, and long spans due to material optimization of the steel and concrete (Sing-Ping, 2016). Therefore, composite elements should be ideal for a tall building.

B Timber

Norway has a long tradition of using wood as the main building material. This is seen in the well preserved Stav-churches that date back to around the end of the Viking Age in Norway, 1150 A.C. These churches were spread throughout Europe, but Norway has the largest amount of well preserved churches. Consequently, it is now considered as a large part of the Norwegian history and culture. On the other hand, concrete and steel have been the main building materials in larger constructions. However, with modern techniques it is possible to build load-bearing timber structures also in high-rise. The increasing interest in wood for high-rise is largely due to the environmental benefits compared to steel and concrete. Every cubic meter of timber releases 1 ton of carbon to the atmosphere. Comparing this to the concrete and steel, the emissions are 81 percent less (Fecht, 2014).



Figure 3.2: Västerbroplan in Stockholm; exterior (Møller, 2015)

Currently Stockholm Wooden Skyscraper, Västerbroplan, by C.F. Møller, shown in Figure 3.2, is under construction (Møller, 2015). This is a 34-story skyscraper where the main building material is glue laminated timber, supported by concrete cores as shown in Figure 3.3. The glue laminated timber has a structure consisting of thin layers of timber elements glued together. The result is a material that is stronger than regular wood, making it possible to have longer spans and large ceiling to floor heights. A desired outcome in high-rise structures.

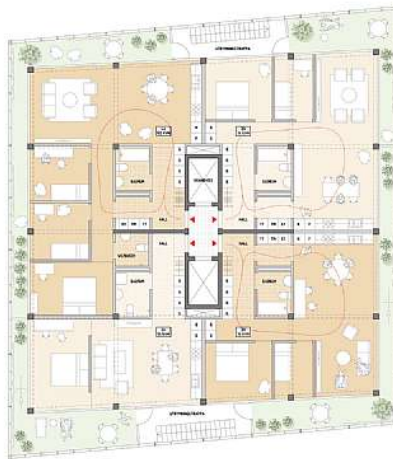


Figure 3.3: Västerbroplan in Stockholm; plan view (Møller, 2015)

As shown in the plan Figure 3.3, the building's load-bearing structure consists of five-by-five columns, two supportive cores and two shear walls. Inside the secondary

support system, walls and ceilings are made of timber, giving it a modernized but traditional Scandinavian design. Glue laminated timber is considered as a fire safe material, requiring a considerable amount of time before it loses its bearing capacity. On the other hand, glue laminated timber is prone to windy and wet conditions. The high-rise in Stockholm has solved this problem by having a winter garden within a glass envelope on the exterior of the wooden structure (Møller, 2015). This creates a transparent envelope with a garden around the main structure. This gives the same sustainable features as for the Shanghai Tower, shown in Figure 3.1. It is therefore possible to implement glue laminated timber as part of the load-bearing system in a high-rise and still maintain a 21st century architectural expression of the building.

C Glass

"Glass is completely new, pure material... It works in the most elementary way. It reflects the sky and the sun; it is like clear water; and it has a wealth of color, form and character which is indeed inexhaustible and which can be a matter of indifference to no person". -Adolf Behne (1919)

The evolution of the glass facade in tall buildings started with the glass curtain wall and has evolved into sustainable solutions. Today, the glass facade can be constructed using up to three layers of glass with air gaps in-between. This leads to an energy efficient facade that also allows for a maximum exposure to daylight and the surroundings. The higher the technology in the glass; the lower the energy consumption, but also the greater the price.

3.2 Designing Sufficiently Against Wind

Wind loads can be subdivided into two basic categories; the dynamic and the aerodynamic. The dynamic loads is time dependent and caused by the changes of pressure on the building over time. Aerodynamic forces take into account the structure interactions with the wind force, creating a different response than the dynamic (Alaghmandan and Elnimeiri, 2013). Aerodynamic forces consist of drag forces, lifting forces and torsional moments. The along wind is generally known as the mean wind with fluctuations, while the cross wind forces act perpendicular and generate vortices (Amin and Ahuja, 2010). By combining the knowledge from architects and engineers, one can design a building with a beneficial aerodynamic geometry and wind optimized structural system. The two governing issues are the discomfort for occupants and the building performance under severe wind conditions (Amin and Ahuja, 2010).

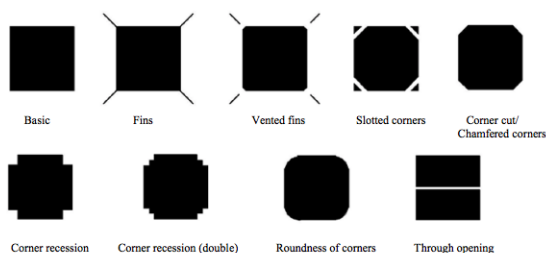


Figure 3.4: Variety of alterations to the plan geometry (Amin and Ahuja, 2010)

Aerodynamic geometries have the characteristic that they confuse the wind acting on the structure. As a result, this reduces the wind pressure (Alaghmandan and Elnimeiri, 2013). In these days, it is common to modify the general geometry with openings, rounded or notched corners and turning or twisting shapes as shown in Figure 3.4. In the building Taipei 101, the corner recessions led to a 25 percent decrease in the overturning moment at the base (Alaghmandan and Elnimeiri, 2013). These solutions will benefit environmentally by having the ability to reduce the volume of structural resisting components.

Types of architectural modifications that have a positive effect on the wind analysis (Alaghmandan and Elnimeiri, 2013; Amin and Ahuja, 2010).

- Taperings. When the building becomes slightly more slender towards the top. The changes lead to a reduction in the across wind loading and effect, which is specially critical in the acceleration analysis of the building. Even so, having a too large tapering on the building will have a negative effect on the damping of the building, causing unwanted excitations.
- Setbacks. This is by the width changing over the vertical distance, leading to the wind having concentrated vortices at different heights of the building. This reduces the wind forces on the building, also leading to varying loads along the height.
- Openings and porous materials. This will give a decrease in the velocity of the vortices, separating the air into paths and consequently decreasing the total wind effect on the building. The openings are usually placed at the top, which largely reduces the across-wind motion, which is generated at this location.
- Turning and twisting. This is an effective way to reduce the vortex shedding along the vertical axis. It reduces the cross-wind since the wind becomes confused with the strongest wind direction. It is worth mentioning that curved design also has a tendency to add strength to the structure.
- Chamfered corners. This architectural correction reduces both along- and cross-wind forces by around 40 percent compared to a regular rectangle, a percentage

that is not altered by changes on the surrounding terrain. The reduction is due to decreasing fluctuating lift, drag and aerodynamic instabilities. However, a few studies conclude that it may have a negative effect on the fundamental mode of the building and damping, especially for low wind velocities. This is mainly when the corner cut is larger than 10 percent of the cross-sectional width.

- Roundoffs. Softening the corners, or adding stepping, also called micro-changes will change and reduce the air flow. For across-wind the effect is noticeable for low and ultimate wind forces, and the response is greatly improved. Nonetheless, other shape modifications are shown to be more beneficial.

In a study done by Iwasa and Hayashida (1990), they investigated the effect of alterations on a 600 meters tall building with an area of 6400 m^2 . They looked at four different geometries: rectangular, circular, rectangular with roundoff corners, and rectangular with notched corners. For the maximum across-wind force, a force of 64.6 m/s , the results show that the best solution was the circular shape, then rectangular with roundoff, next to last the rectangular with notched corners, and lastly the rectangular shape. Consequently, the results show that it is highly favorable to alter the classical rectangular shape to be able to decrease the wind forces on the structure. It is worth mentioning that these results were very different from what was concluded from manually calculated force balancing, which illustrates the immense benefits from using numerical modeling and wind tunnel testing. Another test showed that recessed corners was more effective in vortex shedding than chamfered corners when a building ranged from 240 to 280 meters in height (Amin and Ahuja, 2010).

For a building to become sustainable, it is necessary to implement energy efficiency in the numerical modeling process. The load-bearing structure and the geometry then becomes influenced by environmental performance in a larger extent. During the last decade high-rise buildings have been built with a construction that benefits from the wind force acting on the volume. Buildings have wind turbines and air shafts strategically placed, resulting in a lower energy demand. However, when comparing life-cycle cost to effect, it has been observed that the benefit may not be as great as desired (Al-Chalabi, 2015). Thus, this is not further investigated.

3.2.1 Solutions That Benefit in Oslo, Norway

The main argument for incorporating environmental solutions into buildings is to reduce the energy demand of the building. This is vital in cities where the energy production is governed by oil and fuel production. In Norway, the hydropower plants generally produce more electricity than what Norwegians consume. Consequently, we export the electricity from renewable energy, leading to an annual net export

of electricity for 28 out of the 38 previous years (Statnett, 2017). As a result, the development and innovation in sustainable buildings has only recently reached the country. In the neighboring countries, these solutions have been a part of the construction technique during the last two decades. However, Sweden for example, gain electricity from nuclear power plants, which are not environmental friendly. The drive towards sustainable building techniques in Norway is mainly to reduce the electricity consumption of buildings, with the main goal of lowering the electricity bill. The popularity among the Norwegian population to be environmental-friendly has also led to an increase in demand for residential and office buildings that have the ability to front a sustainable design.

When one considers the overall life-cycle of buildings; the production of materials, construction, operation and demolition; the energy use and carbon dioxide release is substantial. The certification process in Norway to achieve a sustainable building focuses on reuse of materials, energy efficient solutions and even buildings that produce energy in the overall life span. 40 percent of the domestic energy consumption is due to office buildings, an amount the government wishes to reduce (Powerhouse, 2017). This previous decade, the sustainable design in buildings has reached a new threshold; energy positive buildings. An energy positive building produces more energy than what it consumes during the entire life-cycle (Powerhouse, 2017). This engineering innovation has set new standards to building design. In countries where the electricity is governed from non-renewable energy production, this can be seen as a highly beneficial solution for the environment.

Since the electricity in Norway is mainly from hydropower plants, this report focuses on sustainable solutions that reduce the carbon dioxide footprint and not the electricity costs. Therefore, solutions such as solar panels are not considered. This is due to the fact that solar panels are in general placed on the exterior surfaces of roofs or facades, and the material used to implement these solutions can therefore be seen as an additional carbon dioxide emission. This is not sustainable when focusing on CO_2 and not costs. A sustainable building in this report, is considered to be a building that reduces the amount of carbon dioxide emissions by environmental-friendly materials, and reduces the amount of material needed for structural resistance.

A Green Areas

One of the most common implementations of sustainable design is creating green roof gardens. These garden roofs function as rain collectors, air filtration of the city's polluted air, and the principal of giving back the green area that was taken by the building, as stated by Le Corbusier in his *Five Points of Architecture* in Table 2.1. When implementing these green gardens, it is highly necessary to consider the local climate. Norway is situated in the northern hemisphere, and consequently, a large amount of the months have a mean temperature below freezing. One project

that has successfully incorporated plants for water filtration is the Wollishofen Water Plant in Zurich, Switzerland (Butler et al., 2012). Four buildings are here covered in sedum plants, and the project has been a success for over 90 years. The sedum plants are native plants, hence, have been specialized for the local climate by natural selection. The climate in Zurich is comparable to Oslo, and since Norway also has a large variety of sedum plants, it is very likely that an implementation of these species would be a success.

Many of the high-rise structures such as Västerbroplan and Shanghai Tower have implemented vertical gardens by a glass envelope (Møller, 2015; Dupré, 2013). It is highly unlikely that vertical gardens without a glass envelope can survive during the winter months in Oslo due to temperature considerations. These gardens can either be implemented on the exterior of the load-bearing structure or in the core. By having the plants on the exterior, the plants work as a thermal barrier, resulting in less insulation in the building core, due to lower temperature fluctuations. This will be an energy efficient solution that leads to a decrease of insulating material. However, it may lead to an undesired low level of daylight being transmitted into the core. By having a garden placed within the building, the plants will have a controlled temperature environment. The aesthetically effect may be enhanced by having a natural ventilation system constructed with open atriums with a large vertical garden in the center.

B Natural Ventilation

The main purpose of constructing buildings with natural ventilating systems is to decrease the consumption of electrical ventilation, respectively, the electricity bill. The concept and strategies to achieve natural ventilation are dependent on the climate, and therefore vary. The systems implements the outside wind forces as driving forces to achieve a ventilated space. The most common natural ventilation system is the implementation of open atriums. Thermal buoyancy is accumulated in these open spaces, which is the driving force inside the building. By implementation of a natural ventilation system through open atriums, it leads to smaller shafts for mechanical ventilation, therefore less material use. Also, the open area will reduce the amount of material per floor. It is beneficial to implement an atrium solution for office stories, since the floors are in general open and will benefit from the atrium's air quality. For residential floors, the apartments are enclosed and therefore it would be difficult to implement a natural ventilation system. It is possible to combine the open atrium area with a green garden to increase the benefits for this solution. An example of this is shown in Figure 3.5, where a mixed-use building located outside Malmö in Sweden has combined an open atrium with green area and a staircase.

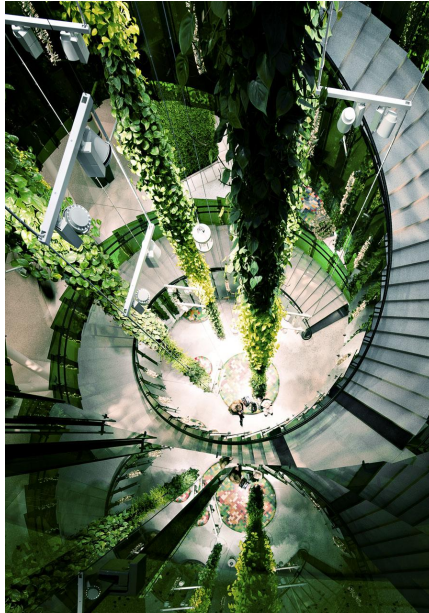


Figure 3.5: Green atrium at Emporia. Photo by Tord-Rikard Söderström

3.3 Existing Skyscrapers and the Publics Feedback

Chicago was the city that evolved the high-rise structure during the 20th century. However, currently the race of achieving the tallest and grandest skyscrapers is mainly in China, Dubai and other Asian countries. These cities have undergone a dramatic change in the skyline over the last decades, and cities have evolved from farming fields. In Europe the eager and trend to build vertically does not have the same intensity as in Asia. When comparing these countries, it is clear that the European countries have a more conservative approach to high-rise, and a stronger connection to building traditions in city centers. Thus, one can say that it is not until the 21st century, when it became possible to combine the traditional European methods with high-rise structures, that the public feedback is becoming increasingly positive.

3.3.1 Oslo and the Publics View on High-Rise

Norway is considered as a small scale country in Europe, with a population of approximately five million people. The need for high-dense buildings due to increased population in the cities has been a part of the agenda only for the past years. Oslo is the capital of Norway with around 650 000 inhabitants, and the city has a

considerable area span (Høydahl, 2010). Current trend is to desire to live as near to the city center as possible, resulting in increasing building prices these last years. Consequently, it is evident that high-rise structures in the city center would be profitable. On the other hand, the population has an highly divided opinion on the aesthetically footprint of skyscrapers and there is a large amount of the population that go under the category; skeptics.

Oslo's city landscape has for many centuries been open to the fjord that encircles the city center. During this past decade the area closest to the fjord has been under construction leading to a new modern area with buildings of 12-18 stories along the coast, known as Barcode. Only a few hundred meters behind the coast one finds the tallest buildings in Norway, Radisson Plaza Hotel and the Post House. The government has in the recent years also approved two to three new high-rise structures next to the Post House. The changes to the architectural expression of Oslo are by some seen as an upgrade to the 21st century, and by some seen as a destruction of the city with a '*picket fence*' skyline as the previous chief commissioner, Erling Lae, stated (Iglebæk, 2012). A large amount of the city's population feel that the new skyline is an unfavorable desire to show the rest of the world Norway's wealth and power. On the other hand, the buildings at Barcode create 5,000 apartments and 20,000 new workplaces. Consequently, others believe this is a modern necessary initiative done by the government.

To this current day, there are restrictions in building high-rise in Oslo. The policies are considered as conservative compared to the rest of Europe. The government argues with the fact that at a latitude of 60 degrees, tall buildings will lead to a highly unfavorable casting of shadows over the surroundings. Each high-rise has to be lean and have a sculptural architectural expression to be approved by the regulations (Iglebæk, 2012). The high-rise strategy, established in 2003, leads to it only being allowed to build 42 meters, 12 stories, in the Oslo region with the exception of Oslo central; where the two tallest are located, Bjørvika where Barcode is situated, and parts of Nydalen.

Even though there are height regulations in Norway, it is the architectonic expression that most likely needs to achieve a positive feedback to be built. Norwegians have a tendency to favor traditions and stability. Change is therefore not always seen as a positive outcome. To build a high-rise in Oslo, it is necessary to incorporate the classical building traditions with a 21st century high-rise. By choosing the right materials, shape and expression this can be possible, but if not done correctly it can also be fatale.

3.3.2 Other Examples in Europe

One can say that Scandinavia has not been a part of the wave of building high-rises. However, during the 21st century new tall buildings has evolved in this region, taller

than ever before. Denmark, Sweden and Norway have cities which are dominated by brick buildings of around five stories. These date as far back as to the 18th century. The style is similar to other European cities such as London and Paris. However, Paris and London have been able to combine these traditional buildings with modern steel constructions in a successful way. Thus, the current change in Scandinavia can efficiently be influenced by these cities and how they evolved today's skyline.

A High-Rise Structures in Paris

Parisians and the French have a strong proudness to the cities culture and architecture. Thus, even though an increasing amount of high-rise projects are being proposed, barely any get approved due to lack of enthusiasm from the Parisians. The debate on tall buildings in the capital started already in the early 20th century by Le Corbusier and other influential architects. The city has made clear regulations against establishing financial districts, instead striving towards a mixed-use city as stated in the book by Saint-Pierre et al. (2010). The development of high-rise structures without sufficient density and variety of functions is seen as a harmful contribution to Paris. In the segment of the book it is stated that there are two governing criteria's for high-rise in Paris; mobility and functionality. It concluded that the prime locations for high-rise was on the outskirts of Paris city, not in the city center. This is mainly due to zero-tolerance for buildings over 37 meters in the city center. However, since that publication, the regulations have changed. This current day it is possible to build high-rise in the city center if Paris, a regulatory change that will make a great impact on the skyline and architecture of Paris, allowing for modern 21st century buildings.



Figure 3.6: The Triangle by Herzog de Meuron (Herzog de Meuron, 2016)

Paris is known for combining the classical brick five floor buildings, with constructions as the Eiffel Tower and Centre de Pompidou. When these buildings were constructed they met massive critiques from the Parisians, but over time have become landmarks and loved by the locals. A new era is on the rise with projects

such as the 180 meters tall Triangle, seen in Figure 3.6, by the architectural firm Herzog de Meuron (Herzog de Meuron, 2016). The asymmetrical triangle is to be completed in 2020, located next to the square Porte de Versailles in the 15ème. With the triangular shape, the height impact on the surrounding buildings and environment is highly reduced, creating a low amount of casting shadows.

'Actually, the pyramid is the ideal configuration for high-rise buildings in a dense urban area...[It] has the practical advantage of admitting more light and air to the street below -William L. Pereira (1969)

With an irregular glass facade, the building opens up to the surroundings by having a transparent footprint. By underlining existing asymmetrical axis of the historical plan of Paris, the structure is specialized for the site. Similar to other high-rise structures, the Triangle was met with skeptics. It was first proposed in 2008, but it was not until 2015 that the structure was approved under a new governmental voting (Herzog de Meuron, 2016).

B Malmö and the Turning Torso

Currently, the tallest building in Scandinavia is the Turning Torso, shown in Figure 3.7, located in Malmö, Sweden. This is a 190 meters tall concrete construction. Due to the 90 degree change of the facade, the building has gotten the name Turning Torso inspired by a sculpture. After the construction period, the building has mainly gotten positive feedback from the public. During the building process, the publics view was in a larger extend negative, gradually changing to more positive. The architectural expression of the building is from the human body and it is represented by the torso and its ability to rotate 90 degrees (Elias, 2004).



Figure 3.7: The Turning Torso in Malmö by Santiago Calatrava (Architecture Magazine, 2015)

A successful expression was then achieved, without specific references to the Swedish culture or building traditions. Its uniqueness compared to other high-rise is what makes this project a success in Sweden. The public has a unique building not seen anywhere else in the world, making it a part of Malmö. This principal of architecture is most likely possible to implement in Oslo. By having a unique structure, it can be seen as a 21st century Norwegian structure, without having clear links to older traditions.

As stated in the article written by Elias (2004), the structure is successful due to the efficient form and geometry. The twisting of the building is a geometrical adaptation that benefits the structural resistance to wind forces. The building is optimized in wind tunnel testing and numerical computational methods. The structure consists of nine vertical cubes that are constructed with a high mix of aggregate concrete. By having five elevator shafts, the structure has a large stabilizing core, that contributes to the stiffness. By using modular concrete elements, the construction was finished in a rapid pace. Malmö is located near the coast, leading to considerable wind forces. Consequently, the building has an exterior secondary support system, constructed with a diagonal steel bracing system (Elias, 2004).

CHAPTER 4

THE GOVERNING STRUCTURAL ASPECTS

From a structural perspective, the main goal for a building, is to withstand the loading that occurs during the entire lifespan. These loads are due to natural incidents such as wind, snow, and seismic activity; as well as loads from human activity. National requirements state the thresholds for motions, forces, stresses and deflections. When a structure is designed it is necessary to determine which loads and which load combinations are the most governing.

For a tall building located in Oslo, Norway, the dominant load is wind. Oslo is situated far from a tectonic plate border, resulting in low seismic activity. The Norwegian codes require the seismic loads to be calculated, and to check if it is within the expectable region. This eliminates further calculations, a situation that is almost always the case. For tall buildings, the fundamental frequencies are low compared to shorter buildings. Therefore, the earthquake's frequencies rarely coincides with the buildings natural frequencies. On the other hand, the wind has varying frequencies that may in a larger extent coincide with the buildings fundamental modes frequencies. This may lead to undesirable oscillation of the building. Damping systems need to be incorporated in the design to avoid oscillation, and detailed numerical analyses are necessary to secure the buildings serviceability.

A Building Use

The safety measures depend greatly on the building use. Office buildings are typically used for an eight hour duration of the day, while residential buildings may be used at all hours. When windstorms occur, the office buildings are usually vacated, and people seek comfort in their homes. Thus, the human comfort in the building during severe weather conditions is dependent on the usage. The residential buildings require greater stiffness and a greater damping system. A mixed-use building needs to take this into account for the acceleration at the different levels, depending on where the office floors are located compared to the residential (Kwok et al., 2015).

4.1 Load-Bearing Structure

When considering which load-bearing system is the most efficient, it is necessary to look at the material properties. The response of the structure will vary according to the strength and stiffness of the materials and cross sections. Which alternative is the best application depends on the forces that will be applied to the structure. For example, concrete has a much greater damping ability than steel, and can therefore be the correct alternative in structures that require structural damping instead of having mass tuned damper. If the building is to be constructed in an area with high seismic activity it is suitable to use a system that has efficient elastic properties; that can absorb the dynamic waves from earthquakes.

Today, there are many different types of structural configurations with reinforced concrete and steel frames. The traditional high-rise buildings from the 20th century had concrete slabs that were supported by steel columns and beams. Technologies have now evolved new methods and solutions, and generally the height is the dominant parameter when choosing the load-bearing system.

The traditional shear frame is efficient for up to around 15 stories. The structure is constructed with a concrete core that stabilizes the building. These structures can either be rigid or semi-rigid, depending on the amount of seismic activity and wind force in the region. When adding a truss system to the exterior or as an addition to stabilize the shear walls, the system becomes stiffer. This is ideal for windy locations with a low degree of seismic activity. As a result, it is possible to exceed the height limitation of 15 stories. Outrigger trusses absorb the wind loads in a very effective way, and lead these forces vertically to the ground, without following the load path through the concrete core. Thus, it is possible to decrease the volume of the concrete shear core (Bing, 2016). Even so, many feel that outrigger trusses architecturally are outdated, since this was the popular building technique in the late 20th century.

Another alternative is to build with concrete cores and supplementary shear walls. The shear walls are ideally located with a large as possible distance from the center of rigidity. Consequently, the overturning moment and amount of torsion in the structure is reduced. The shear walls will absorb the wind loads perpendicular to the length axis, leading the forces vertically to the ground (Bing, 2016). Shear walls are ideal for residential buildings, where the walls are situated to also function as separating walls between apartments.

A third possible system that has a suitable geometry for tall buildings, is to have multiple concrete cores supported by an additional truss system between these cores. The truss system will couple the cores, and as a result the loads are transferred between the cores, dividing and sharing the loads efficiently.

Since the building should be designed for mixed-use, it is possible to implement the shear walls for the residential stories, and the truss system for the office stories.

Both systems need to be support by additional columns and beams to efficiently transfer the loads to the core. The wind forces will be transferred from the envelope, to the slabs, and further into the concrete cores. If one implements lean columns and beams, these function mainly to support the live and dead load from the slabs only. If the load-bearing system is supported by stiff enough columns, the wind loads can be transported vertically through this stiff system, without the loading being transferred to the core.

4.1.1 Height Considerations

When deciding on the height of a building, it is necessary to relate the floor height to the function of the story. Common practice is to have a ground floor categorized as a soft-story. A soft story reduces the buildings stiffness dramatically and has immense negative effects on the structures ability to withstand seismic loads (Bing, 2016). This floor usually has a height of around 6-7 meters for office buildings. The floor-to-floor height of each story differs for residential and office buildings.

- Typical office floor height: 3.35 m -4.25 m (2.5 m -2.9 m clear)
- Typical residential floor height: 2.45 m - 3.45 m (2.3 m - 2.75 m clear)

It was decided to implement a ground floor of 6.2 meters, while the office and residential floors has a height of 4.0 and 3.4 meters respectively. To achieve a top story that could be implemented as a rooftop bar and restaurant space, this floor has a height of 5.7 meters. It is desired to have a soft story at mid-height of the building, to use for recreational space for the public. Concluding, the building has altogether a height of 122.0 meters.

The aspect ratio is the ratio of the height versus the width footprint, commonly denoted as H/B-ratio. There is a tendency to build more and more slender structures, increasing the aspect ratio (Bing, 2016). This leads to lighter structures that are more prone to wind forces. The engineering task to design a suitable structure that has enough stiffness, has become a highly complex problem. It is preferable to have an aspect ratio lower than six, to achieve a sufficient amount of stiffness (Bing, 2016). Thus, when a building is of 122 meters in height, the width should be at least 20 meters.

4.2 Introduction to Wind Loads

When analyzing wind loads it is necessary to look at both static and dynamic analyses for a tall building. The static behavior of the wind will lead to story drift and all-over displacement; a parameter that is governing serviceability. The dynamic

behavior results in oscillation and vibration due to the dynamic and time-varying behavior the wind has (Kwok et al., 2015). It is in the dynamic varying load the occupant comfort is critical and it is usually calculated by the acceleration of the building.

Wind effects on structures are dependent on the following (Kwok et al., 2015).

- Site conditions
- Geometrical shape
- Height of the structure
- Dynamic characteristics; mass distribution, modal shapes, vibration periods, lateral stiffness

The wind force and pressure that generates load patterns on the building is highly complex and difficult to calculate. A building usually has a service life of 50 years in Norway, thus, the site conditions and stories of neighboring structures may vary during the life span. If there is an increase in tall neighboring structures, the original wind pattern will then have interference by the new surrounding structures, creating a new force pattern on the building. The geometrical shape of the structure has a large influence on how the wind force will be transferred to loading. Since most buildings are streamlined they can be seen as bluff bodies. This leads to drag forces on the building in the wind direction, lift forces perpendicular and torsional moment (Bing, 2016). The wind pressure will result in vortex shedding that creates vibrations. The changes in the wind force over time may also lead to turbulence, that again creates new patterns of vibrations (Kwok et al., 2015).

4.2.1 Method of Calculating Wind Response

Wind can generally be divided into three types; prevailing winds, seasonal winds, and local winds. All of these vary over time, and a mean value is usually used in calculations. However, the mean is also time dependent. Therefore, a one-hour average wind speed may be 14 m/s while the same wind has 38 m/s as a minute average.

Today, the most correct procedure to determine a buildings response to time-varying wind is through wind tunnel testing. The results obtained from such experiments are close to what the structure will experience when constructed. Wind tunnel testing is a tedious experiment and sufficient wind data, over short time intervals, are needed. Many wind codes do not provide values for the short period wind speeds, which in most cases are governing. Consequently, simplified assumptions have to be made. For tall buildings it is necessary to conduct wind tunnel testing before actual construction. By using thresholds and requirements from National Codes it is possible to do conservative calculations of the wind response, a method that is sufficient for conceptual design stage of a project. For Norway, the Eurocode NS-EN 1991-1-4, CEN (2005), and corresponding National Annex provide the calculation

method for deflections and accelerations of a building under wind loading. In NS-EN 1991-1-4 the following serviceability requirement is stated; *'For serviceability assessments, the maximum along-wind displacement and the standard deviation of the characteristic along wind acceleration of the structure at height z should be used'*, CEN (Section 6.3.2, 2005). The code also provides the method of calculating the static wind forces on all the surfaces of the envelope structure.

4.2.2 Building Drift, Lateral Deflection and Displacements

Deflection is a governing issue for high-rise structures since the wind loads vary over the height and the total force is large due to a large surface area. Displacements will lead to an increase in local and global stresses in the structure, which again may lead to failure and occupant discomfort. However, design codes do not specify a limiting value for service limit state deflection at global level. Each element should be checked for ultimate limit state failure due to deflection. The former is mainly studied in the conceptual design, since the global response of the structure is of the most interest.

'For the performance of a structures resistance to horizontal displacement to be adequate, the peak inter-story drift must not exceed 1/300-1/500 of the story height under un-factored loads' is stated in an article by Amin and Ahuja (2010). The horizontal drift is determined by analyzing the first two bending modes of the building, the along-wind and the across-wind response. The torsional moment may also be governing for building drift, usually a higher order bending mode. The control of the inter-story drift is an indicator to check whether the stiffness of the building is adequate. When the buildings have alternations over the vertical height, the inter-story drift has a greater tendency to be governing. The total lateral displacement of the building has also limiting values depending upon national requirements. In the recent years, this limiting value has become a more used practice than inter-story drift for wind loads. The limit is the ratio between the lateral drift at the top story and the total height of the building (Amin and Ahuja, 2010).

The only serviceability criteria that is given in the National Standards for maximal deflection is *'defined for the individual project'*, CEN (Table NA.A1(904), 2002). Consequently, there is no general limiting value for the maximum deflection. A design requirement for the structure must thus be set from considering previous projects and the structural engineering field's preferred threshold.

In the doctoral dissertation by Honfi (2013), 20 key personnel in the community at Lund University in Sweden were interviewed to determine the recommended value of maximum deflection. The value were for buildings designed with reinforced concrete, steel and timber. The result of the interviews are shown in Table 4.1. In the table the loading G refers to permanent loads, and Q refers to variable loads.

Type of answer	Deflection limit
General limit	L/400 L/200- L/300
Different limits with different load combinations	L/400(G+Q) L/300(G+Q) L/600(Q); L/600(G); L/300(G+Q)
Different limits based on building importance	L/400 for public buildings, big contractors L/300 for less important buildings, small contractors
Different limits for different materials	steel: L/250 to L/600 concrete beams: L/500 timber: L/450 to L/600

Table 4.1: Recommended values for maximum deflection form doctoral dissertation (Honfi, 2013)

As Table 4.1 illustrates, the preferred limiting value of maximum deflection varies upon person to person. When a structure has alterations on the general shape and it is considered as unique and untraditional, it is desired to be on the safe side. This ensures safety of the structure. Consequently, since the structure for the aim of this thesis has never been built before, it is desired to be conservative. The service limit state maximum deflection is set to $L/500$. This value provides a conservative limit for all the different materials, as well it is lower than the recommended limit for public buildings. For a 122 meter tall building, this leads to the limit for maximum deflection being set to 0.244 m as shown in Equation 4.1.

$$\Delta_{max} = L/500 = 122 \text{ m}/500 = 0.244 \text{ m}. \quad (4.1)$$

4.2.3 Acceleration of Buildings

The acceleration of the wind is directional sensitive, and a limit is set to ensure occupant comfort under strong winds conditions. Tall buildings are subjected to wind excitations not only in a direction parallel to the wind but also in the perpendicular direction. The response from excitations is sway, where the accelerations is the resonant component of the dynamic response. The maximum acceleration may occur from the along-wind, across-wind or torsional vibration (Kwok et al., 2015). For tall slender buildings the governing acceleration is usually from the across-wind, which is problematic since National Codes only have calculation methods for determining the along-wind accelerations. Overall, the results that are calculated are approximate methods, and the results have a very low accuracy compared to wind tunnel testing.

The acceleration is usually measured in the peak value or the standard deviation. The peak value and the standard deviation, are taken as a value over a period of a few minutes up to a hour. The difference in these two values are however significant as Kwok et al. (2015) discusses in their book. The wind excitations create different waveforms or acceleration signatures. All are narrow banded with

the same frequency, therefore only the envelope form is varying. Consequently, the difference in the peak value may be significant for the same standard deviation. The wave form and duration has a great importance in the occupants comfort, and a basic peak value is often not sufficient. People generally tolerate vibrations over a short period only, and a short period between each vibration will lead to discomfort (Kwok et al., 2015).

For slender buildings with a high H/B-ratio, the buildings usually have a fundamental period of 3-8 seconds. This period commonly coincides with the monthly occurring vortex shedding, leading to oscillation if the structure is in-sufficiently designed with a low amount of dampers. In these cases, the coded procedure that uses the 1-10 year return-period wind is insufficient (Kwok et al., 2015).

Dynamic wind can be analyzed in the time or frequency domain. When analyzing in the time domain, the results will derive the exact solution. However, in the frequency domain the results only derive the peak resultant. The peak resultant is the square root of the sum of squares; SRSS. When the last method is used and the spectrum has peak values that do not coincide, the results obtained are highly conservative (Kwok et al., 2015).

Using the NS-EN 1991-1-4 it is possible to calculate the peak acceleration in the frequency domain (CEN, 2005). The method calculates the standard deviation of the acceleration which is then multiplied by a top factor. However, NS-EN 1991-1-4 does not address the limiting values for the accelerations. These limits need to be found in the ISO Standards. There are two different alternatives for finding the threshold values for the acceleration, both alternatives require to re-calculate the acceleration retrieved from NS-EN 1991-1-4. Alternative one is to use ISO 10137. It has a limiting acceleration value depending on the natural frequency and the usage of the building. However, the limiting value is set for a 1 year return period acceleration, while the National Standard NS-EN 1991-1-4 calculates a 50 year return period acceleration. The second alternative is to use ISO 2631-1 and ISO 2631-2 to calculate and compare a frequency weighted acceleration. The latter is considered as a more conservative approach since the limiting value is lower than for the method using ISO 10137. To be able to use the latter approach, the fundamental frequency needs to be larger than 1 Hz.

4.3 Torsional Moment

Torsion is considered as the third component of the building motion. It occurs when there is an imbalance between each faces instantaneous pressure distribution. The structure then tends to rotate around the center of resistance, creating torsional moments. Since the moment is a product of the distance from the stiffness center, the moment and rotation varies over the plan section. Consequently, the largest torsional moment is furthest from the center of resistance (Amin and Ahuja, 2010).

When calculating the torsional moment it is necessary to use the 10-minute reference wind speed. The wind pressure is then calculated by considering a triangular wind pressure acting on the facades. The results of torsional moment are then represented through shear force and the equivalent eccentricity. The method for calculating torsional moment is given in Eurocode NS-EN 1991-1-4.

4.4 Seismic Considerations

Earthquake engineering deals with the effects of earthquakes on people and their environment. When an earthquake occurs, body waves and surface waves are produced. Three characteristics of the ground motion are important in earthquake engineering (Yu, 2016).

1. Peak ground shaking, such as peak ground acceleration (PGA). Will influence the vibration amplitude and is used to design the earthquake design spectra and acceleration time histories.
2. Duration of strong ground shaking. The severity of earthquake motion is highly affected by the duration of the strong motions. If the PGA is large but over a very short period of time, it is unlikely to inflict and cause damage to structures.
3. Frequency content. The frequency of the ground motion will cause severe damages if it is inflicted and close to the natural frequency of the structure. Oscillation may then occur, and stability of the structure is highly reduced.

It is necessary to design the building against earthquake motions, and to do this through dynamic analysis. For dynamic analysis it is possible to not only get the magnitude of loadings and stiffness of the elements; but also the frequency characteristics of loads, and the dynamic properties of the structure. A building has natural damping force through the different elements material stiffness and elasticity. It dissipates the energy in the system through friction at connections and material damping such as cracks in concrete (Yu, 2016).

Eurocode NS-EN 1998-1 and National Annex are mainly used as calculation methods in Norway. It is then necessary to take into account the site's response to the ground movement. Soil usually has larger damping than bedrock, and damping has a greater effect on the high-frequency components of the ground motion. Therefore, for certain soil profiles it leads to de-amplification of the high-frequency waves, and amplification of the lower-frequency waves. This is undesired for buildings, which are prone to the lower frequencies. Thus, it is ideal to have a building situated on a site that has bedrock as close as possible to the building's ground level (Yu, 2016). For buildings that have an height larger than 73 meters, it is necessary to use dynamic procedures in earthquake calculations (Mwafy et al., 2006).

For seismic activity the main concern is structural failure and human discomfort under earthquake conditions. In NS-EN 1990, the design values for seismic load combinations are given in CEN (Table A1.3, 2002). The load participation factors for seismic conditions are equal to 1.0 under ULS conditions and thus, it is possible to analyze both the ultimate limit state and service limit state with the same load combination equations. Serviceability limits are given in the percentage inter-story building drift (Dymiotis-Wellington and Vlachaki, 2004).

4.4.1 Fundamental Modes and Fundamental Frequencies

When a structure is subjected to an impulse force, the building is set into motion. The behavior of the building motion is influenced by the mass and stiffness of each story. When subjected to a force, the structure moves with a behavior equal to the least resisting sway-motion. For tall slender buildings, it is common to obtain high fundamental periods, and consequently, low fundamental frequencies. With high periods, the motion-sway is slow but with large deflections. Under loading, the building will have forced motion; and after, the building will continue to move until the damping of the system resists the motion all together (Yu, 2016).

Fundamental modes are the shapes of the building under motion. For a sufficiently stiff high-rise the first and second fundamental modes are the most governing; being cantilever like displacement in x- or y-direction. The third mode is commonly torsional rotation about the center of rigidity.

A general rule of thumb is that the natural period is equal to $T = \frac{\text{number of stories}}{10}$ (Yu, 2016). The building is of 31-stories; when including the roof as a story, leading to a period of 3.1 seconds. Seismic activity generates wave propagation with a much lower period. Consequently, oscillation due to earthquake loading will not occur for this structure.

4.4.2 Response Spectrum and Time History Analysis

There are different methods to calculate the buildings motion due to seismic activity. The results vary with what method is used, some are highly conservative while others may be inaccurate. The response spectrum is a plot of the peak value of a response quantity, as a function of the natural vibration period, T_n , of the system or the natural vibration frequency, f_n . The most common response spectrum is for acceleration (Yu, 2016). The results gained from these spectrums are the pseudo-spectral acceleration for each of the structure's modes under earthquake vibration.

Seismic input to nonlinear dynamic analysis of structures are commonly defined in terms of acceleration. This results in time-history functions, varying in time,

where the response spectrum is compatible to specified target response spectrums. Time-history functions give the response of the structure during and after loading. It is most common to define the target spectrum in either time or frequency domain. The frequency content of the ground motion is related to the magnitude, as the higher frequency components of the spectrum attenuate; decrease in seismic energy, more rapidly (Yu, 2016). For tall buildings that have irregularities, an earthquakes motion is in a larger extent comparable to the time-history functions than the response spectrum. This is the case since the time-history analysis is a function of time, and due to site specific considerations (Mwafy et al., 2006). For high-rise structures these parameters are more governing than for lower buildings.

A Calculation Method Used in NS-EN 1998-1

When calculating the response to seismic activity, it is necessary to use values of the ground acceleration for that specific site. The only method to do this for Oslo, Norway, is through NS-EN 1998-1. It is possible to create a horizontal and a vertical elastic response spectrum from the ground conditions at the local site and the characteristic value of the seismic action at that site. *'The reference peak ground acceleration chosen by the National Annex, corresponds to the reference return period T_{NCR} of the seismic action for the no-collapse requirement'* as stated in CEN (Section 3.2.1(3), 2009). Since the load combinations used for seismic response are the same for ultimate limit state and service limit state, the elastic response spectrum will be equivalent for both cases.

4.4.3 Inter-Story Drift

Inter-story drift limits are suitable to determine a buildings serviceability under seismic actions. Total structural deflection is not an ideal limiting value since the mode shapes for the building are not only creating horizontal displacements. Inter-story drift is a method of determining the horizontal displacement for one story compared to the under-laying story. Limitations are usually given in percentage values. In Norway there is no general limiting value, and it is necessary to determine the design limiting inter-story drift percentage for this project. Table 4.2 compares different limiting values.

Reference	Limiting inter-story drift in %	Determination of value
Beretero et al. (1991)	0.06 – 0.6	Range of limit from Eurocode 1998-1
Beretero et al. (1991)	0.3	Field observations
Saito et al. (1996)	0.5	SLS criteria for member yielding
Ghobarah et al. (1997)	0.7	Elastic limit state critical value
Esteva et al. (2002)	0.3	Recommended value for 10 year return period seismic activity

Table 4.2: Critical inter-story drift values for SLS

Summarizing Table 4.2, it is possible to set the inter-story drift to 0.3%. This can be seen as a conservative value.

4.4.4 Overturning Moment

The building motion will lead to displacements and forces that again will lead to overturning moments. The stiffest members of the structure will have the largest overturning moment, that decreases with increasing vertical height. The magnitude of the seismic force is directly related to the magnitude of the base overturning moment and base shear. When considering different geometries it is thus, necessary to compare the values of the overturning moment for each alternative.

5.1 Property Location

It is necessary to determine the location of the building to be able to achieve the correct calculations for the wind and seismic loads. The forces will be factored by the geometry and vertical shape of the building, which again is restricted to a site boundary. Oslo is a city that is currently under major construction changes, therefore finding a property that fulfills all the desired credentials is a challenge.

Desired factors for the sought after property.

- Daylight for the tall building, but maintaining sunlight for adjacent buildings.
- Access to public transportation.
- Access to surrounding nature; parks, forest, ocean.
- Lucrative space for residential and office space.
- Lucrative property as a tourist attraction and possibility of stores and restaurants in the complex.
- Parks and other green areas shall remain untouched.

The main construction and development projects in Oslo are currently in an area called Bjørvika. This is situated along the coast, with an ideal location for public transportation and nature. As a result, it was desired to find a property in this area. Nonetheless, when overviewing the regulation plan, it is clear that all the possible sites surrounding the projects that are in the construction stage, are part of later phases in this project. It was therefore required to consider other properties instead.

The desire is to build a mixed-use high-rise. The main difficulty is to find a property that can serve for an office space and for apartments. Office spaces desire easy access to public transportation and a location close to other office buildings. Residential spaces on the other hand, wish to be in an area sheltered from noise, close to the outdoors and nature, in quite surroundings. The nature aspect is especially important to Norwegians, who desire the unique combination of nature and wildlife while also living in a concrete jungle.

When considering other areas than Bjørvika in Oslo, it is natural to look at the

areas in close distance to the main public commute stations; National Theater, Oslo Central Station and Majorstua Station. These are all located in lucrative areas that have green spaces in a close proximity.

The National Theater is close to the Royal Castle, the main shopping street in Oslo, office buildings and apartments. The Royal Castle is also situated with a surrounding park, and consequently this area meets the requirements. In a close distance one also finds Aker Brygge and Tjuvholmen, areas that have been completely renovated at the start of the 21st century. These locations are ideal, but there is no available space in this area. When overviewing possible locations where existing buildings are located, considering demolition of the current buildings, the governing issue is the daylight restrictions a tall building would yield on the surroundings. Due to the currently strict high-rise policies in Oslo, it is highly unlikely that a high-rise that prevents daylight reaching historically old buildings, would be approved.

Majorstua Station has an excellent park, Vigelands park, right next to it and also easy access to the forest. There is a great amount of other business buildings in the area. However, when viewing the map, it was clear that the road map and adjacent buildings in the area prohibit a development of the desired building or building complex. The infrastructure here is also less attractive than for the two other stations. Also, since the location is in a significant distance from the newly developed areas Tjuvholmen and Bjørvika, the site is not as lucrative.



Figure 5.1: Overview of the development in Bjørvika (Plan- og bygningsetaten, 2016)

Oslo Central Station is located next to the ongoing project in Bjørvika. This project covers the main coast of the city center. The project includes monumental buildings such as the Opera House, Munch Museum and Deichmanske Main Library, as well as a large complexes for housing and offices. An overview of the area is shown in Figure 5.1.

As Figure 5.1 illustrates, the new development is highly modern and the buildings have a large focus on sustainable design. These structures have roof gardens, public spaces, low energy consumption design and irregular 21st century architectonic expressions. The central station is located on the periphery of the project site. Consequently, the access to public transportation is ideal.

Due to the project development in Bjørvika, the surrounding area is undergoing a great increase in popularity. The area that catches one's interest is on the leeward side of Ekeberg Hill. The area is located next to historical sights from the Viking Age in Norway, while also being next to Bjørvika. Ekeberg Hill is also an excellent neighborhood for nature walks. The location will have the green surroundings as well as a view towards the fjord. To this current day, the area around Mosseveien is under-developed by having low-cost housing. For this reason, it can be seen as a site with an un-used potential. The properties in this area are only a 10-minute walk from the offices and residential apartments at Bjørvika, and therefore it is a lucrative area for restaurants and possibly stores. It is most likely necessary to have a property with a certain distance from the hill itself, to achieve the desired daylight from the south-east direction.



Figure 5.2: Overview of the desired property (Kartverket, 2017)

The governing negative aspect of this sight is the public transport vessel that is located between the sight and the coastline. Even though it is not on the current governmental agenda, it is believed that this vessel will undergo an upgrade in just a few years. The Bjørvika-plan has gotten consensus in most of the regulatory changes in this area, and the plan requires that the railway system is constructed underground within 10 years (Jernbaneverket, 2012). Thus, it is highly likely that the

railway will be constructed in a tunnel as described in the regulation plan established by Asplan Viak and Jernbaneverket, now called Bane NOR (Jernbaneverket, 2012). The desired site for the high-rise is shown in the map in Figure 5.2. As seen in the Figure 5.2, the area of the property is approximately $3000 m^2$.

5.2 Shading Considerations for Buildings Location

The Norwegian Government has made clear restrictions on maximum building height in Oslo. This is mainly due to the amount of shading from tall buildings situated far on the northern hemisphere. To be able to achieve a lucrative concept, it is necessary to place buildings such that they do not cast shadows over the existing surroundings.

The sun will travel from the east to the west, but mainly appear in the south. Shading will thus appear behind the northern facade, but also north-west in the mornings, and north-east in the afternoons. It is desired to place the building such that the shading is mainly covering the roads and not existing buildings or green areas. If the building has an irregular plan geometry the shading may be controlled in a larger extent, by having less surface area on the northern facade. On the other hand, it is desired to have a large surface area against the south; both due to the sun path and also due to the view in this direction. These two aspects are contradiction since a large southern facade creates a large shading area behind the northern facade. When considering the site location shown in Figure 5.2, showing the property in a shaded blue, it is ideal to place the building furthest to the east. This will lead to the roundabout and intersecting roads being exposed to shade and not the existing buildings. The shape of the building is less important in the shading aspect since the distances to the nearest buildings are considerable for this placement.

5.3 Options for the Shape and Plan Geometry

Traditionally the skyscraper was a rectangle structure that was symmetric over the height. During these past decades the shape and form has changed dramatically to favor geometries that enable resistance against wind forces in a greater extent. This has led to buildings with rotations, twists, openings, and abnormal geometry over the height (Pignataro et al., 2014). By numerical software methods the shapes and geometries can be optimized to account for location specified loads. In places where typhoons, earthquakes and winds are an issue, software can optimize the geometry to have the ideal combination of stiffness against the wind loading, while maintaining flexibility for earthquake loads.

To achieve a basic geometry for the building, it was necessary to conduct wind analysis for various geometries. Ideally, one can create a three dimensional model with a load-bearing system that is changeable. However, when using the desired software program Revit, this was impossible. It was necessary to have a static envelope to be able to conduct load tests. Consequently, another program was used to achieve the envelope geometry. This was done by using Rhinoceros and Grasshopper to design the geometries, and then implementing these into Autodesk Flow Design. Autodesk Flow Design is a computational program that conducts basic wind tunnel tests. This program calculates the drag forces; when applying uniform three dimensional wind loading. By doing this, different plan geometries can be compared and it is possible to construct an envelope that is designed for wind loads.

5.3.1 Drag Coefficients and Drag Forces for Different Geometries

The software program Autodesk Flow Design only takes into account the given mean wind speed and performs a primitive wind tunnel test. Gust winds and the other components of the time varying wind is not taken into account. Thus, this program was used to conclude on which geometrical shapes were best suited for minimizing the drag forces and thereby, the drag coefficients. Drag forces are the along-wind forces, which act in the direction of the mean wind.

As explained in the book by Simiu and Scanlan (1996), the turbulent component can enhance the flow entrainment in the wake, thus, cause stronger suction and larger drag forces. On the other hand, if the B/H-ratio is sufficiently large, the turbulence can cause flow reattachment which would not have occurred in uniform flow. This again will lead to lower drag forces. However, since the building is tall and lean, it is not likely that the B/H-ratio will be large enough to reduce the drag forces. Consequently, the resulting forces from the Autodesk Flow Design will be further enhanced by the turbulent wind forces.

The wind pressure that is applied on the building surfaces will result in net forces and moments. The forces in the structure due to the along-wind, will lead to drag forces, while the across-wind forces will lead to lifting forces (Simiu and Scanlan, 1996). The drag, lift and moment are affected by the shape of the body and the Reynolds number. The Reynolds number takes into account the surface texture and roughness of the shape. To simplify the analysis, all the different shapes that were studied had a smooth surface, although, in reality the surface is not smooth.

The goal was to achieve a structure that had as low as possible wind pressure acting on the surface. The surface facing the wind direction will experience positive pressure, while the other sides will in most cases experience negative pressures. The leeward surface will have a wake that is dependent on the geometry. The wake

causes disturbances, vortices, and wind flow that is circular in-plane and vertically.

The results that are shown in the program Autodesk Flow Design are the drag forces and the drag coefficients. The net wind pressure is often described in a dimensionless value known as the drag coefficient, C_D . This value takes into account the wind speed, direction, surface area, shape, Reynolds number, Froude number and Mach number (Simiu and Scanlan, 1996). The drag coefficient is a reorganization of the drag forces, F_D , as shown in Equation 5.1.

$$C_D = \frac{F_D}{0.5 \times \rho \times U^2 \times B} \quad (5.1)$$

5.3.2 Deciding on the H/B-Ratio

To be able to compare the results in an efficient way, it was decided to construct shapes that all had a height of 120 meters. This is an ideal height since the other tall buildings in Oslo are around this height; with Plaza Hotel at 117 meters and Post House at 111 meters.

When deciding on the width, the H/B-ratio needs to be considered. If the value is larger than six, up to ten special features are needed to improve the wind comfort (Bing, 2016). If the height-to-width ratio should be lower than six, it is necessary to have a width that is larger than 20.33 meters. If one considers a width of 20 meters in a circle, this creates a plan with an areal of 400 square meters. Consequently, plan geometry with a total area of around 400 meters was designed in Rhinoceros and then transferred to Autodesk Flow Design for software wind tunnel analysis.

The shapes and areas that were studied in Autodesk Flow Design.

1. Circle: $A = \pi \times r^2 = \pi \times 12^2 = 452 \text{ m}^2$
2. Ellipse: $A = \pi \times r_1 \times r_2 = \pi \times 7 \times 18 = 396 \text{ m}^2$
3. Square: $A = B^2 = 20^2 = 400 \text{ m}^2$
4. Rectangle: $A = B \times L = 18 \times 22 = 396 \text{ m}^2$
5. Hexagon: $A = 6 \times 6 \times 6 \times \sqrt{3} = 375 \text{ m}^2$
6. Octagon: $A = n \times r^2 \times \tan(\pi/n) = 8 \times 12^2 \times \tan(\pi/8) = 477 \text{ m}^2$
7. Triangle: $A = 2 \times 20 \times 20/2 = 400 \text{ m}^2$

5.4 Results from Autodesk Flow Design

The main results from the drag coefficients and drag forces were compared. However, the analysis also displayed how the uniform wind affected the structure over time. The results showed that the different shapes gave substantial differences in amount of vortices, speed of the resulting wind forces from the created turbulent components, and also pressure forces on the exterior facades. However, this components were

only represented by illustrations and not numerical values, and results could not be obtained.

The values of the drag forces and drag coefficients are highly affected by the angle and which surface is on the windward side, perpendicular to the wind. Consequently, it was necessary to run the wind tunnel testing at different angles of the structure. The wind can appear theoretically in all directions and is never only from one direction. The results are shown in Table 5.1 and Table 5.2.

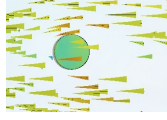

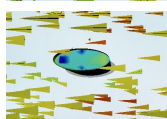
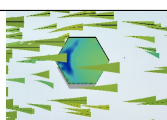
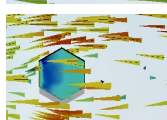
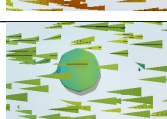
Plan geometry	Illustration of wind direction on shape	Drag coeff.	Drag force
Circular		0.68	113 <i>kN</i>
Ellipse		1.64	409 <i>kN</i>
Ellipse		0.79	80 <i>kN</i>
Hexagonal		1.02	150 <i>kN</i>
Hexagonal		0.67	160 <i>kN</i>
Octagonal		0.92	150 <i>kN</i>

Table 5.1: Results from Autodesk Flow Design for various shapes, part 1


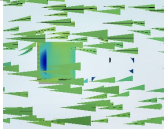
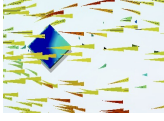
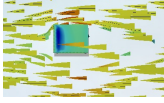
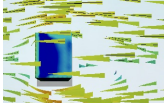
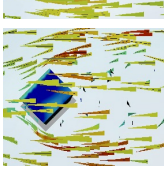
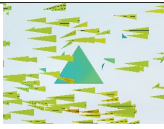
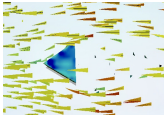
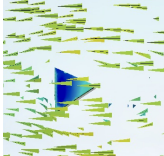
Plan geometry	Illustration of wind direction on shape	Drag coeff.	Drag force
Octagonal		0.97	140 <i>kN</i>
Square		1.28	180 <i>kN</i>
Square		1.39	272 <i>kN</i>
Rectangle		1.13	143.5 <i>kN</i>
Rectangle		1.38	211.6 <i>kN</i>
Rectangle		1.51	296 <i>kN</i>
Triangle		1.07	240 <i>kN</i>
Triangle		1.45	252 <i>kN</i>
Triangle		1.60	327 <i>kN</i>

Table 5.2: Results from Autodesk Flow Design for various shapes, part 2

From the results of the wind tunnel testing it is clear that sharp corners are highly unfavorable, since these shapes lead to high drag forces and high drag coefficients. The circle had the most favorable geometry, second was the octagon with smoothed corners. This is logical since there is limited difference between these two shapes. The triangle, square and rectangle showed highly unfavorable results. Consequently, these shapes are not used in further analysis. Further computation was therefore conducted with a circle, ellipse shape, hexagonal shape and octagonal shape. The ellipse shape was included even though the results were not promising, but this was due to the large difference between the two radii. The difference in the results between the hexagon with six edges and the octagon with eight edges is largest when the wind is applied on the corner. The wind is then forced onto the interacting sides, leading to a higher value for the hexagon shape, since the total windward surface area is larger.

CHAPTER 6

DETERMINING THE GEOMETRY

In this chapter the software programs Rhinoceros and Ladybug has been used to illustrate how the sun path and wind directions influence the placement and geometry of the structure. In Ladybug it is possible to upload weather data from different cities all around the world. Here, Fornebu which is situated in Oslo, Norway, has a record of weather data for a ten year period. This file can be uploaded from the internet site EnergyPlus (U.S. Department of Energy's Building Technologies Office, 1991). The hourly wind speed, temperature, wind direction, sun path, humidity, and other parameters are given in this file. Hence, it is possible to compute and study how the given weather data may influence the geometry and placement of the building. The geometrical shapes were also analyzed in Autodesk Flow Design, testing the shapes in a primitive wind tunnel test. Therefore, it is possible to compare the wind tunnel analysis results with the results from Rhinoceros and Ladybug. Consequently, an optimal rotation, geometry and placement of the building can be achieved by comparing the results from wind test to wind directions, temperature, and other factors from Ladybug and Rhinoceros.

6.1 Governing Wind Directions

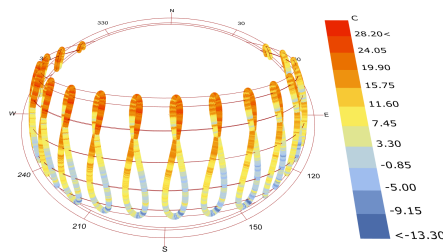


Figure 6.1: The solar path over the year in Oslo

It is desired to have a large southward facing facade, such that solar lighting is substantial even in the winter months. It is also worth mentioning that the southward direction is the one with the most prominent view, a large facade on this side is therefore desired for both apartments and offices. Using Rhinoceros and

Ladybug it possible to to construct a sun path over the annual period. From this diagram, shown in Figure 6.1, it is clear that the sun is governing in the southward direction.

However, it is also necessary to take into account the direction of the wind. Usually there is a dominant wind direction, especially for crucial wind speeds. Using Rhinoceros and Ladybug it possible to to construct a wind rose using variable parameter inputs. From an architectural standpoint it interesting to observe which direction is best suited for natural ventilation. Parameters that are of interest are then the temperature and wind speed. Natural ventilation can only be beneficial when the air is hot enough and the wind is substantial. Thus, when restricting the temperature to be above 16 degrees and the wind speed to more than 1 m/s, the wind rose is illustrating the possible natural ventilation directions.

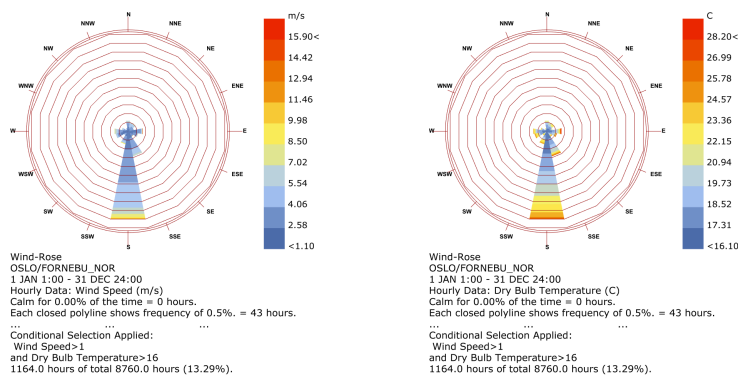


Figure 6.2: The wind rose for Oslo when temperature is over 16 degrees and wind speed is larger than 1 m/s

The results, shown in Figure 6.2, show that the warm wind is governing from the southward direction. This is the same direction as the sun. Therefore, this facade should have components for natural ventilation and a facade that can benefit from the sun and warm wind. It is also clear for Figure 6.2 that the wind is dominantly under 4 m/s, being a breeze that is beneficial for ventilation.

In the winter months it is necessary to have a significant amount of insulation in the dominant wind direction. When changing the wind rose to cover the cold wind that has a temperature lower than 0 degrees, and also a wind speed larger than 1 m/s, the resulting wind rose is of interest.

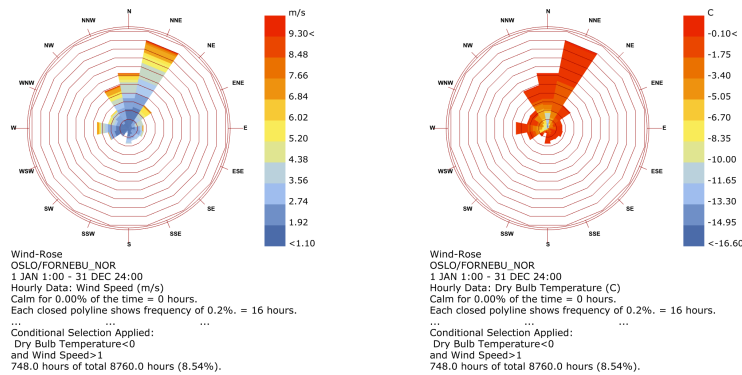


Figure 6.3: The wind rose for Oslo when temperature is under 0 degrees and wind speed is larger than 1 m/s

From Figure 6.3, it is clear that the cold wind comes dominantly from the north and north-east direction. Thus, the northward facing facade should have a different construction that is more insulating than the other facades. The temperature of the wind is mainly around freezing, but it is clear that the wind has a higher wind speed in the winter months than for the summer months. Consequently, the wind forces upon the structure will be larger in this direction than those from the south in the summer.

6.1.1 Influence on the Geometry

Since this building is designed for a mixed-use for both residential and office floors, it is desired to have a shape that is suited for these purposes. The results from the sun path and wind rose analysis retrieved in Rhinoceros and Ladybug show that it is desired to have a structure that is largely facing the south. This favors the ellipse and hexagonal shapes in a larger extend then the circle and the octagon. However, having a large facade in the wind direction leads to a large surface area that undergoes wind pressure, thus increasing the loading on the structure. To achieve a minimal amount of forces one wishes to have a structure that has minimal drag forces in the dominant wind directions. These two factors are contradicting, and consequently it is necessary to decide which is governing.

When comparing the surface area of the north with the drag forces, it is clear that the ellipse shape with the wind on the elongated side is highly unfavorable. This is due to the forces the wind will conduct on the structure. The hexagonal shape is the shape that has the second to largest area facing the southward direction. By having an orientation such that the wind will be perpendicular to one of the six faces, this geometry is favorable. However, twisting along the vertical axis may lead to a disadvantageous surface pressure on the structure. The circular shape will be

the shape with the lowest surface area towards the south facade, but it is an ideal shape for the wind pressure. Twisting and other vertical geometrical changes will most likely not affect the amount of drag force on a circular structure.

Concluding, it is most likely that the hexagonal shape or the circular shape is the most favorable. An intermediate may be even more beneficial, leading to an octagon with smooth edges. For this reason the circular, hexagonal, octagonal and elliptical shapes are studied in a further degree, while the rectangular and triangular shapes are rejected.

6.2 Additional Changes to the Geometry

When deciding on the most effective geometry for the building by using results from Autodesk Flow Design, the two governing aspects are the drag forces and the surface area in the north and north-east direction. It is necessary to consider modifications to the geometry to reduce both the drag force and the surface area towards the north.

The alterations that were focused on.

- Twisting of the structure 45 degrees.
- Twisting of the structure 90 degrees.
- Tapering over 2 meter in radius over the height.
- Soft corners of a 5 meter radius.

The four remaining plan geometries; the hexagon, octagon, circular and ellipse, underwent these changes. Then they were analyzed in the wind tunnel test in Autodesk Flow Design.

Plan geometry	Original shape	Twisting 45 degrees	Twisting 90 degrees	Tapering	Soft corners
Circular	$C_D = 0.68$ $F_D = 113kN$	$C_D = 0.68$ $F_D = 113kN$	$C_D = 0.68$ $F_D = 113kN$	$C_D = 0.84$ $F_D = 129kN$	$C_D = 0.68$ $F_D = 113kN$
Ellipse: short side	$C_D = 0.79$ $F_D = 77kN$	$C_D = 0.62$ $F_D = 84kN$	$C_D = 1.0$ $F_D = 179kN$	$C_D = 0.45$ $F_D = 2.0kN$	$C_D = 0.79$ $F_D = 77kN$
Ellipse: long side	$C_D = 1.64$ $F_D = 411kN$	$C_D = 1.12$ $F_D = 252kN$	$C_D = 1.17$ $F_D = 210kN$	$C_D = 1.21$ $F_D = 160kN$	$C_D = 1.64$ $F_D = 411kN$
Hexagonal: corner	$C_D = 1.02$ $F_D = 148kN$	$C_D = 0.73$ $F_D = 113kN$	$C_D = 0.96$ $F_D = 156kN$	$C_D = 0.97$ $F_D = 127kN$	$C_D = 0.91$ $F_D = 132kN$
Hexagonal: flat side	$C_D = 0.68$ $F_D = 114kN$	$C_D = 0.84$ $F_D = 133kN$	$C_D = 0.91$ $F_D = 144kN$	$C_D = 0.87$ $F_D = 132kN$	$C_D = 0.72$ $F_D = 111kN$
Octagonal: corner	$C_D = 0.92$ $F_D = 153kN$	$C_D = 0.76$ $F_D = 124kN$	$C_D = 0.82$ $F_D = 134kN$	$C_D = 0.88$ $F_D = 138kN$	$C_D = 0.64$ $F_D = 104kN$
Octagonal: flat side	$C_D = 0.97$ $F_D = 150kN$	$C_D = 0.85$ $F_D = 136kN$	$C_D = 0.87$ $F_D = 140kN$	$C_D = 0.94$ $F_D = 132kN$	$C_D = 0.89$ $F_D = 138kN$

Table 6.1: Results From Autodesk Flow Design for Geometrical Alterations, part 1

The results shown in Table 6.1 illustrate how the modifications change the drag forces imposed on the structures. From the table it is clear that twisting the structure vertically 45 degrees is highly more favorable than 90 degrees. It is also possible to conclude that adding soft corners to the hexagon and octagon will lead to a lower drag forces. The results show that the elliptical shape is unfavorable, with larger drag coefficients and drag forces than the other shapes.

It is important to emphasize that the wind in the wind tunnel test performed by Autodesk Flow Design is uniform. Thus, the wind profile is uniform over the height. In reality, this is not the case. The wind increases with height, until reaching a boundary layer where it then becomes uniform. This leads to the wind forces being larger at the top than at ground level.

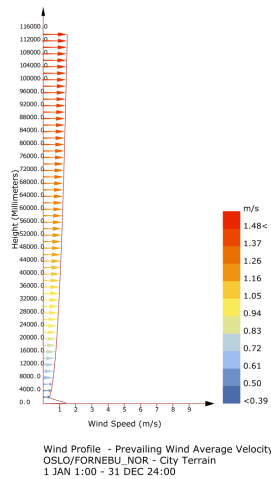


Figure 6.4: The 10-year mean wind profile for hourly wind speed over the height, in Oslo

Figure 6.4 shows how the hourly mean wind profile varies with the height. This is the mean wind over a 10 year recorded period. It is worth mentioning that this value cannot be compared to the 50 year return period wind that is calculated using the Eurocodes, as shown in Appendix A. However, since the Autodesk Flow Design model illustrate wind forces from a uniform wind profile, while in reality is is parabolic, the results from the analysis are conservative and with errors. It is clear that since the actual wind force increases with height, the beneficial effect of tapering would be greater that the results from Autodesk Flow Design. Also, it is in a larger degree necessary to have the most beneficial geometry towards the top.

The shapes were further altered to include multiple modifications; 45 degree twisting vertically, roundness of corners, and tapering. The shapes that were analyzed were the octagon, hexagon and the circular shapes. The results from Autodesk Flow

Design resulted in less beneficial drag coefficients and drag forces, than for only one alteration. Therefore, from a drag force standpoint it is not ideal to apply multiple alterations to the original geometry. The vertical modifications may have resulted in the mesh not working as effectively and correctly as for the uniform geometries. Thus, the results from this analysis are inconclusive. On the other hand, the wind is a dynamic force where the drag force is not considered as the governing issue for tall buildings. From a vortex shedding perspective, theories conclude that these changes will lead to more favorable geometries under wind induced loading.

6.3 Plan Section and Structural Bearing

When deciding on the conceptual design, it is necessary to consider which shapes are the most beneficial for subdivision of the plan geometry. The plan geometry should be suited for both apartments and offices. It is desired to have load-bearing columns and walls that separate the apartments. It is simpler to divide a plan section with corners and straight facades than one with a curved facade. Problems arise when one desires to achieve an optimal subdivision of a plan structure when the entire facade is curved. This shape is especially unsuited for bedrooms, bathrooms and kitchen where it is ideal to have straight walls. As a result, the circular shape was seen as undesirable.

Secondly, it is vital to examine how the load-bearing components will transfer loads for the various geometries. When having hexagonal and octagonal shapes with sharp corners, it is possible to have load-bearing columns at these corners. Tapering and twisting is more complex for load-bearing components. This will lead to it being problematic for optimal load transfer between the stories. Tapering will result in the columns not being placed vertically aligned, a highly unideal situation for a tall building. Twisting the structure will result in the same challenges. Even so, both of these alterations are widely used for tall buildings and thus, it should be possible to implement these alterations beneficially.

CHAPTER 7

IMPLEMENTATION OF THE STRUCTURAL ASPECTS

It is desired to design a building that has a enveloping glass facade with glue laminated timber elements surrounding the main structure. This will result in an aesthetically unique exterior. With this layout, it is possible to create a static core building, and add the alterations mainly to the envelope structure. On that account, this chapter focuses on the structural aspects of the static structure and how to optimize the building against the exterior wind loads. To do this, calculations for the wind components are needed and then to implement these into the stability calculations. Since the site has been determined, it is also possible to design the elastic response spectrum, taking into account the seismic considerations. The polygonal shapes are further investigated, while the other fundamental geometries showed unfavorable results in Chapter 6.

7.1 Achieving a Suitable Load-Bearing Structure

It is essential to achieve a load-bearing structure that has columns placed conveniently for load transfer. This is problematic when twisting and tapering modifications are added to the shapes. A service core placed near the center of the plan section will not be altered by tapering or twisting of the structure envelope. For this reason, service cores close to the center of the plan section are desired. Contradicting, when designing to resist torsional moment, it is optimal to have shear walls far away from the center of mass.

7.2 Wind Loads on the Structure

Since the site has been chosen, it is possible to calculate the 10-minute mean wind speed for a 50 year return period wind load using NS-EN 1991-1-4, as shown in Figure 7.1. The detailed results for these calculations are shown in Appendix A.



Figure 7.1: Mean wind speed, $v_m(z)$

The results shown in Figure 7.1, show that the mean wind speed differs for the summer and winter months, with the forces being larger in the winter months.

To find the wind forces acting on the structure, it is necessary to determine the peak pressure, $q_p(z)$, and the turbulence intensity, $I_v(z)$. The fluctuating components of the wind are then taken into account. The wind forces that the exterior surfaces were exposed to were computed by using two different methods. Alternative one, was to subdivide the envelope surface into segments using CEN (Figure 7.5, 7.6; and Eq. (5.3), 2005). The final equation, calculating the wind force, for method one, is shown in Equation 7.1.

$$F_w = c_s c_d c_{pe,10} q_p(z_e) A_{ref} \quad (7.1)$$

The second alternative is to calculate a resulting force for the whole structure, taking the geometry into larger considerations by using Equation 7.2, from CEN (Eq. (5.4), 2005).

$$F_w = c_s c_d \times \sum_{elements} c_f q_p z_e A_{ref} \quad (7.2)$$

From the results and figures it is clear that the first method, Equation 7.1, is the most used and accepted method.

7.2.1 Torsional Moment

From the wind force calculated by method one; Equation 7.1, calculations of the torsional effects have been computed. This is carried out by changing the wind force

to a triangular force distribution over the windward facade, as shown in Figure 7.2. The computed turbulence moment is shown in Figure 7.3. Detailed calculations and procedures are given in Appendix A. The turbulence generates overturning moment, increasing towards the base.

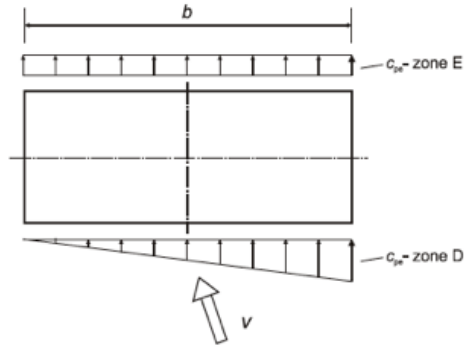


Figure 7.2: Wind force to calculate torsional moment, from CEN (Figure 7.1, 2005)

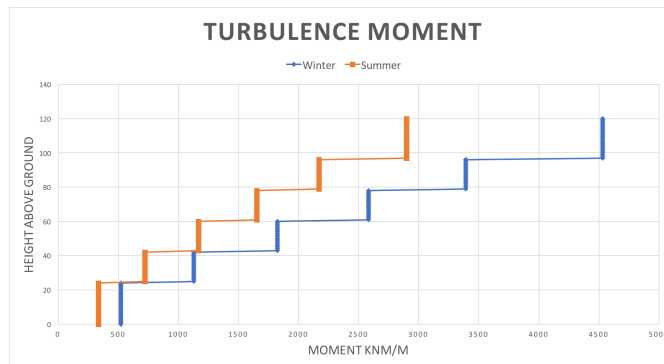


Figure 7.3: Overturning moment due to turbulence

Figure 7.3 indicates that the maximum overturning moment is approximately 4500 kNm/m for the upper stories, and segmentally decreasing towards the base. The stiffness of the core structure needs to resist the total torsional moment, by the stresses being lower than the material strength of the service cores.

7.3 Determining the Service Cores

The cores need to resist the total overturning moment from the torsional wind loads. Since there are additional load-bearing elements in the structure, it is not crucial that the stresses in the service core are well within the design strength.

It is decided to have two service cores; one for the elevator shafts and, another for an emergency staircase. The two cores are each in a distance of 2.75 meters from the center of the building. By having this configuration, it is possible to have an open atrium in the open space between the two service cores. The open atrium is a desired architectonic expression that can be implemented in the office stories. The core that has the elevator shafts, house two elevators, it is however possible to add an additional elevator if needed. The addition will also increase the stiffness of the structure. It is therefore conservative to only calculate with two elevator shafts.

7.3.1 Calculations of the Torsional Stresses in the Service Cores

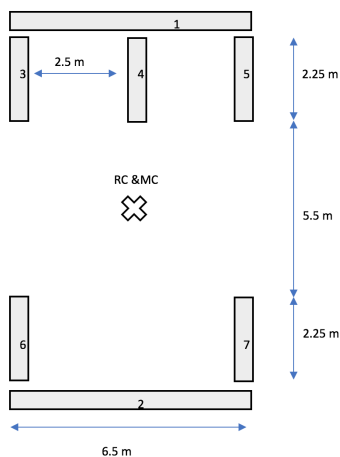


Figure 7.4: Illustration of the service core

For the calculations of the overturning moment, it was decided to do conservative calculations. Consequently, the cores are uncoupled and the walls with openings for the elevators and staircase are not included. In reality, the shear walls in the core are an intermediate between coupled and un-coupled. This meaning that the shear stress distribution is to a larger degree distributed over the entire system. A schematic representation of the service cores is shown in Figure 7.4.

Parameter	Equation or value
Thickness of all elements	$t = 0.5 \text{ m}$
Height of all elements	$H = 122 \text{ m}$
Width and length of structure	$B = 26.4 \text{ m}$
Length of each element, varies	L
Area	$A = t * L \text{ m}^2$
Second moment of inertia	$I = \frac{t * L^3}{12}$
Concrete E-modulus for B45-strength	$E = 36 \text{ MPa}$
Concrete design compressional strength, B45	$f_{cd} = 25 \text{ MPa}$
Bending stiffness	$K_b = \frac{3EI}{H^3}$
Shear stiffness	$K_s = \frac{EA}{3H}$
Total wall stiffness	$K = \frac{1}{\frac{1}{K_s} + \frac{1}{K_b}}$
Rotational stiffness x-coordinate	$x_t = 0.5B \times \frac{\sum K_{y,i} x_i}{\sum K_{y,i}}$
Rotational stiffness y-coordinate	$y_t = 0.5B \times \frac{\sum K_{x,i} y_i}{\sum K_{x,i}}$
Rotational stiffness	$K_{rot} = \sum ((x_i - x_t)^2 \times K_{y,dir} + (y_i - y_t)^2 \times K_{x,dir})$

Table 7.1: Equations and parameters used to calculate the stress due to torsion

Table 7.1 includes the governing strength parameters and equations needed for the calculations. All the walls are continuous through the entire height of 122 meters, and they all have a thickness of 0.5 meters.

Wall	Strong axis	L [m]	I [m ⁴]	A [m ²]	K _b [kN/m]	K _s [kN/m]	K [kN/m]
1	K _{x1}	6.5	11.443	3.250	680.57	319672.13	679.13
2	K _{x2}	6.5	11.443	3.250	680.57	319672.13	679.13
3	K _{y1}	2.25	0.475	1.125	28.23	110655.74	28.22
4	K _{y2}	2.25	0.475	1.125	28.23	110655.74	28.22
5	K _{y3}	2.25	0.475	1.125	28.23	110655.74	28.22
6	K _{y4}	2.25	0.475	1.125	28.23	110655.74	28.22
7	K _{y5}	2.25	0.475	1.125	28.23	110655.74	28.22

Table 7.2: Equations and parameters used to calculate the stress due to torsion

Calculations have been carried out to find the rotational center and the stiffness contribution from each wall as shown in Table 7.2. As seen in Table 7.2, the stiffness of the service cores is mainly due to walls 1 and 2. When calculation the rotation center it coincides with the mass center, being placed at the center of the building. The efficient stiffness contribution from each wall and further calculations are shown in Table 7.3.

Wall	$x = x_i - x_t$	$y = y_i - y_t$	xK_y [kN]	yK_x [kN]	x^2K_y [kNm]	y^2K_x [kNm]
1	0	5.25	0	3565.40	0	18718.37
2	0	-5.25	0	-3565.40	0	18718.37
3	-3	4.125	-84.66	0	253.99	0
4	0	4.125	0	0	0	0
5	3	4.125	84.66	0	253.99	0
6	-3	-4.125	-84.66	0	253.99	0
7	3	-4.125	84.66	0	253.99	0
Sum					1015.95	37436.75

Table 7.3: Equations and parameters used to calculate the stress due to torsion

The total torsional moment of 18123.821 kNm, was added as a point load at a height equal to $z = 3H/5 = 73.2$ m. The calculations are shown in Appendix A,. From this it is possible to find the stress distribution for each wall. The stress is derived from the overturning moment, M_{twist} , at the base. The results showed that wall 1 and 2 contribute immensely to the stiffness, as shown in Table 7.3.

Wall	$H_{twist,y}$ [kN]	$H_{twist,x}$ [kN]	$M_{twist,y}$ [kNm]	$M_{twist,x}$ [kNm]	σ_y [N/mm ²]	σ_x [N/mm ²]
1	0	1680.47	0	123010.68	0	34.94
2	0	-1680.47	0	-123010.68	0	-34.94
3	-39.90	0	-2920.96	0	-6.92	0
4	0	0	0	0	0	0
5	39.90	0	2920.96	0	6.92	0
6	-39.90	0	-2920.96	0	-6.92	0
7	39.90	0	2920.96	0	6.92	0

Table 7.4: Results for overturning moment

As the results in Table 7.4 show, the stresses in the two x-directional shear walls, wall 1 and 2, are too high. The maximum compressional strength for grade C45/55 concrete is $f_{cd} = 25.5$ MPa. In tension, the concrete has a much lower strength, and a large amount of reinforcement is needed. However, since the models include additional support systems, and one of the large advantages of alterations is reduced overturning moment, it is believed that this model will still be applicable. It is however necessary to include the elevator and staircase opening walls in x-direction,

to see how they affect the stress distribution. The y-directional shear walls are well within the limit.

7.3.2 Additional the Walls with Openings

New calculations were computed for when the walls with elevator and staircase openings were included. This will describe the actual situation in a larger extent.

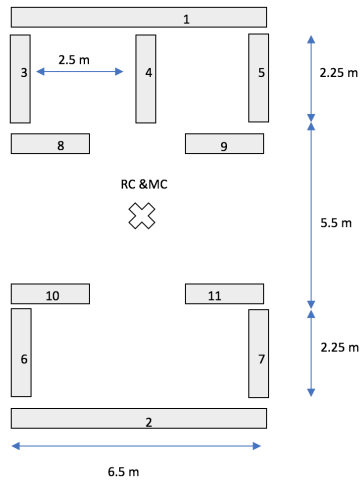


Figure 7.5: Illustration of the service core, with additional walls

As the Figure 7.5 shows, the placement for the openings of the elevator is not calculated correctly. However, the results will not be altered in a large degree when changing to two openings instead of one larger.

When computing the calculations for the new design the total stiffness of the service cores changes. Since additional stiffness is added in the x-direction, the two over-loaded walls from the previous calculations, experience a lower degree of stress. The calculations shows that the longest walls, wall 1 and 2, are now experiencing a stress equal to $\sigma = \mp 28.62 \text{ MPa}$. The stress value is now very close to the design compressional resistance. The cores are believed to be within the requirements. If one also calculates the contribution from the additional composite columns and shear walls, the base stress in each element is going to be reduced.

7.4 Seismic Loading and Natural Frequencies

For earthquake loads, it is necessary to check the ultimate limit state collapse and serviceability limitations. Seismic activity is highly dependent on the ground conditions and to what degree they transfer the wave motion to the structure. Soft soil is the most destructive since the waves are then generated with high amplitudes due to low resistance in the foundation (Yu, 2016). The foundation at the site is considered to be of clay of around 10-20 meters before reaching bedrock. This foundation is greatly favorable compared to Bjørvika which rests on reclaimed land with over 80 meters to bedrock (Kartverket, 2017).

It is necessary to construct the elastic response spectrum using NS-EN 1998-1, to achieve how the local site affects the propagation of seismic waves. The soil profile is most likely in C-category; *'with a soil profile consisting of deep deposits of dense or medium-dense sand, clay or gravel with thickness from several tens to many hundred meters'* as stated in CEN (Table (NA.3.1), 2009). From NS-EN 1998-1, it is possible to conclude that Oslo has peak ground acceleration of $a_{g40Hz} = 0.5 \text{ m/s}^2$, with a return period of 475 years (Figure (NA.3(901)), CEN, 2009).

7.4.1 Elastic Response Spectrum

Input in Spectrum	Input in Spectrum
The soil factor	$S = 1.40$
Lower limit of the period of the constant spectral acceleration branch	$T_B(s) = 0.10$
Upper limit of the period of the constant spectral acceleration branch	$T_C(s) = 0.30$
Value defining the beginning on the constant displacement response	$T_D(s) = 1.5$
Lower bound factor	$\beta = 0.2$

Table 7.5: Inputting values for elastic response spectrum

Values due to the ground conditions were incorporate into the elastic response spectrum, given in Table 7.5 (Table NA.3.3, CEN, 2009).

Figure 7.6 illustrates the horizontal elastic response spectrum for the different ground site conditions. The importance class of the building is dependent on the service use. Since this is a building mainly used for offices and apartments it belongs to class III; *'ordinary buildings not belonging in categories such as schools, hospitals and fire stations but that are taller than 15 stories'* as stated in CEN (Table NA.4(902), 2009). By definition we have $\gamma_l = 1.4$. This leads to the design ground acceleration being equal to $a_g = \gamma_l a_{g40Hz} = 0.76 \text{ m/s}^2$, as defined in CEN (Equation (3.5), 2009).

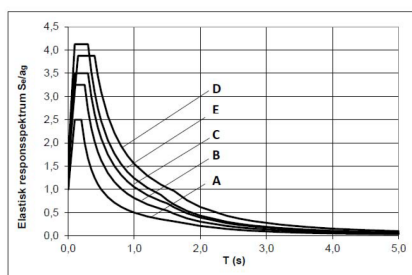


Figure NA.3(903) – Horizontal elastic response spectra for use in Norway for ground types A to E

Figure 7.6: Figure of elastic response spectrum from (Figure NA.3(903), CEN, 2009)

It is further assumed that the building can be placed under the category of DCL; Ductility Class Low. This leads to the range of the reference values of the behavior factor being equal to $q \leq 1.5$, as stated in CEN (Table NA.6.1, 2009). This can be assumed since the structure is located in a region with very low seismic activity and the connections are assumed to be fixed; thus lateral movement is in a larger extent resisted than for hinged connections. Also the acceleration is lower than $a_g/g < 0.08$, with the value being 0.076 (CEN, 2009).

8.1 Deciding on the Most Efficient Building Software Program

The governing load; wind, results in static and dynamic actions on the building. Therefore, manual calculations would be a limiting approach to achieve results for the structures response to the loads. It was desired to create BIM models for the different geometrical alternatives, that could be analyzed under both static and dynamic loads. Results could then be compared to given serviceability thresholds.

The structures that were modeled.

1. Hexagonal structure
2. Hexagonal structure with twisting over the vertical height
3. Hexagonal structure with twisting and tapering over the vertical height
4. Octagonal structure
5. Octagonal structure with twisting over the vertical height
6. Octagonal structure with twisting and tapering over the vertical height

In the models, it was decided that the interior space should equal 400 m^2 . This creates a H/B-ratio > 6 for the main structural system. To be able to implement space on the exterior as either balconies or green garden areas, an additional 2.4 meters was added to the width. This resulted in a plan section with maximum width and length equal to 26.4 meters.

To be able to compare these models, analysis results are needed for wind and seismic loads. The aim was to be able to create a parametric model, that could easily be modified. For example, to be able to change the width of the building, and have all the connected elements over the height adjusted automatically. Alterations could then be finely tuned and the building could be optimized for the site specific loads.

8.1.1 ETABS

After trying numerous software programs, it was decided to use the software program ETABS version 2016. ETABS created by Computers and Structures, Inc., is well suited for tall buildings. This program had previously been used by the student in a tall buildings course at Nanyang Technological University. Consequently, the student knew that the program would be suitable for the desired models and results. The program applies user-defined loads, and various National Standards calculations are encoded in the program. However, ETABS is restricted to NS-EN 1992 and NS-EN 1993, resulting in only correct analysis results for steel and concrete elements. It was decided to also have glue laminated timber, thus, the results will not show utilization and stresses for these cross sections. Even so, the program was used to create the six different models, and loads from dead, live, snow, wind and seismic actions were analyzed for all the six geometries.

8.2 Basic Steps to Generate the Models

When entering the software program, one determines which codes to calculate with. Here the material codes for steel and concrete were implemented. For the loads, the codes for general actions, NS-EN 1991; wind loads, NS-EN 1991-1-4; and seismic loads, NS-EN 1998-1, were used. The next step is to define the total amount of stories, which is 32 when including the base and roof as separate stories. A grid system is created, and the plan section can be drawn and multiplied for each story. The elements that were included in the models were the service cores, shear walls for residential stories, load-bearing composite columns, glue laminated timber columns and beams, and concrete slabs. The exterior envelope of the glass curtain wall is not included in the model and consequently, calculations for the glass facade has not been computed.

8.3 Limitations to ETABS

ETABS generates beams, columns and frame elements that are three dimensional. The analysis includes biaxial bending, torsion, axial deformation and biaxial shear deformations for elements of concrete and steel. The interface simplifies the process of creating cross-sections, and for concrete and steel elements it is possible to create groups of cross sections. When running the analysis the program will choose the optimal cross section from the group; resulting in optimal utilization of each element. However, this feature was not applicable for costume designed cross sections, which in reality all the elements in the models were.

When running the analysis for concrete cross sections, reinforcement was supposed

to be added automatically. This feature was not applicable since ETABS would terminate when trying to add the reinforcement. As a result, the concrete cross sections were designed without reinforcement. This includes the service cores, shear walls, slabs and composite columns. However, the program was able to retrieve the amount of necessary reinforcement to withstand the loads, but not show design results for the correct placement of the reinforcement.

When designing the load pattern for the wind load, it was not possible to apply torsional wind. This is when the wind has a triangular load pattern, according to NS-EN 1991-1-4. The manual calculated torsional moment and subsequently, overturning moment was therefore not comparable to analyzed ETABS results.

It is also worth mentioning that for the hexagonal model that was twisted and tapered, the duration of the analysis was exceptionally long. The results from the analysis did not show any clear deviations from the other models. When running the analysis the mesh generation was the time consuming aspect, and most likely the mesh is not constructed correctly.

8.3.1 Composite Columns

For composite columns, the cross-sections were easily created, but it was not possible to create these as grouped cross sections. Consequently, analysis had to be run, utilization had to be checked, and then the user had to exit the analysis mode, change the cross sections, and re-run the analysis. This was a tedious process. When creating the cross sections, the preferred reinforcement diameter is selected and the analysis can design the amount of bars needed in longitudinal and transverse direction. However, this was not applicable for the composite columns. Thus, the sections are of a steel HE-A profiles enclosed in concrete rectangular cross sections, and not actual composite columns with reinforcement. The concrete grade was C45/55 and the steel grade was S355.

8.3.2 Glue Laminated Timber

For the glue laminated timber cross sections it was necessary to define the material properties of the desired GL32c. This was done by creating a concrete cross section and editing all the material properties.

Material Name and Type	
Material Name	GL32c
Material Type	Concrete, Orthotropic

Modulus of Elasticity	
E1	185000 MPa
E2	112000 MPa
E3	112000 MPa

Shear Modulus	
G12	650 MPa
G13	650 MPa
G23	65 MPa

Coefficient of Thermal Expansion	
A1	0.000003 1/C
A1	0.000003 1/C
A1	0.000003 1/C

Poisson's Ratio	
U12	0.35
U13	0.35
U23	0.35

Figure 8.1: The specified material properties for GL32c

Figure 8.1 shows how the glue laminated timber material data was added. Then, a variety of rectangular cross sections for this material was defined, and used for the different elements. The analysis generated the correct loading for each glue laminated timber element, but checks were not conducted. Therefore, manual calculations had to be computed for these elements.

8.3.3 Hollow Concrete Slabs

It was desired to use concrete slabs with hollow cores of concrete grade C45/55. These are optimal to withstand loading, while maintaining a low volume of concrete. This was desired from an environmental perspective. For the upper 17 stories, the slabs were designed as HCS200 elements, while the lower stories were of HCS265. The sections were designed as regular compact slabs, using effective thickness as the design thickness. The cores were resisted to only transfer longitudinal loading. Consequently, each element can be seen as a simply supported element, between the glue laminated timber beams and columns. Each hollow core slab had a width of 1.2 meters. The wind load is generated as a load that is forced upon the the extent of the entire slab diaphragm. This horizontal loads are transferred to the service cores by moment resisting connections between the hollow core slabs and the service cores.

When running the analysis, the software program is designed to create the required reinforcement in the slabs to withstand the governing factored loads. This was not possible for the hollow core slabs. However, since these are not the main elements of interest, further results of the slabs performance has not been looked at.

8.4 Modeling the Plan Section

Since some of the models included alterations, it was necessary to decide on the correct placement of the columns close to the exterior. For sufficient load transfer between the stories, it is ideal that the columns were placed directly aligned with the vertical z-axis. The total tapering effect over the height was decided to be of 2 meters in the plan radius. The twisting over the structure height was created with a total of 45 degrees. As a result, vertical columns were placed with a distance of 2.6 meters from the envelopes periphery. By having this design, the columns could remain aligned vertically over the total height of 122 meters. To underline the actual twisting of the building, additional tilted columns were added to the exterior facade. These followed the corners of the octagonal or hexagonal plan sections. Consequently, there were placed six exterior columns for the hexagonal models, and eight for the octagonal models, in each story.

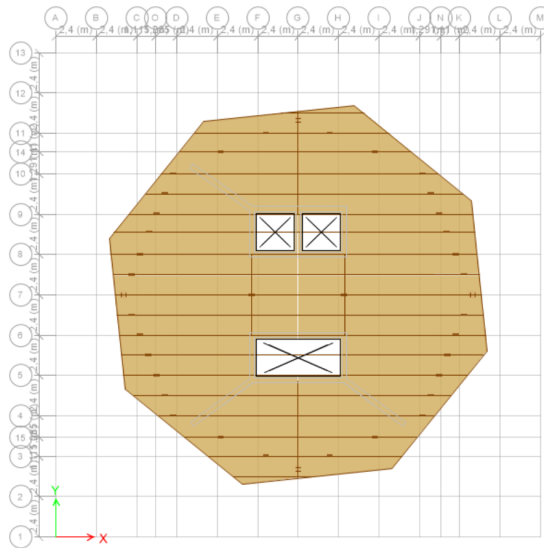


Figure 8.2: The plan view and 3D view of octagon with twisting and tapering alterations

Figure 8.2 illustrates how the octagon models were modeled in ETABS. As the plan section shows, the concrete slabs have a width of 1.2 meters and are supported by the service cores and the glue laminated timber beams, shown in darker brown color. The section also illustrates the placement of the glue laminated timber columns in a distance of 2.6 meters from the envelope. Figure 8.2 shows how these columns remained static throughout the height.

8.5 Static Load Cases

The load cases shown in Table 8.1, were added to each structure by following guidelines given in CEN (2002, 2005). As Table 8.1 shows, the snow load for Oslo is equal to 2.8 kN/m^2 .

Description of Loading	Value
Self-weight generated by ETABS for each element	Varies
Imposed dead load, floor finish all stories except roof	1.0 kN/m^2
Imposed dead load, floor finish roof	0.5 kN/m^2
Live load for residential and office stories	3.0 kN/m^2
Live load for roof	0.75 kN/m^2
Snow load on roof area, from	2.8 kN/m^2
Wind load	$v_m = 22.0 \text{ m/s}$

Table 8.1: Loading on the structures

8.5.1 Wind Loading

The wind loading generated in ETABS is specified in the 'Lateral Loads Manual' by Computers and Structures, inc. (2016). All together there are four user defined parameters; where one is code specific while the rest are common for all the codes. These parameters determine; the exposure height of the wind load, the plan area extent of the load, the terrain category, and wind coefficients. The wind loading is set to be implemented to the structure in a multi-stepped angle from 0 degrees from the x-direction, to 45 degrees rotation from the x-axis. It is treated as a single load case (Computers and Structures, inc., 2016).

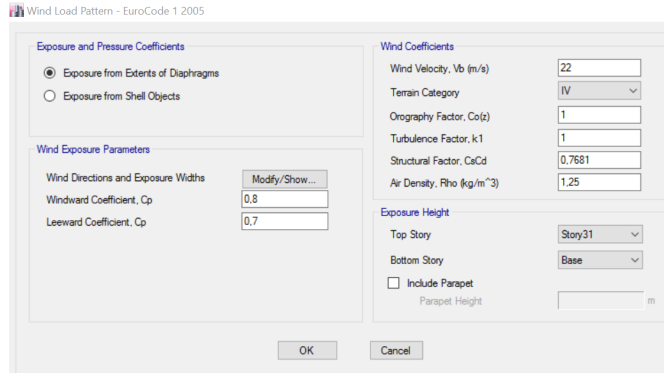


Figure 8.3: Implementing the wind loading in ETABS

The wind load was applied to the models as shown in Figure 8.3. The implementations of the four required parameters to construct the wind pattern is shown. This load is equivalent to method 1 in Appendix A, by only adding the windward and leeward pressures. The wind loads are determined based on the wind pressure, w , shown here in Equation 8.1, from CEN (Eq.(5.1) and Eq.(5.6), 2005).

$$w = c_s c_d q_p(z) c_{p,windward} + c_s c_d q_p c_{p,leeward} \quad (8.1)$$

The program does not implement the National Code defined load for the torsional rotation due to uneven wind loads, calculated in Chapter 7. Consequently, the overturning moment at the base from torsion, is in ETABS for when the load is applied in the most governing angle from the x-axis. The value retrieved from this calculation is not directly related to the manually calculated overturning moment in Chapter 7, but is an indication of the rotational forces due to wind loads.

8.6 Earthquake Loads

The seismic loads can be generated using NS-EN 1998-1 input parameters; Figure 8.4, as response spectrum, or time-history functions. All methods are applicable according to '*Lateral Loads Manual for ETABS 2016*' (Computers and Structures, inc., 2016). In total, four different seismic loads were created using the acceleration and other parameters obtained from site considerations in Oslo, Norway.

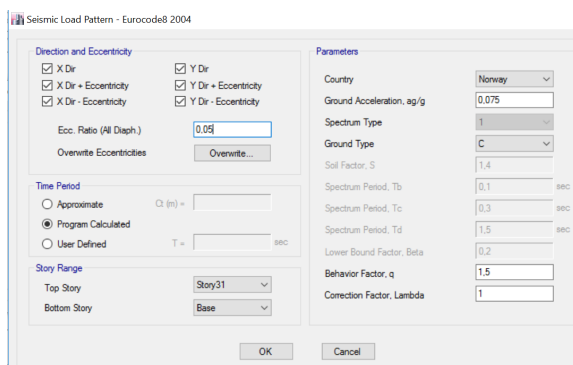


Figure 8.4: Seismic: NS-EN 1998-1 implementation

Earthquake forces are considered as dynamic, since they vary in time. The earthquakes excitations are generated using both response spectrum and time history functions. The response spectrum is applied in both x- and y-direction. The damping ratio was set to 0.05 for all the structures, which is a commonly used value (Mwafy et al., 2006). If one plots the peak displacements versus the natural period, T_n , for a given value of the damping ratio, one obtains the displacement response spectrum. Similarly, by getting the peak velocity and peak acceleration, velocity spectrum and acceleration spectrum is retrieved. The acceleration response spectrum is implemented into ETABS as shown in Figure 8.5.

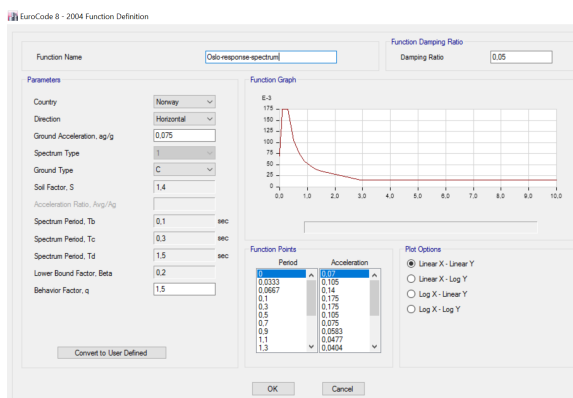


Figure 8.5: Response spectrum

The synthetic time history function is computed by ETABS generating the ground acceleration over time from the response spectrum function. This is done in two ways; using the frequency domain and the time domain, shown in Figure 8.6 and Figure 8.7 respectively.

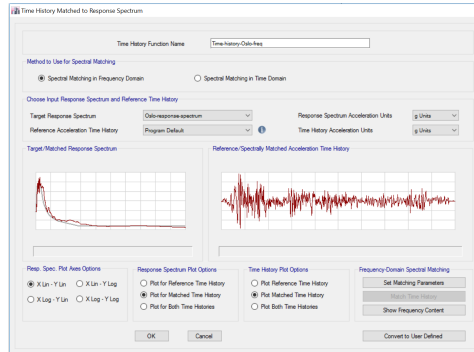


Figure 8.6: Time history analysis in frequency domain

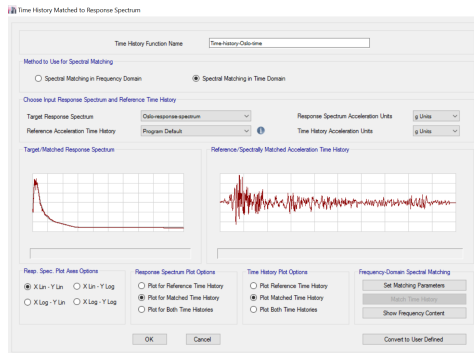


Figure 8.7: Time history in time domain

Since the four different load combinations, shown in Figures 8.4 - 8.7, are generated from the same parameters, idealistically they should retrieve the same results. On the other hand, as described in Chapter 4, the various methods may lead to inaccuracies and deviating results. One value of a standard deviation may lead to a variation of peak accelerations and durations, and such variations will be shown in ETABS.

8.6.1 ETABS Implementation of Seismic Load Pattern

The analysis results that are shown for the governing loads are retrieved from an algorithm based on CEN (Section 4.3.2, 2009). ETABS calculates the spectral design spectrum, $S_d(T_1)$. The calculations are accordingly the base shear, F_b , shown in Equation 8.2 (Eq.(4.5), CEN, 2009).

$$F_b = S_d(T_1)W\gamma \quad (8.2)$$

The base shear is distributed over the height resulting in forces per story given in Equation 8.3 (Eq. (4.11,) CEN, 2009).

$$F_{story,i} = \frac{w_i h_i F_b}{\sum_{story=-i}^n w_i h_i} \quad (8.3)$$

8.7 Load Combinations

Load combinations are generated to follow the Norwegian requirements. ETABS automatically generates load combinations that are based on steel and concrete elements ultimate limit states. Since serviceability is governing for the comfort criteria, SLS load combinations were also added, as well as load combinations for the four seismic loads. The governing load combinations in ETABS are shown in Table 8.2.

Name	Equation
DCon5	$1.35 \times Dead + 1.05 \times Live + 1.50 \times Wind$
DCon6	$1.35 \times Dead + 1.05 \times Live - 1.50 \times Wind$
SLS1	$1.00 \times Dead + 0.70 \times Live + 1.00 \times Wind$
SLS2	$1.00 \times Dead + 0.70 \times Live + 1.00 \times Wind + 0.70 \times Snow$
ULSeis1	$1.00 \times Dead + 1.00 \times Response\ spectrum$
ULSeis2	$1.00 \times Dead + 1.00 \times Seismic$
ULSeis3	$1.00 \times Dead + 1.00 \times Time - history - time$
ULSeis3	$1.00 \times Dead + 1.00 \times Time - history - frequency$

Table 8.2: Governing load combinations in ETABS

8.8 Changes Due to Results from Analysis

The final model results were achieved by repeating the analysis process to obtain a utilization range of 0.65–0.95 for the composite columns. Consequently, the volume of concrete and steel was minimized for these columns.

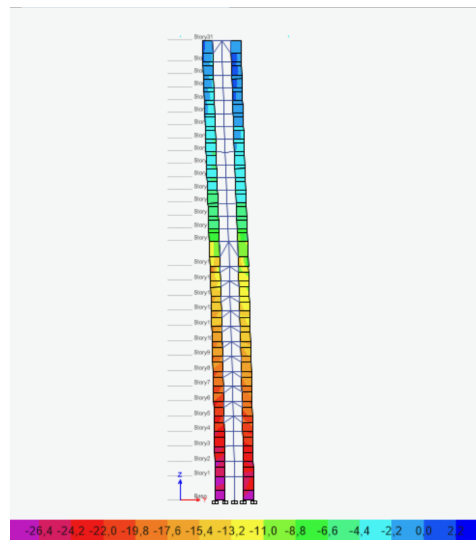


Figure 8.8: The truss system in each model. Stresses shown in the service core as well

From the first results, it was clear that the displacement was too large due to the uncoupling between the two service cores. As a consequence, an additional truss system was added in-between. This leads to the two cores having the same displacement and stress pattern. They cores have different values depending on where the loading is implemented. The truss system was created using glue laminated timber, and was added to the top story and office stories; with the exception of the four lowest stories. It was desired to have an open atrium in the office stories, and the atrium would have a greater architectonic benefit if the truss system was not added to the lower floors. By doing this, the opening between the cores would be enhanced, and increase the spatial feel. All the joints of the truss system were moment and torsional free hinges. Figure 8.8 illustrates the configuration of the truss system and at which floors this system was added.

All the six models were constructed with the same elements at equal locations from the center of the plan section. However, the interior glue laminated columns were placed at a distance of 2.6 meters from the base exterior envelope. This results in a varying placement for the hexagon and octagon models. Wind and seismic loads were applied over the diaphragm for each story, while the live and dead load were gravitational forces applied to each slab.

The models were optimized such that the utilization for the composite columns was within 65-95 percent, without additional reinforcement. First, all the models were analyzed with the required composite cross sections from the plain hexagon and octagon models. When adding modifications to the shapes, it led to specific columns having either a very low or higher utilization, and the cross sections were changed. This method of optimizing the models was chosen since it was the only way of achieving load efficient design of the composite columns.

Manual calculations were computed for wind accelerations and the glue laminated timber elements. The glue laminated timber elements were only design checked and resulting cross sections found, for the octagon tapered and twisted model. ETABS results of the forces, fundamental frequencies and mass per story were retrieved to compute the manual calculations. It was believed that the loading in the glue laminated timber columns would show minimal deviation between the models.

The plain hexagonal model is unique, this is seen in the utilization shown in Figure 9.1. The elevation in Figure 9.1 is located in the center of the model plan in the x-direction. It is clear that the composite columns closest to the windward direction are barely loaded compared to the other models. The columns in the upper stories have a cross section of HE100A steel profiles enclosed in concrete. The model required composite columns that had 1/3 of the area required for other models.

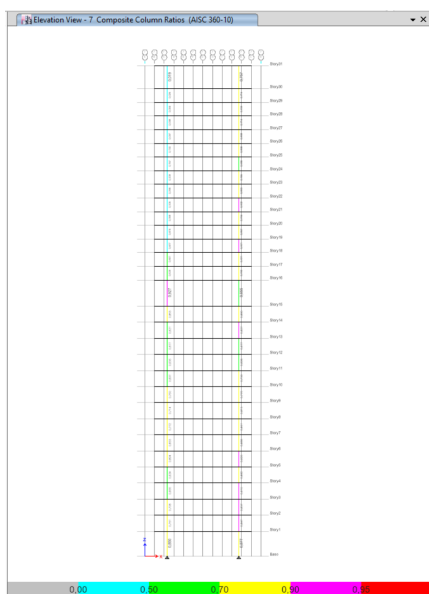


Figure 9.1: Utilization degree for composite columns at elevation 7

Changing the columns in Figure 9.1 to achieve the desired utilization, also leads to the model being prone to seismic displacements and accelerations, due to the low mass and stiffness. Consequently, the results for displacement due to seismic loads in the hexagonal plain model are immense, as a result of this low mass in the upper stories. From the results it is clear that this model is constructed with errors. The model results are discussed further in Appendix G, but not included in this chapter.

9.1 Main components

The structures had a total height of 122 meters. Where there were three floors; the base, story 16 and story 30; that could be considered as soft stories. The office floors had a height of 4.0 meters, while the residential floors had a height of 3.4 meters.

The main load-bearing components were the elevator and staircase cores that were symmetrically placed in a distance of 2.75 meters from the mass center of each story. These walls function as shear walls and absorb the horizontal wind loads. The wind loads are mainly transferred to the concrete cores, however, the stiffest composite columns also contribute to the resistance. The secondary load-bearing system consisted of elements that carry the slabs and the gravitational forces for each story. It was desired to have this system in glue laminated timber elements. Consequently,

the majority of the columns and all the beams are of glue laminated timber. At the most critical load-bearing locations of the columns, the glue laminated timber was exchanged into composite columns, that have a much larger load capacity.

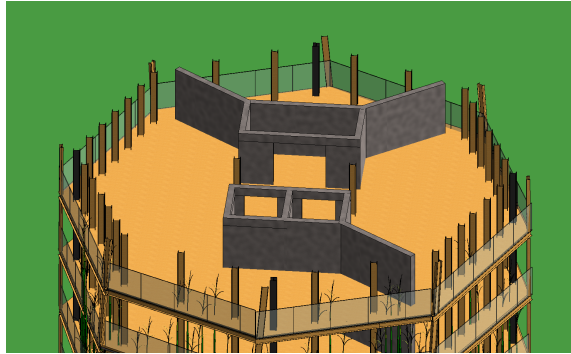


Figure 9.2: Illustration of the plan section, shown by octagon tapered and twisted in Revit

Since it was desired to have both a tapering and a twisting effect over the vertical height, it was crucial to place the beams and columns efficiently. As a result, the majority of the columns are placed 2.6 meters from the edge, as explained in Chapter 8. A few of the exterior glue laminated timber columns follow the edges of the envelope. This leads to these columns twisting over the height due to both the tapering and the rotation of the building. The load transfer for these columns are tilted in both the vertical and horizontal plane. The effect is having a non-beneficial load transfer, but having a underlined architectonic expression for the exterior facade. In Figure 9.2 the plan section is shown. Here the composite columns are colored black, and the glue laminated columns have a wooden finish. Figure 9.2 is of a residential story, also showing the placement of the additional shear walls for these stories.

9.2 Results from ETABS for Wind Analysis

For the wind analysis there were two main results that determined the efficiency for the structural analysis. These were the displacement of the structures due to the wind loads, and the acceleration of the buildings. Both of these limits are given as indicators of the occupants comfort, and the loads had to be applied in serviceability limit state. The overturning moment at the base due to wind loads was also looked at.

9.2.1 Load combinations

The worst load combination for the serviceability limit state wind load is shown in Equation 9.1.

$$SLS_{worst,wind} = 1.0 \times \text{Dead} + 1.00 \times \text{Wind} \quad (9.1)$$

An increase of mass will most likely lead to a stiffer structure, and this will decrease the displacement and acceleration. Therefore, it is logical that snow loads will decrease the displacement and the load combination with applied snow load is not governing.

9.2.2 Displacement and drift

The displacement limit to satisfy the occupant comfort criteria was set to $H/500 = 122/500 = 244 \text{ mm}$. This was a conservative value to be certain that all the materials, cross sections and the global models were within the limit for occupant comfort.

Model	Displacement	Drift Ratio	Overturning Moment
Octagon plain	230.02 <i>mm</i>	0.224%	2038477 <i>kNm</i>
Octagon twist	209.33 <i>mm</i>	0.212%	2074058 <i>kNm</i>
Octagon taper	184.32 <i>mm</i>	0.181%	1830328 <i>kNm</i>
Hexagon twist	226.16 <i>mm</i>	0.221%	2087755 <i>kNm</i>
Hexagon taper	196.83 <i>mm</i>	0.211%	1834469 <i>kNm</i>

Table 9.1: Results from ETABS for wind displacement, drift ratio and overturning moment

As the results show in Table 9.1, all the models have a displacement within the given limit. The drift results display the maximum drift percent for each story. A limit has not previously been set for the wind loaded drift ratio, as it is more common to look at the buildings total displacement. However, the drift ratio is of interest when the structure has varying stiffness and plan geometries over the height. The results showed that the drift ratio was most commonly largest at the soft story at mid-height, situated at the 16th-17th story. This floor height was of 6.5 meters. The maximum inter-story displacement is usually set to the same limit as for total displacement, and therefore it is $H/500 = 6.5/500 = 13.0 \text{ mm}$ for the soft story (Bing, 2016). When calculating the percentage drift, it is equal to, $H/500 = 0.2\% \times H$. Consequently, the octagon model that is tapered and twisted, is the only model that has a maximum story drift ratio within this limit.

Table 9.1 also show the values for overturning moment at the base. These values are not comparable to torsional moment in the service core and the resulting

overturning moment. The results show the total moment at the base due to the load combination given in Equation 9.1. The values however demonstrate that the overturning moment at the base is decreased when adding alterations to the models.

9.2.3 Wind Acceleration and Modal Results

The results from Table 9.2 show that the fundamental period is within a region of 4.1 s - 4.44 s for all the shapes. Table 9.2 shows that when adding alterations to the basic shapes, the fundamental period decreases.

Model	Fundamental Period	Fundamental Frequency
Octagon plain	4.423 s	0.226 s ⁻¹
Octagon twisting	4.393 s	0.228 s ⁻¹
Octagon taper	4.130 s	0.242 s ⁻¹
Hexagon twisting	4.437 s	0.225 s ⁻¹
Hexagon taper	4.123 s	0.243 s ⁻¹

Table 9.2: Results from ETABS for modal periods and frequencies

$$f = \sqrt{\frac{k}{m}} \quad (9.2)$$

Equation 9.2 shows the function for determining the natural frequency for a SDOF system. The divisor in Equation 9.2 is the stiffness of the system. When adding alterations, the mass decreases. Since the frequency increases with alterations, as shown in Table 9.2, the stiffness does not decrease. This is a desired result, and can be seen as a frequency tuned structural design.

Values of the mass per story were retrieved from the ETABS models. The calculation method to determine the wind acceleration for the octagon tapered and twisted model is shown in Appendix B. Table 9.3 shows the two varying accelerations, depending on which method was used to find the equivalent mass for each model. When the equivalent mass is retrieved from an integrated mass per story, the values are larger than those computed with a mean mass. The mean mass method is when an equivalent mass is calculated by taking the mean value of the mass for the upper third of the height. The integrated mass method is considered to be the most correct, since the calculations are integrated over the actual mass for each story. Table 9.3 shows that the acceleration is within a range of 0.18 – 0.21 m/s² for all the models.

Model	Acceleration Mean Mass	Acceleration Integrated Mass
Octagon plain	0.190 m/s^2	0.206 m/s^2
Octagon twisting	0.183 m/s^2	0.198 m/s^2
Octagon taper	0.198 m/s^2	0.206 m/s^2
Hexagon twisting	0.189 m/s^2	0.203 m/s^2
Hexagon taper	0.205 m/s^2	0.213 m/s^2

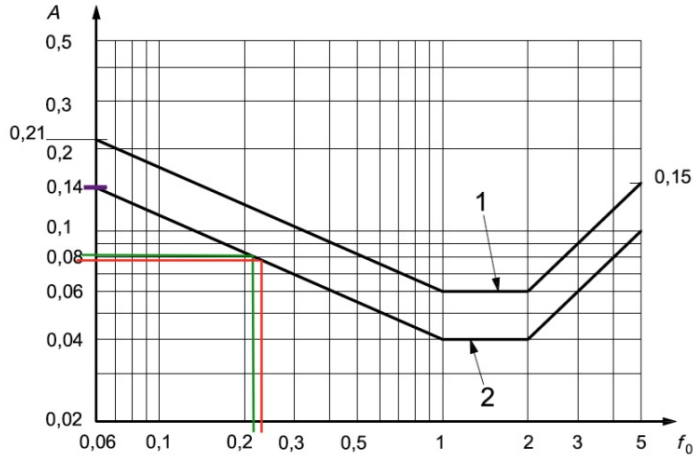
Table 9.3: Results from manual calculations for acceleration

9.2.4 Calculations for ISO 10137

The standard ISO 10137, sets the limiting acceleration to be approximately $0.08 m/s^2$ for residential buildings, but varies due to a buildings fundamental frequency (ISO, 2007). Since the upper portion of the mixed-use building is of residential stories it is correct to use this value, instead of the one for office buildings. However, the limit is for a peak acceleration with a return period of 1 year, and not a 50 year return period as calculated in the results shown in Table 9.3. Consequently, the mean wind speed needs to be modified. The factor c_{prob} is altered to change the return period. When the value is changed to a two year return period, c_{prob} is reduced from 1.0 to 0.6956. The resulting mean wind speed is then decreased from $v_{m,50} = 22.68 m/s$ to $v_{m,2} = 15.78 m/s$. The two year return period is used instead of a one year return period since the c_{prob} -factor is based on a Poisson-process for annual probability.

Model	Acceleration ISO Mean Mass	Acceleration ISO Integrated Mass
Octagon plain	0.0700 m/s^2	0.0756 m/s^2
Octagon twisting	0.0671 m/s^2	0.0726 m/s^2
Octagon taper	0.0723 m/s^2	0.0754 m/s^2
Hexagon twisting	0.0694 m/s^2	0.7473 m/s^2
Hexagon taper	0.0750 m/s^2	0.0778 m/s^2

Table 9.4: Results from manual calculation for acceleration according to ISO 10137



Key

A peak acceleration, m/s^2

f_0 first natural frequency in a structural direction of a building and in torsion, Hz

1 offices

2 residences

Figure D.1 — Evaluation curves for wind-induced vibrations in buildings in a horizontal (x, y) direction for a one-year return period

Figure 9.3: Limiting acceleration from ISO (Figure D.1, 2007)

Table 9.4 shows the calculated peak accelerations with a one year return period. Figure 9.3 shows the limiting value set by ISO (2007). The purple line indicates the discarded hexagon plain model that had a very low frequency. The hexagon and octagon models with both tapering and twisting had a fundamental frequency of approximately 0.225 Hz . The limiting value for these was set to 0.078 m/s^2 , and is indicated by the red line in Figure 9.3. The remaining plain octagon model, and twisted octagon and hexagon models are limited by a peak acceleration of 0.08 m/s^2 , as shown by the green line in Figure 9.3.

When comparing Figure 9.3 with the calculated values in Table 9.4, all the acceleration values were within the limits. The fundamental frequency of each model is dependent on the mass per story. When adding alterations, the fundamental frequency increases since the equivalent mass decreases. Consequently, as shown in Figure 9.3, the variation between the different models peak accelerations can be seen as insignificant. These results can be seen as an indication of sufficiently designed models and functioning alterations, since all values are within the acceleration limit. The actual stiffness is constant even with a decreased amount of load-bearing structure when adding alterations.

9.2.5 Calculations for ISO 2631-1 and ISO 2631-2

The standard ISO (2003), gives a limiting frequency weighted acceleration of $0.02 m/s^2$. However, as stated in the title of the International Standard, the limiting acceleration requirement can only be applied to buildings that have a fundamental frequency in-between $1 - 80 Hz$. If the fundamental frequency is lower, other limitations need to be considered (ISO, 2003). As a consequence, it is not possible to use ISO 2631 for any of these models.

9.2.6 Overturning Moment

In Chapter 7, the overturning moment according to NS-EN 1991-1-4 was calculated. The calculations were for uncoupled walls, and therefore, they can be regarded as conservative calculations. Calculations were for cores; without including the wall with opening for the staircase and elevator door, and calculations when these walls were included.

When including the walls with the door openings, the governing stress was equal to $\sigma = \pm 28.62 MPa$. This calculation is more correct than when the additional walls were not included. As the results show, the stress level is just above the design limit, $f_{cd} = 25.5 MPa$. Consequently, since the cores are in reality more coupled it is considered that the service cores are sufficiently designed to withstand the overturning moment. In addition, the service cores are not the only elements that function in the vertical load-bearing structure. The models also have composite columns. These columns have a width of around $500 - 600 mm$ for the lower stories, and will contribute to resisting the torsional moment. Since these composite columns are placed further away from the mass and stiffness center, their contribution to moment resistance is large.

A ETABS and Overturning Moment

ETABS generates values for global overturning moment and forces for each type of element. The global overturning moment is not comparable to the manual calculations, but the moment, M33, is. This is the moment in the shear walls about the x- and y-direction and similar to the torsional moment calculated manually. However, the wind load is not directly following the pattern with a triangular load distribution over the width, as shown in Figure 7.2. On the other hand, the wind load is uniform but with the most governing angle from the x-direction. This will result in a torsional moment that needs to be checked against the design limit for ultimate limit compressional strength for C45/55 concrete, $f_{cd} = 25.5 MPa$. The configuration of the service core in ETABS is more equivalent to reality, with cores that are coupled shear elements.

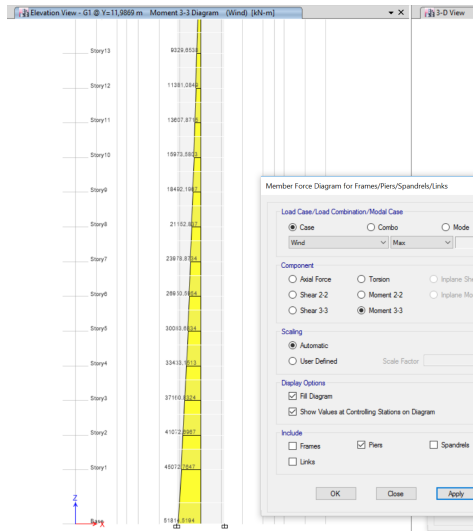


Figure 9.4: Overview of moment, M33, in shear walls

Figure 9.4 is retrieved from ETABS for the lower stories. The results show the moment in one of the two governing core walls that is parallel to the x-axis. The overturning moment at the base is equal to 51814.52 kNm . This is equal to a base stress of 14.72 MPa . A value which is lower than the limiting design strength. Consequently, considering the loading generated in ETABS, the models have a service core that can withstand the applied wind load.

9.3 Results from ETABS for Seismic Loads

There were four different seismic load patterns that were added to the ETABS models, as shown in Table 9.5. When comparing the results in Table 9.5, it is evident that the NS-EN 1991-1-4 has larger displacements than the corresponding load patterns. This is due to the conservative period that is generated when using the coded parameters. The load generated as response spectrum has equivalent loading, but the duration of the peak acceleration was shorter (Mwafy et al., 2006). The time-history functions are the only loads varying with time. Consequently, these loads demonstrate the earthquakes ground excitations in a larger extent. As a result, the variation between the results illustrate the conservative approach used in NS-EN 1998-1 when designing the response spectrum. The constant application of the peak acceleration, PSA, leads to higher displacements and stresses for the response spectrum loads than the time-history loads, as shown in Table 9.5.

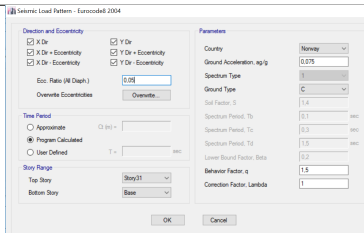

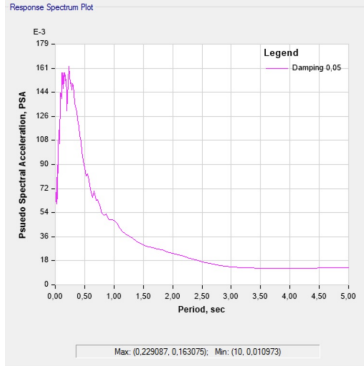
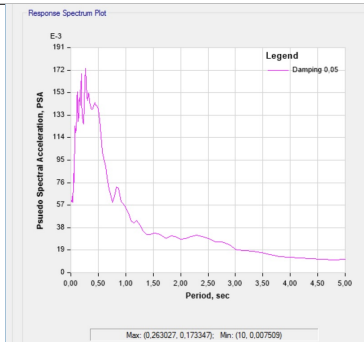
Load Pattern	Implementation in ETABS	Displacement	Overtuning Moment	PSA
Values from NS-EN 1991-1-4		94.57 mm	1.406×10^6 kNm	not given
Response Spectrum		54.69 mm	1.333×10^6 kNm	0.175
Time-History, time domain		28.63 mm	1.326×10^6 kNm	0.160
Time-History, frequency domain		28.63 mm	1.326×10^6 kNm	0.170

Table 9.5: Comparing the results for the seismic loads in octagon tapered and twisted model

9.3.1 Displacement and drift

The inter-story drift limit was set to 0.3%, as a conservative value chosen from various publications. This value is more accurate than total displacement of the building for seismic load situations.

Model	Displacement Seismic	Drift Seismic	Seismic Overturning Moment
Octagon plain	107.25 mm	0.106%	1520920 kNm
Octagon rotate	106.473 mm	0.105%	1564049 kNm
Octagon taper	94.57 mm	0.093%	1406066 kNm
Hexagon rotate	112.65 mm	0.113%	1562790 kNm
Hexagon taper	97.83 mm	0.104%	1395705 kNm

Table 9.6: Results from ETABS for seismic displacement

It is clear from the results shown in Table 9.6 that the total lateral displacement from the seismic load, is not governing compared to the results from wind loads. The drift ratio results display the maximum drift percent for each story, and the results show that all the models are within the limit of 0.3%. The results shown in Table 9.6 illustrate that the displacement, drift ratio and overturning moment decreases with increasing alterations to the shape. These results show how the mass is not the only parameter that defines the stiffness. From only a mass standpoint, the displacement should increase when adding alterations, since the mass decreases. The results therefore indicate that the alterations also have a positive effect on the serviceability under earthquake loading.

9.3.2 Acceleration and Modal Results

The acceleration results from ETABS are for the top story's acceleration under the seismic response spectrum function load. Therefore, the results are not comparable with the requirements for the accelerations due to wind loads.

Model	Acceleration	Fundamental Period	Fundamental Frequency
Octagon plain	753.53 mm/s ²	4.423 s	0.226 s ⁻¹
Octagon rotate	761.29 mm/s ²	4.393 s	0.228 s ⁻¹
Octagon taper	914.57 mm/s ²	4.13 s	0.242 s ⁻¹
Hexagon rotate	808.81 mm/s ²	4.437 s	0.225 s ⁻¹
Hexagon taper	981.36 mm/s ²	4.123 s	0.243 s ⁻¹

Table 9.7: Results from ETABS for acceleration and mode shapes

The results from Table 9.7, show that the fundamental period is within a region of 4.1 s - 4.44 s. Table 9.7 shows that when adding alterations to the basic shapes, the acceleration increases while the fundamental period decreases. Explained by Equation 9.2 for the natural frequency, the models lower mass leads to higher frequencies when the stiffness is constant.

Earthquakes ground excitations lead to motion in the soil underneath the structure. Therefore, the acceleration at the top story is in a larger degree influenced by the frequency than for wind loads. When the frequency increases, so will the acceleration, as shown in Table 9.7. The results in Table 9.7 indicate that the tapered and twisted octagonal geometry is more ideal than the tapered and rotated hexagonal model when considering accelerations at the top story.

When comparing the results Table 9.7 in to the results of the displacements, it is clear that when adding alterations and consequently decreasing the mass for the upper stories, the displacement decreases while the acceleration of the displacement increases. Human comfort is more prone to the acceleration of the structure under story sway than the actual displacement in a measured distance. Therefore, the occupant comfort is reduced with increasing alterations.

9.4 Amount of Concrete and Steel

Since the building has an aim to be sustainable, and reduce the amount of concrete and steel, it is necessary to compare the total mass of the different models.

Model	Total Mass Steel	Total Mass Concrete
Octagon plain	3822.42 <i>kN</i>	86305.17 <i>kN</i>
Octagon rotate	3803.80 <i>kN</i>	86299.71 <i>kN</i>
Octagon taper	3733.26 <i>kN</i>	78517.53 <i>kN</i>
Hexagon rotate	4040.80 <i>kN</i>	85708.50 <i>kN</i>
Hexagon taper	3809.61 <i>kN</i>	79532.60 <i>kN</i>

Table 9.8: Results from ETABS for mass

The results in Table 9.8 show that in general, the amount of concrete and steel decreases when adding alterations to the general octagonal and hexagonal shapes. The results also indicate that the amount of concrete and steel is lower for the octagon model that is tapered and twisted, than the tapered and twisted hexagonal model. The percentage decrease from the plain octagonal geometry to the final tapered and twisted model is, 2.33% for steel, and 9.02% for the concrete.

9.5 Glue Laminated Timber Elements

The forces due to ULS loads were retrieved from ETABS, for the glue laminated timber exterior columns and truss system. It was decided to have a uniform width of 280 mm for all the sections, mainly due to aesthetic considerations. When calculated, almost all the elements had sufficient strength with a cross sectional height of 225 mm.

9.5.1 Axial Force Design of Columns

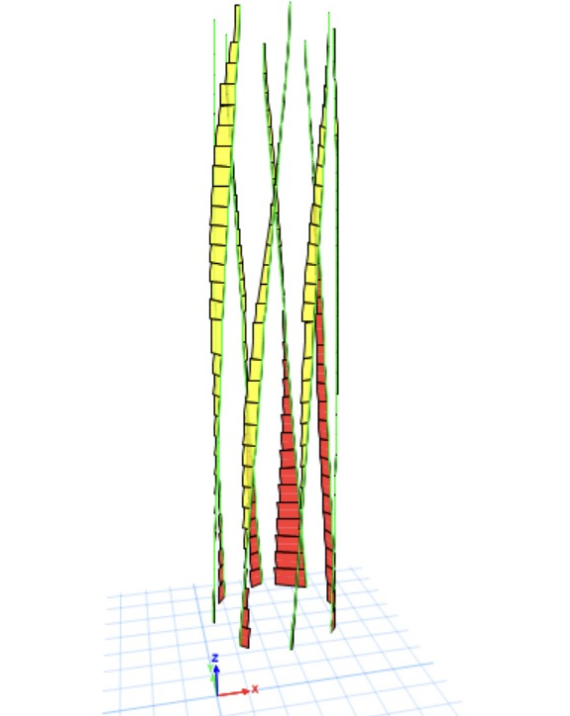


Figure 9.5: Axial force distribution in the exterior glue laminated timber columns

Figure 9.5 illustrates how the axial loading is applied over the exterior columns. The red indicates compression, while yellow indicates tension. Under the governing ULS load combination, the uppermost stories are under tension, and this is largest at the windward facade. The lower stories have columns in compression, which is largest at the leeward facade.

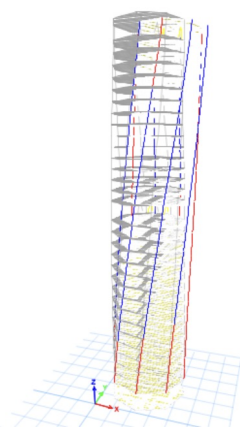


Figure 9.6: Axial force distribution in the exterior glue laminated timber columns with displacements

Figure 9.6 illustrates the displacement due to the wind loading on the structure, where the exterior columns are highlighted. Here, the red color columns are in compression while the blue colored columns are in tension.

9.5.2 Cross Sectional Dimensions



Figure 9.7: Cross sections for the glue laminated columns

A few of the columns had to have an increased cross sectional height to withstand the governing loading. In Figure 9.7 the columns in green color are designed with cross section $B \times H = 280 \times 225 \text{ mm}^2$, the red colored columns have $B \times H = 280 \times 270 \text{ mm}^2$ and the purple colored columns have $B \times H = 280 \times 360 \text{ mm}^2$. The cross sections that had to be increased are those who undergo the largest compressional axial force on the leeward side. For the truss system of glue laminated timber, all the elements were efficient when designed with a cross section of $B \times H = 280 \times 225 \text{ mm}^2$.

From the results, it is clear that the glue laminated elements have not been applied with substantial loads. This is desired since the elements contribute as a secondary load-bearing system. The results indicate that the columns only function as supports for gravitational loads such as dead and live load.

9.6 Final Model in Revit

Due to the results obtained from the different models, the octagon tapered and twisted was considered as the all-over best designed structure. The structure obtained the lowest displacement, drift ratio and overturning moment results under both seismic and wind loading. The seismic acceleration was lower than for the hexagonal tapered and twisted model, by approximately 10 percent. Consequently, the stiffness of the octagon tapered and twisted was greater, even with a lower amount of steel and concrete, than the tapered and twisted hexagon model. The octagonal tapered and twisted model was exported to Revit for architectural illustrations.



Figure 9.8: Octagon tapered and twisted model in Revit

Figure 9.8 shows how the whole structure is designed. The exterior structure consist of a glass curtain wall supported by twisted glue laminated timber columns. Inside the glass, the office stories have a glass covered garden, while the residential stories have balconies. The architectonic effect of the glass, wood elements and green objects create an appealing 21st century skyscraper. The facade underlines the sustainable focus of the building. Figure 9.8 also shows the roof garden with the desired sedum plants that have sustainable features, as described in Chapter 3.

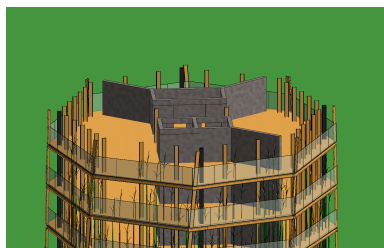


Figure 9.9: Octagon tapered and twisted model in Revit, section view

Figure 9.9 shows the section plan of a typical residential story. The two service cores are shown, as well as the shear walls that function as load restraining elements and apartment separators. Due to the twisting over the vertical height, the balconies have unique configurations for each story. The student believes that the balcony and green garden area will still serve its function, even with an abnormal shape. It is desired to have wooden finish for the ceilings and floors, to enhance the relation to the Norwegian building traditions. At the corners of the service cores, non-load carrying walls are to be placed as entrances for the different apartments. Glass facades are also to be placed to enclose the apartments from the balcony space. Figure 9.10 shows the building design from ground view.



Figure 9.10: Octagon tapered and twisted model in Revit, ground perspective

The aim of this thesis was to create a conceptual structural design of a mixed-use skyscraper, focusing on the architectural and structural aspects. When regarding the architectural aspects, it was desired to create a building with a unique plan geometry and facade. If well designed, it would receive positive feedback from Norwegians, and also function as a tourist attraction by representing the city's skyline. Given current and future focus on sustainability, it is of outmost importance to implement this in the design of the building. For this purpose the secondary load-bearing system was designed with glue laminated timber elements. The facade of the building consists of a glass curtain wall, enveloping a garden and balcony area. This garden surrounding the inner structure will reduce the required amount of insulation, creating a green and eco-friendly footprint. These gardens and the semi-transparent glass will make the skyscraper stand apart from existing high-rise buildings in Norway.

Creating a skyscraper for a city such as Oslo, will always be met by some skepticism. The majority of the buildings are five story complexes, and thus, a contrasting 30 story building would have to complement the existing buildings. In the recent years, the city skyline has changed, by new and modern architectural designs as the ragged line of Bjørvika, named Barcode; the hypermodern design of the new Opera House; and Tjuvholmen, that is partly built on reclaimed land. These projects have changed the perception of what well functioning architecture is. Norwegians have embraced these projects by the common understanding being that they give the city identity and character. Since the building enhances the traditional use of timber, with a modernized form of the facade, it may be a well-functioning architectural solution for Oslo. The expression of the building is blending the future and the past together.

Due to the great height of skyscrapers, they are specially prone to wind loads. Since the building is situated in an area far from a tectonic plate border, the wind loads were governing in structural stability calculations. As a combination of both the architectonic and structural aspects, it was desired to add alternations to the basic shape. Changing the geometry over the vertical height will increase the complexity of the structure. This was considered as a beneficial factor for the publics appeal of constructing a skyscraper in Oslo city center. From a structural standpoint, wind alterations will lead to an increased stability and resistance.

The following basic plan geometries were considered; rectangle, square, circular, triangular, ellipse and two polygonal shapes. After running these geometries in a primitive software wind tunnel testing and considering the sun path for the specific site; the polygonal shapes were considered as the best fit. Alterations were then added. After re-running in the software wind tunnel test, it was clear that modifications such as tapering and twisting over the vertical height, and round-offs at the corners, would increase the structures resistance to uniform wind loads.

The remaining two fundamental geometries, the hexagon and octagon, had a plan area equal to approximately 500 square meters; when including the surrounding garden space. It was of interest to model these in a BIM program and add alterations, to see how these modifications would improve the structural stability of the building. Consequently, six models were created so that the effect of tapering and twisting over the vertical height could be analyzed. Round-offs at the corners was considered as an ideal alteration to reduce the wind forces, but was discarded due to the then problematic placement of the efficient load-bearing corner columns.

The six models were designed in ETABS and analyzed for wind and seismic loads according to National Standards. The results were then compared, to see which model was best fitted to withstand the site specific loads. From the results, it is possible to conclude that the alterations generated beneficial effects for wind loads, but increased the acceleration under earthquake loads. This was due to lower mass for the uppermost stories, as a consequence of the tapering effect over the height.

Under the analysis, the governing load combinations were in serviceability state, and the behavior had to be within certain threshold for occupant comfort. For wind loads these were; total lateral displacement and acceleration. For the seismic conditions it was the inter-story drift ratio. When adding alterations, the displacement and drift ratio decreased with increasing alterations. The acceleration under wind loads was equivalent for all the models, while the seismic acceleration increased with increasing alterations due to the increased fundamental frequency.

Concluding, modifications to the basic geometry increased the resistance against the governing loads applied. Due to optimization of the composite columns and the tapering modification, the alterations also reduced the total volume of load-bearing elements. When considering the combination of all the results from ETABS, the octagonal tapered and twisted structure was the most optimized against the site specific loads in Oslo, Norway.

This master thesis covers only the conceptual design stage. Consequently, analysis and results for the slabs, beams and columns are not covered extensively. The results are from wind loads according to NS-EN 1991-1-4, which is largely based on static and dynamic loading. Wind tunnel testing is required to obtain the actual aerodynamic behavior of the wind and its influence on the structure.

BIBLIOGRAPHY

- Ábalos, I. and Herreros, J. (2003), *Tower and Office: From Modernist Theory to Contemporary Practice*, first edn, MIT Press, Cambridge, Mass.
- Al-Chalabi, M. (2015), ‘Vertical farming: Skyscraper sustainability?’, *Sustainable Cities and Society* **18**, 74 – 77.
URL: <http://www.sciencedirect.com/science/article/pii/S2210670715000700>
- Alaghmandan, M. and Elnimeiri, M. (2013), ‘Reducing impact of wind on tall buildings through design and aerodynamic modifications (architectural and structural concepts to mitigate wind effect on tall buildings)’, *American Society of Civil Engineers* **3-5**.
- Amin, J. A. and Ahuja, A. K. (2010), ‘Aerodynamic modifications to the shape of the buildings: a review of the state-of-the-art’, *Asian Journal of Civil Engineering (Building and Housing)* **11**(4), 433–450.
- Architecture Magazine (2015), ‘Turning torso’.
URL: <http://www.architectmagazine.com/project-gallery/turning-torso>
- Beretero, V. V., Anderson, J. C., Krawinkler, H. and Miranda, E. (1991), Design guideline for ductility and drift limits: Review of state-of-the-art in ductility and drift-based earthquake-resistant design for buildings, Technical Report UCB/EERC 91/15, University of California at Berkeley.
- Bing, L. (2016), Wind effects and wind load. Lecture notes from CV6108: Tall Buildings at Nanyang Technological University.
- Butler, C., Butler, E. and Orians, C. M. (2012), ‘Native plant enthusiasm reaches new heights: Perceptions, evidence, and the future of green roofs’, *Urban Forestry Urban Greening* **11**(1), 1 – 10.
URL: <http://www.sciencedirect.com/science/article/pii/S1618866711000951>
- CEN, ed. (2002), *NS-EN 1990 Eurocode 0: Basis of Structural Design*, Norsk Standard, Brussels.
- CEN, ed. (2005), *NS-EN 1991-1-4 Eurocode 1: Actions on structures - Part 1-4: General actions. Wind actions*, Norsk Standard, Brussels.
- CEN, ed. (2009), *NS-EN 1998-1:2004/AC:2009 Eurocode 8: Design of structures for earthquake resistance. Part 1: General rules, seismic actions and rules for buildings*, Vol. 1, Standard Norge, Brussels.

- CEN, ed. (2010), *NS-EN 1995-1-1:2004+A1:2008+NA:2010 Eurocode 5: Design of Timber Structures. Part 1-1: General Common Rules and Rules for Buildings*, Vol. 1, Standard Norge, Brussels.
- Computers and Structures, inc. (2016), *Lateral Loads Manual for ETABS 2016*, second edn, Computers and Structures, inc., USA.
- Dupré, J. (2013), *Skyscrapers*, first edn, Black Dog Leventhal : Distributed by Workman.
- Dymiotis-Wellington, C. and Vlachaki, C. (2004), Serviceability limit state criteria for the seismic assessment of r/c buildings, in '13th World Conference on Earthquake Engineering', number 2269 in '16', WCEE, Vancouver, Canada.
- Elias, H. (2004), 'Turning torso twists new life into cubism', *The Architect's Journal* **220**(8), C4-C7.
- Esteve, L., Díaz-López, O., García-Pérez, J., Sierra, G. and Ismael, E. (2002), 'Life-cycle optimization in the establishment of performance-acceptance parameters for seismic design', *Structural Safety* **24**, 187-204.
- Fecht, S. (2014), 'Tree houses', *Popular Mechanics* **191**(4), 12-12.
- Ghobarah, A., Aly, N. M. and El-Attar, M. (1997), Performance level criteria and evaluation, in 'Proceedings of the International Workshop on Seismic Design Methodologies for the Next Generation of Codes', Slovenia, pp. 207-215.
- Goldsmith, M. (1953), *The tall building: The effects of scale*, Architectural, Illinois Institute of Technology, Chicago, Illinois.
- Herzog de Meuron (2016), 'Triangle'.
URL: <https://www.herzogdemeuron.com/index/projects/complete-works/301-325/307-triangle.html>
- Honfi, D. (2013), *Design for Serviceability - A probabilistic approach*, Paper, Lund University, Sweden.
- Høydahl, E. (2010), 'Befolkningsvekst rundt oslo', *Statistics Norway* **5**(6).
URL: <https://www.ssb.no/befolkning/artikler-og-publikasjoner/befolkningsvekst-rundt-oslo>
- Iglebæk, O. (2012), 'Høyhus i norden - til begjær og besvær!', *Plan* **44**(6), 28-33.
- ISO, ed. (2003), *ISO 2631: Mechanical vibration and shock. Evaluation of human exposure to whole-body vibration. Part 2: General requirements*, Vol. 1, International Standard ISO, International Standard ISO, ISO 2631-1:2003(E).
- ISO, ed. (2007), *ISO 10137: Bases for Design of Structures - Serviceability of Buildings and Walkways Against Vibrations*, Vol. 1, International Standard ISO, International Standard ISO, ISO 10137:2007(E).

- Iwasa, Y. and Hayashida, H. (1990), ‘Aerodynamic shape effects of tall building for vortex induced vibration’, *Wind Engineering and Industrial Aerodynamics* **1**(33), 237–242.
- Jacobs, J. (1961), *The Death and Life of Great American Cities*, 10 edn, Pimlico 2000.
- Jernbaneverket (2012), Planforslag til plan- og bygningsetaten (pbe) 22. juni 2012, Reguleringsplan UOS-00-A-36030, Jernbaneverket.
- Kartverket (2017), ‘Kartkatalogen-geodata’.
URL: <http://www.kartverket.no/Kart/>
- Kwok, K., Burton, M. and Abdelrazaq, A. (2015), *Wind-Induced Motion of Tall Buildings - Designing for Habitability*, Vol. 22, 22 edn, American Society of Civil Engineers (ASCE).
- Le Corbusier (1989), *Towards a New Architecture*, thirteenth edn, Butterworth Architecture, London.
- Moelven (2015), *Karakteristiske fasthet- og stivhetsegenskaper for gran og trykkimpregnert limtre*, Moelven, Oslo.
- Møller, C. F. (2015), ‘HSB 2023 Västerbroplan’.
URL: <http://www.cfmoller.com/p/HSB-2023-Vasterbroplan-i3048.html>
- Mwafy, A., Elnashai, A., Sigbjörnsson, R. and Salama, A. (2006), ‘Significance of severe distant and moderate close earthquakes on design and behavior of tall buildings’, *Structural Design of Tall and Special Buildings* **15**(4), 391–416.
- Pignataro, M. A., Lobaccaro, G. and Zani, G. (2014), ‘Digital and physical models for the validation of sustainable design strategies’, *Automation in Construction* **39**, 1 – 14.
URL: <http://www.sciencedirect.com/science/article/pii/S0926580513002094>
- Plan- og bygningsetaten (2016), ‘Nå blir det liv i bjørvika’.
URL: <http://byplanoslo.no/content/na-blir-det-liv-i-bjorvika>
- Powerhouse (2017), ‘Energy positive buildings’.
URL: <http://www.powerhouse.no/en/energy-buildings/>
- Saint-Pierre, C., Becue, V., Diab, Y. and Teller, J. (2010), Case study of mixed-use high-rise location at the greater paris scale, in C. A. Brebbia, S. Hernández and E. Tiezzi, eds, ‘The Sustainable City VI’, Vol. Ecology and Environment, WIT Press, Rio, pp. 251–262.
- Saito, T., Abe, S. and Shibata, A. (1996), Reliability based seismic design criteria for reinforced concrete buildings in japan, in ‘CD-ROM Proceedings of the Eleventh World Conference on Earthquake Engineering’, number 758, Acapulco, Japan.
- Simiu, E. and Scanlan, R. H. (1996), *Wind Effects on Structures: Fundamentals and Applications to Design*, Vol. 10, third edn, John Wiley Sons, Inc.

Sing-Ping, C. (2016), Introduction to composite construction. Lecture notes from CV6107: Behavior and Design of Steel and Composite Structures.

Statnett (2017), 'Data fra kraftsystemet: import og eksport'.

URL: <http://www.statnett.no/Kraftsystemet/Data-fra-kraftsystemet/Import-og-eksport/>

U.S. Department of Energy's Building Technologies Office (1991), 'Energyplus: Energy simulation program'.

URL: https://energyplus.net/weather-location/europe_wmo_region6/NOR//NOR_Oslo.Fornebu.01

Yu, Y. (2016), Seismology and earthquakes. Lecture notes from CV6103: Structural Dynamics.

APPENDIX *A*

The following Appendix includes calculations to find the mean wind speed at the site, and the two alternative methods to calculating the forces acting upon the envelope structure due to the wind loads. Vortex shedding and wake buffeting is also studied, to see if they are a concern for the building. The Appendix uses NS-EN 1991-1-4 and the corresponding National Annex for the calculations (CEN, 2005). The referencing equations and sections from Eurocode are shown in *slanted writing*, while the numbering according to this thesis is shown in regular font.

A.1 Mean Wind Calculations

A.1.1 Basic Wind Velocity

The reference value of the basic wind velocity, v_b , shown in Equation A.2, is the characteristic 10 minutes mean wind velocity at 10 meters above ground, in an open terrain. Reference values of wind velocity are determined with annual probability of exceedance equal to 0.02, which is equivalent to a mean return period of 50 years (CEN, 2005).

The mean wind speed is dependent of the height above ground, denoted z . Near ground, the mean wind velocity is decreasing much due to frictional forces caused by the terrain. It is equal to zero at the ground level. At heights above 10 meters the wind speed is increasing, until reaching the boundary layer. The thickness of the boundary layer, or gradient height, depends on the ground roughness. The larger the roughness, the larger the gradient height (CEN, 2005). At the boundary layer and after, the wind speed is constant. The wind speed has a parabolic relationship with the height.

$$v_{b,0} = 22 \text{ m/s} \quad (\text{A.1})$$

$$v_b = c_{dir} \times c_{season} \times c_{alt} \times c_{prob} \times v_{b,0} \quad (\text{A.2})$$

Reference values based on the 50 year return period are used to find the basic wind speed. The reference value is denoted $v_{b,0}$, and is shown in Equation A.1, *from Table NA.4(901.1) for Oslo in the National Annex*. When taken into account the local site factors it is possible to calculate the basic wind speed, v_b , as shown in

Equation A.2, from *NS-EN 1991-1-4 Equation (NA.4.1)*. The required parameters to calculate Equation A.2 are found in Table A.1.

Description of factor	Site considerations	Input value
Height above water level	Site at sea level	$c_{alt} = 1.0$
Directional factor	Conservative to use 1.0	$c_{dir} = 1.0$
Seasonal factor	Winter months <i>NA.4.2(2P(901.3))</i>	$c_{season,winter} = 1.0$
Seasonal factor	Summer months <i>NA.4.2(2P(901.3))</i>	$c_{season,summer} = 0.8$
Return period factor	Use return period of 50 years	$c_{prob} = 1.0$

Table A.1: Site factors that alter the basic wind speed

Due to the seasonal factor, there will be one basic wind speed for the winter months, Equation A.3, and another for the summer months, Equation A.4.

$$v_{b,1} = c_{dir} \times c_{season} \times c_{alt} \times c_{prob} \times v_{b,0} = 22 \text{ m/s} \quad (\text{A.3})$$

$$v_{b,2} = c_{dir} \times c_{season} \times c_{alt} \times c_{prob} \times v_{b,0} = 17.6 \text{ m/s} \quad (\text{A.4})$$

A.1.2 Mean Wind Speed

The mean wind velocity $v_m(z)$ is varying with height, z . This is not the same as the basic wind speed derived above since it also accounts for the terrain, orography and the building height. The equation to calculate the mean wind speed is given in Equation A.5, from *NS-En 1991-1-4 Equation (4.3)*.

$$v_m(z) = c_r(z)c_0(z)v_b \quad (\text{A.5})$$

Terrain roughness is in category four, according to *Annex A, Figure A.1*. This is for city area with at least 15 percent of the area covered by buildings where the building height is over 15 meters (CEN, 2005). There might be lower percentage of tall buildings this current day, but most likely the area will be under development during the next decades. It is assumed that the building is located 5 meters above sea level.

Description of factor	Site considerations	Input value
Roughness length	Table NA.4.1 for category IV	$z_0 = 1.0$ m
Minimum height	Table NA.4.1 for category IV	$z_{min} = 16$ m
Terrain factor depending on z_0	Table NA.4.1 for category IV	$k_r = 0.24$
Maximum height	Taken from Equation (4.5)	$z_{max} = 200$ m

Table A.2: Site factors that alter the mean wind speed

From Equation A.5 it is necessary to determine the parameters $c_r(z)$ and $c_0(z)$. The $c_r(z)$ takes into account the ground roughness and is given in Equation A.6 and Equation A.7, depending on the location of z , from Equation (4.3). For the values of $z < z_{min} = 16$ m.

$$c_r(z) = c_r(z_{min}) = k_r \times \ln\left(\frac{z_{min}}{z_0}\right) = 0.24 \times \ln\left(\frac{16}{1}\right) = 0.6654 \quad (\text{A.6})$$

For the values of $z_{min} < z < z_{max}$

$$c_r(z) = k_r \times \ln\left(\frac{z}{z_0}\right) = 0.24 \times \ln\left(\frac{z}{1}\right) \quad (\text{A.7})$$

The c_0 - value expresses the terrain orography and takes into account the increase in wind velocity due to terrain. It is assumed that Ekeberg hill, close to the site, is far enough away from the site. Consequently, we have $c_0 = 1.0$. The mean wind speed variation over the height is shown in Figure A.1, for both the winter and the summer months.

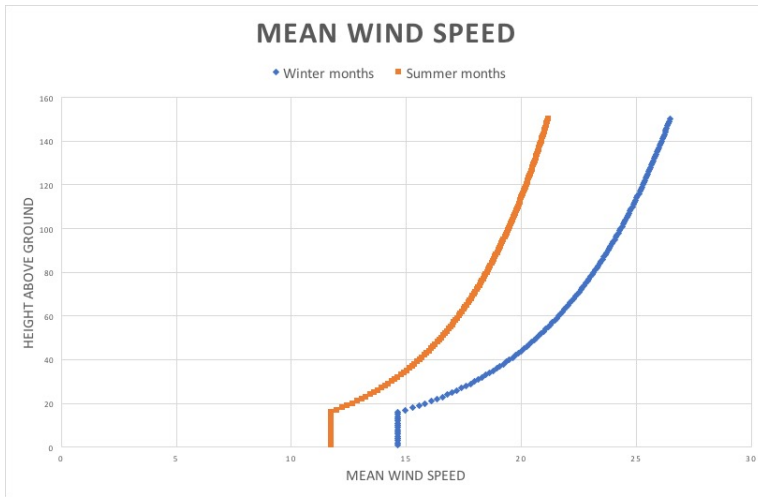


Figure A.1: Mean wind speed, $v_m(z)$

A.2 Peak Velocity Pressure

A.2.1 Wind Turbulence

The turbulence intensity, $I_v(z)$, is defined as the standard deviation of the turbulence by the mean wind velocity over the height. The standard deviation of the turbulence σ_v , given in Equation (4.6) with the recommended value $k_l = 1.0$, is calculated for both winter and summer months. The general equation is shown in Equation A.8, while the calculations for the winter and summer months is shown in Equation A.9 and Equation A.10 respectively.

$$\sigma_v = k_r v_b k_l \quad (\text{A.8})$$

$$\sigma_{v,1} = k_r v_b k_l = 0.24 \times 22 \times 1.0 = 5.28 \text{ m/s} \quad (\text{A.9})$$

$$\sigma_{v,2} = k_r v_b k_l = 0.24 \times 17.6 \times 1.0 = 4.22 \text{ m/s} \quad (\text{A.10})$$

The turbulence intensity, given by Equation (4.7), is expressed in two equations, depending on the height of z . Equation A.11 expresses the turbulence intensity when $z < 16 \text{ m}$. Equation A.12 expresses the turbulence intensity for greater heights. For $z < z_{min}$

$$I_v(z) = I_v(z_{min}) = \frac{\sigma_v}{v_m(z_{min})} \quad (\text{A.11})$$

For $z_{min} < z < z_{max}$

$$I_v(z) = \frac{\sigma_v}{v_m(z)} \quad (\text{A.12})$$

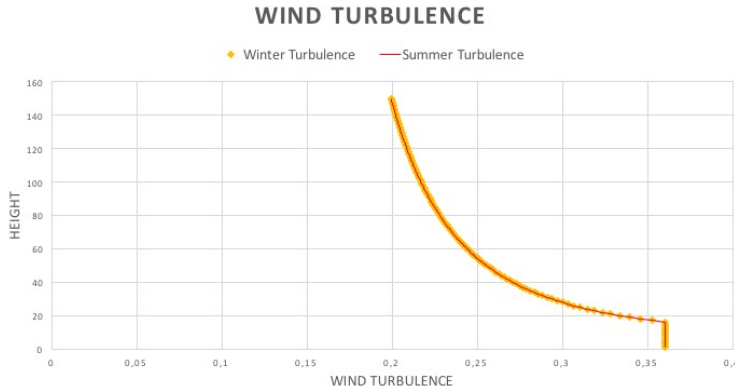


Figure A.2: Wind turbulence over the height, $I_v(z)$

As seen in Figure A.2, the variation of the turbulence intensity between the summer and winter months is negligible.

A.2.2 Peak Velocity Pressure

The peak velocity pressure includes both the fluctuating short-term velocity and the mean, *given in Equation (4.8)*, shown here in Equation A.13.

$$q_p(z) = 0.5\rho v_m^2(z) \times (1 + 2k_p I_v(z)) \quad (\text{A.13})$$

The density of the air is dependent on the temperature and pressure but can be taken as $\rho = 1.25 \text{ kg/m}^3$. The top factor is set to $k_p = 3.5$.

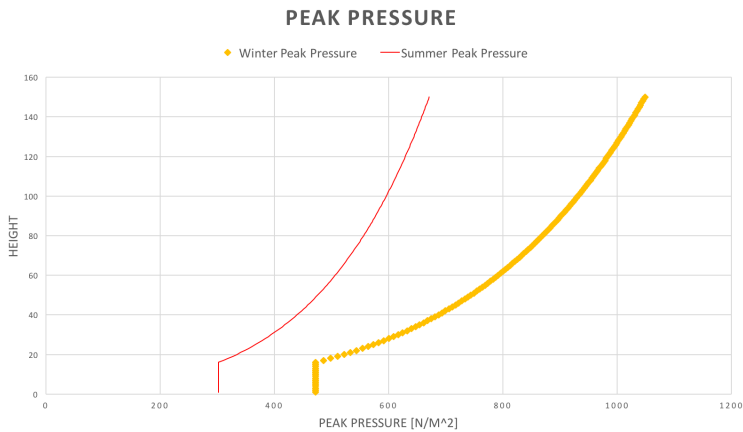


Figure A.3: Peak velocity pressure over the height, $q_p(z)$

The results for the peak pressure is shown in Figure A.3. It shows that there is a large deviation between the winter and summer months in the pressure acting over the height. The wind pressure is considerable greater in in winter months.

A.3 Wind Actions

A.3.1 Wind Pressure on External Surfaces

To find the external pressure it is necessary to determine the reference height. The wind pressure equation is shown in Equation A.14, *obtained from equation (5.1)*.

$$w_e = q_p(z_e)c_{pe} \tag{A.14}$$

Since this is a high-rise building we have that $h > 2b$. The pressure is then assumed subdivided into three parts, where the top and bottom height is uniform with a midsection that is increasing by linear subparts, from *Figure (7.4) (CEN, 2005)*, shown here in *Figure A.4*.

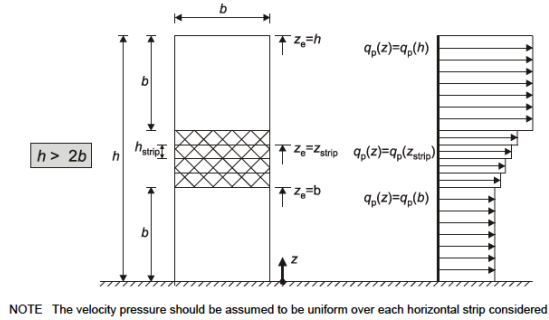


Figure 7.4 — Reference height, z_e , depending on h and b , and corresponding velocity pressure profile

Figure A.4: Wind profile over the height (CEN, 2005)

To be able to construct the correct wind profile and further calculations, it is necessary to implement the geometrical values of the structures; shape, width and height. The value of the pressure coefficients, c_{pe} , are determined by the geometry of the building. Since the surface area is larger than 10 m^2 , it is correct to use $c_{pe,10}$ instead of $c_{pe,1}$, from *Figure (7.2) in NS-EN 1991-1-4*.

A.3.2 Calculation of $c_s c_d$

Two different methods were used to calculate the wind forces on the structure. For the first alternative of calculation, the structure is subdivided into segments, and one calculates the forces for each of these segments separately. The axial forces on the structure is given in Equation A.15, from *Equation (5.3)*.

$$F_w = c_s c_d q_p(z_e)c_{pe,10}A_{ref} \tag{A.15}$$

The second alternative is to have a summarized total wind force over the structure. This method is in a larger extent based on the geometry of the structure. The total force F_w is given in Equation A.16, from *Equation (5.4)*.

$$F_w = c_s c_d \sum_{elements} c_f q_p(z_e) A_{ref} \quad (\text{A.16})$$

For both methods it is necessary to calculate the value of $c_s c_d$, which is a structural factor. The factor $c_s c_d$ takes into account the effect of wind actions from the non-simultaneous peak wind pressures and the effect of vibrations of the structure due to turbulence (CEN, 2005).

The equation to determine $c_s c_d$, given in Equation (6.1), is only valid if the structure corresponds to one of the basic building shapes, from Figure 6.1, and if the along-wind vibration in the fundamental mode is significant, stated in 6.3.1(2)P. These requirements are considered to be fulfilled. Resulting in the factor being computed by Equation A.17, from Equation (6.1).

$$c_s c_d = \frac{1 + 2k_p I_v(z_s) \times \sqrt{B^2 + R^2}}{1 + 7I_v(z_s)} = \frac{1 + 2 \times 3 \times 0.2337 \times \sqrt{0.534 + 2.464 \times 10^{-6}}}{1 + 7 \times 0.2337} = 0.7614 \quad (\text{A.17})$$

Description of parameter	Considerations	Input value
Reference height for structural factor	From Figure 6.1, $H < \frac{z_{max}}{0.6} = 333$ meters	$z_s = 0.6h = 73.2$ m
Reference height	Given in Equation (B.1)	$z_t = 200$ m
Reference length scale	Given in Equation (B.1)	$L_t = 300$ m
Turbulence intensity at reference height z_0	$L(z_s)$ from Equation (B.1)	$L_z(z_s) = 151.30$
Background factor due to lack of correlation of the pressure on structure	From Equation (4.5)	$B^2 = 0.534$
Fundamental frequency estimate	Using Equation (F.2), $H > 50$ m	$n_1 = 46/h = 0.3833$
Non-dimensional frequency	Given by Equation (B.2)	$f_L(z_s, n) = 3.2106 \text{ s}^{-1}$
Non-dimensional power spectral density function	Given by Equation (B.2)	$S_L(z_s, n) = 0.0619$
Resonance response factor due to turbulence	Taken from Equation (B.6)	$R^2 = 2.464 \times 10^{-6}$
Peak factor. Ratio of maximum fluctuating part of response and its standard deviation	From Equation (B.4)	$k_p = 3.0$

Table A.3: Parameters used to calculate $c_s c_d$

Values used to calculate $c_s c_d$ in Equation A.17, are given in Table A.3. The calculated values are shown for the winter months, which is governing compared to the summer months. The calculations used a rough estimate of the mass per unit height of the building by considering the main concrete and timber elements.

A.3.3 Wind Force Calculations Using Method 1

When using Equation A.15, it is necessary to determine the external pressure coefficients and height of each uniform loaded area. The facade is subdivided into five parts, where the windward side is denoted D, and the leeward side is denoted E. The facade surfaces that are parallel with the wind direction are divided into three segments per face; denoted A, B, and C. The $c_{pe,10}$ - values and width of each segment is shown in Table A.4.

Facade face	Input value $c_{pe,10}$	Width of area
Windward facade	$c_{pe,10,D} = 0.8$	24 m
Side facade closest to windward side	$c_{pe,10,A} = -1.2$	9.6 m, both sides included
Middle side section facade	$c_{pe,10,B} = -0.8$	38.4 m, both sides included
Side facade closest to leeward side	$c_{pe,10,C} = -0.5$	0 m
Leeward side facade	$c_{pe,10,E} = -0.7$	24 m

Table A.4: Parameters used to calculate w_e

The results for the wind forces are varying over the height and the calculations are shown in Figures A.5-A.8.

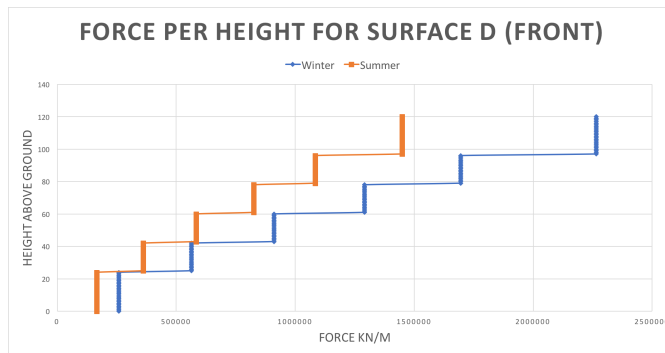


Figure A.5: Wind profile over the height for surface D

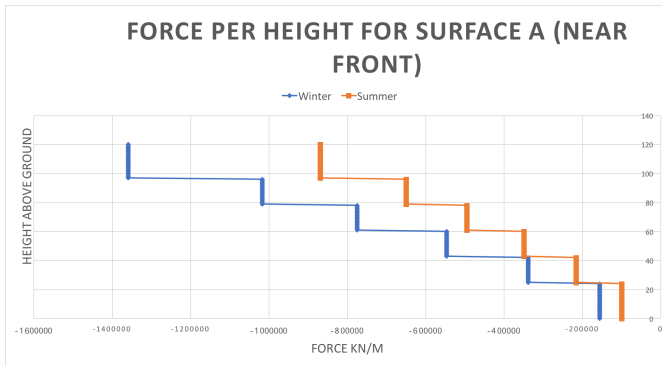


Figure A.6: Wind profile over the height for surface A

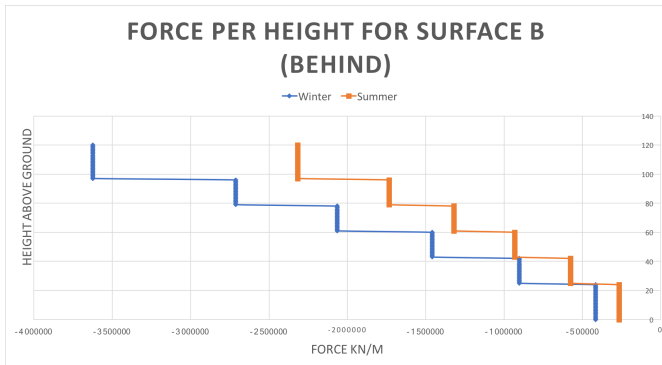


Figure A.7: Wind profile over the height for surface B

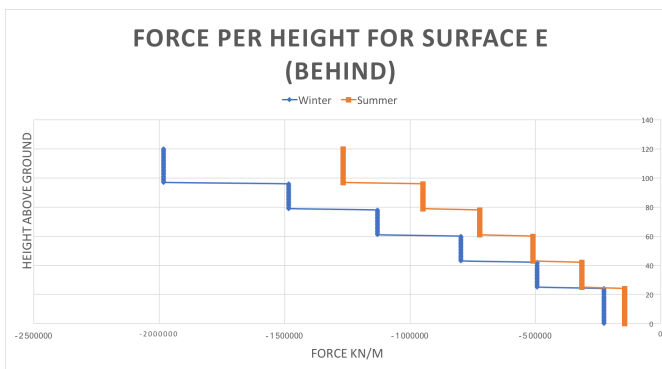


Figure A.8: Wind profile over the height for surface E

A.3.4 Wind Force Calculations Using Method 2

This method calculates the resultant force over the whole structure based on values of $c_s c_d$ and c_f . To calculate the value of c_f , it is necessary to take into account the general plan geometry and the Reynolds number. The Reynolds number is a dimensionless velocity that takes into account the surface texture. The value Re is determined by Equation A.18, from Equation (7.15).

$$Re = \frac{b \times v_m(z_e)}{\nu} \tag{A.18}$$

The result is $Re = 40.4 \times 10^6$ for summer months, and $Re = 32.4 \times 10^6$ for the winter months. Consequently, the values are larger than 3×10^5 , leading to $c_{f,0,hexagon} = 1.60$ and $c_{f,0,octagon} = 1.30$, from Table 7.11 (CEN, 2005). When multiplying this value with the end-effect factor, defined by Figure 7.36 and Table 7.16, one achieves the values of $c_{f,hexagon} = 1.456$ and $c_{f,octagon} = 1.001$. The wind force over the structure height is shown in Figure A.9 and Figure A.10 for the two different plan geometries. These method generates greater positive values for the wind force acting on the structure than method 1.

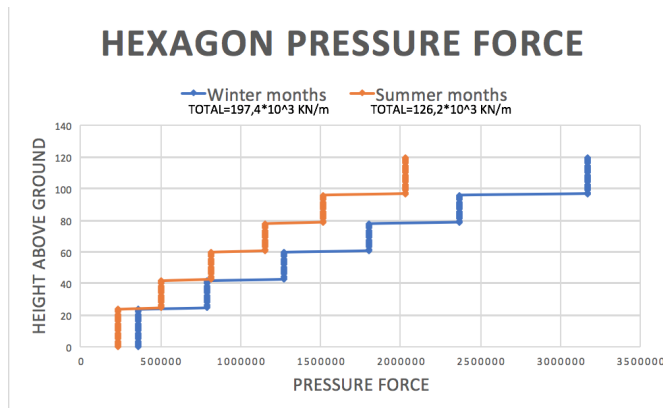


Figure A.9: Wind profile over the height for hexagon

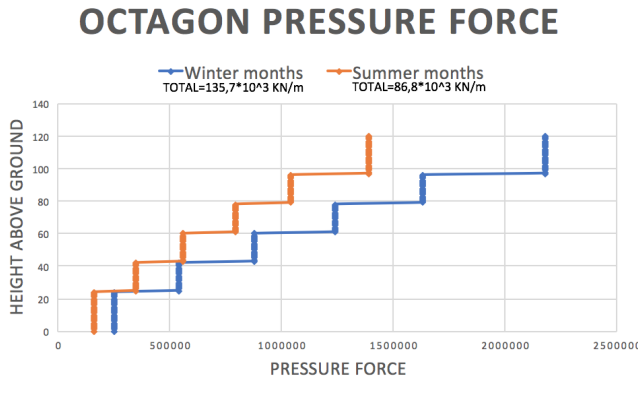


Figure A.10: Wind profile over the height for octagon

A.4 Wake Buffeting

For slender buildings; defined as $h/b > 4$, it is necessary to take into account the effect of increased turbulence in the wake of nearby structures, *stated in Section 6.3.3*. This is only applicable when the site has more than one tall structure. Therefore, this aspect is not further examined since this structure is situated at a site with considerably lower buildings. This conceptual design thesis also focuses only on constructing one building at the site.

A.5 Vortex Shedding

Vortex shedding are vortices that are generated at the leeward side of the structure. This effect creates fluctuations of the wind pressure. If Equation A.19 is satisfied, it is not necessary to investigate the vortex shedding effect, *as stated in Equation (E.1) in NS-EN 1991-1-4*.

$$v_{crit,1} > 1.25v_m = 31.60 \text{ m/s} \quad (\text{A.19})$$

In Equation A.19, the mean velocity is implemented as the value obtained for the top of the building, which is the largest value. Consequently, it is the most conservative to implement.

$$v_{crit,1} = \frac{b \times n_{l,0}}{S_t} = \frac{24 \times 0.3833}{0.18} = 55.37 \text{ m/s} \quad (\text{A.20})$$

Equation A.20 shows the implemented values of the critical velocity, with an assumed fundamental frequency. As shown, the value is greater than the product of $1.25v_m$.

As a result, vortex shedding will not occur. In Equation A.20, the Strouhal number, S_t , is for cylinder structures, *taken from Table E.1*.

It is however worth mentioning that even though the procedure in NS-EN 1991-1-4 results in the structure not having vortex shedding, it is likely that vortex shedding to at least some degree will occur. Further theories and references for these assumptions are given in Chapter 4.

APPENDIX *B*

This Appendix includes the calculations for achieving the correct dynamic acceleration of the building due to wind loads. The wind induced acceleration is calculated for all the six models that were designed in ETABS, but the procedure is shown for the octagon model that is tapered and twisted. The final calculated result for each building is shown in Chapter 9. The calculation method takes into account the dynamic response by using the mass per story and fundamental frequencies of the building as parameters from ETABS. The method is retrieved from NS-EN 1998-1 and the corresponding National Annex. The method takes dynamic parameters to compute a static acceleration (CEN, 2009). The referencing equations and sections from Eurocode are shown in *slanted writing*, while the numbering according to this thesis is shown in regular text.

B.1 Wind Acceleration Calculations

A buildings response to wind loading is limited by the serviceability requirements. The limitations are with respect to human comfort, and general building sway and motion. The wind induced acceleration is a referencing value of the human comfort. In this Appendix the accelerations are calculated for the first fundamental frequency.

The octagonal tapered and twisted building has the dynamic response with the first natural modal period equal to 4.13 seconds, and the first fundamental frequency equal to 0.242 s^{-1} . These values were retrieved from the ETABS analysis. The acceleration is only calculated for the first mode, since this is the mode with the lowest period and can be considered as the governing mode.

The characteristic peak acceleration is given in Equation B.1, *from in Section 6.3.2(1) in NS-EN 1991-1-4 by using Annex B and Equation B.4(4) (CEN, 2005)*.

$$a_{char,peak} = \sigma_{a,x}(z) \times k_p \quad (\text{B.1})$$

The peak acceleration, Equation B.1, is determined by using the natural frequency as upcrossing frequency $v = n_{1,x} = 0.242$. The standard deviation of the acceleration

is given by Equation B.2, *from Equation (B.10)*. As stated in Chapter 4, the standard deviation can lead to varying peak accelerations. Thus, depending on the method used, the results retrieve different peak accelerations. This is one of the main errors and difficulties with using coded calculations for the structures response to earthquake motion.

$$\sigma_{a,x} = R \times K_x \times \Phi_{1,x}(z) \times \frac{c_f \times \rho \times b \times I_v(z_s) \times v_m^2(z_s)}{m_{1,x}} \quad (\text{B.2})$$

The peak factor, k_p , is obtained from Equation B.3, *form Equation (B.4) (CEN, 2005)*. The averaging time for the mean wind velocity is set to $T = 600$ s, *given in Equation (B.4)*.

$$k_p = \min \left(3.0 \text{ and } \sqrt{2 \ln(v \times T) + \frac{0.6}{\sqrt{2 \ln(v \times T)}}} \right) \quad (\text{B.3})$$

As a result, the peak factor is equal to; $k_p = \max(3.0 \text{ and } 3.3456)$. Thus, it is set to $k_p = 3.3456$.

B.1.1 Calculation of the Standard Deviation

Table B.1 shows the required values to calculate the standard deviation according to NS-EN 1991-1-4 and the corresponding National Annex. The values in Table B.1 also implement the results retrieved from ETABS.

Calculation parameter	Abbreviation	Value
Air density, <i>from Section 4.5(1)</i>	ρ	1.25 kg/m ³
Fundamental frequency for model	$n_{1,x}$	0.242 s ⁻¹
Reference height, <i>using figure 6.1</i>	z_s	73.2 m
Roughness length, <i>given in Table 4.1</i>	z_0	1.0 m
Minimum height, <i>defined by Table 4.1</i>	z_{min}	16 m
Maximum height, <i>from Eq. (4.5)</i>	z_{max}	200 m
Reference height, <i>from Eq. (B.1)</i>	z_t	200 m
Reference length scale, <i>from Eq. (B.1)</i>	L_t	300
Width of the building	b	26.4 m
Height of the building	h	122 m
Turbulent length scale, <i>from Section B.1(1)</i>	$L_{z,s}$	152.9867
Mean wind velocity, <i>from Section 4.3.1(1)</i>	$v_{m,z,s}$	22.6680 m/s
Turbulence intensity, <i>from Section 4.4(1)</i>	$I_{v,z,s}$	0.23293
Background factor, <i>from Eq. (B.3)</i>	B^2	0.53109

Table B.1: Values form NS-EN 1991-1-4

A Calculation of the Non-Dimensional Coefficient and Equivalent Mass

To compute the calculations for the standard deviation, $\sigma_{a,x}$, it was necessary to calculate the non-dimensional coefficient, K_x , given in Equation B.4, *from Equation (B.11)*.

$$K_x = \frac{\int_0^h v_m^2(z) \times \Phi_{1,x}(z) dz}{v_m^2(z_s) \times \int_0^h \Phi_{1,x}^2(z) dz} \quad (\text{B.4})$$

However, due to the flat terrain at the site location, giving $c_0 = 1.0$, and that the fundamental mode shape can be calculated from, $\Phi_1(z) = (\frac{z}{h})^\zeta$, the equation can be generalized to Equation B.5, *from Equation (B.12)*.

$$K_x = \frac{(2\zeta + 1) \left\{ (\zeta + 1) \left[\ln\left(\frac{z_s}{z_0}\right) + 0.5 \right] - 1 \right\}}{(\zeta + 1)^2 \times \ln\frac{z_s}{z_0}} \quad (\text{B.5})$$

The fundamental mode shape may be calculated using Equation B.6, *from Annex F.3 Equation (F.13)*.

$$\Phi_1(z) = \left(\frac{z}{h}\right)^\zeta = \left(\frac{z}{122}\right)^\zeta \quad (\text{B.6})$$

The values were computed for each vertical meter, z . The component ζ was set to 1.5, since the building can be seen as a slender cantilever with a concrete core,

stated in Section F.3(1). This led to the calculated value of the non-dimensional coefficient, $K_x = 1.41659$.

Corresponding, the equivalent mass per unit length was integrated for each meter using Equation B.7, from Equation (F.14). Here, the actual mass per story is retrieved from ETABS for all of the six models.

$$m_e = \frac{\int_0^l m(s) \times \Phi_1^2(s) ds}{\int_0^l \Phi_1^2(s) ds} \quad (\text{B.7})$$

The resulting equivalent mass per unit length, m_e , was calculated by using the trapezoidal method for numerical integration in Excel. The mass was equal to 63454.85 kilograms per unit height for the octagon model that was tapered and twisted.

However, it is also possible to use a simplified method, stated in Section F.4(2). This is when a building can be simplified to a cantilever structure. Then, the equivalent mass can be approximated as the average mass of the upper third of the structure. This method gave the average mass per unit length equal to 67737.63 kilograms. Both methods were used to calculate the acceleration, and the results were then compared.

B Calculation of c_f

The force coefficient, c_f , is determined by Equation B.8, from Equation (7.19).

$$c_f = c_{f,0} \times \omega_\lambda \quad (\text{B.8})$$

The free-end flow force, $c_{f,0}$ -coefficient, is determined by the shape of the plan section. The structures have no roundness to the sharp corners and they have Reynolds number larger than $Re > 2 \times 10^5$. Consequently, it leads to the octagonal structures free-end force coefficient being set to $c_{f,0} = 1.30$, from Table (7.11).

The value of ω_λ is determined from the effective slenderness λ , from Figure (7.16). With an octagonal plan shape and a height over 50 meters, the effective slenderness is equal to $\lambda = 1.4 \times h/b = 6.470$. The value of the end-effect factor is $\omega_\lambda = 0.68$. This is due to the solidity ratio being equal to 1.0 since it is a closed building, from Figure (7.36).

Consequently, the value of the force coefficient, from Equation B.8 is $c_f = 0.68 \times 1.30 = 0.884$.

C Calculation of R^2

The value of R^2 determines the resonance response factor due to turbulence in the vibration mode. Equation B.9 expresses the equation to determine the value, *from Equation (B.6)*. The values shown in Table B.2 were necessary for the calculation of Equation B.9.

$$R^2 = \frac{\pi^2}{2\delta} \times S_L(z_s, n_{1,x}) R_h(\eta_h) R_b(\eta_b) \quad (\text{B.9})$$

Calculation parameter	Abbreviation	Value
Total logarithmic decrement of damping given in Section F.5	δ	0.05
Non-dimensional power spectral density function, Eq. (B.2)	$S_L(z_s, n_{1,x})$	0.0927
Calculating value for Eq. (B.8)	η_b	1.2965
Calculating value for Eq. (B.7)	η_h	5.9913
Aerodynamic admittance function for width, Eq.(B.8)	R_b	0.4961
Aerodynamic admittance function for height, Eq. (B.7)	R_h	0.1530

Table B.2: Values to determine R^2

Concluding, the calculated value from Equation B.9 was $R^2 = 0.69468$.

B.1.2 Results of the Acceleration

The peak acceleration was calculated for both methods to determine the equivalent unit mass values, as shown in Table B.3.

Calculation method	Abbreviation	Value
Method with integrated equivalent mass	$a_{char,peak,1}$	0.206 m/s^2
Method with simplified equivalent mass	$a_{char,peak,2}$	0.198 m/s^2

Table B.3: Results for acceleration calculation

The results in Table B.3 show the acceleration at the top of the building, $z = H = 122 \text{ m}$, for the octagon model that was tapered and twisted. The height $z = 122 \text{ m}$, is where the largest acceleration will occur. Comparison of these values to the required thresholds given in ISO 10137 and ISO 2631-1, are given in Chapter 9. The results in Table B.3 show that since the simplified method for calculating the equivalent mass had a larger mass, the structure becomes stiffer, leading to a lower amount of acceleration in the building.

APPENDIX C

This Appendix covers the manual calculations of the glue laminated timber elements. The elements that were focused on were considered to be the elements with the largest values of applied forces. As a result, only the exterior columns and the truss system was looked at, as shown in Figure C.1. The manual calculations are for the octagon model that is tapered and twisted. This model has the exterior columns twisting over the vertical height, a situation that is more prone to forces than the un-twisted models. The calculations in this appendix include biaxial bending, compression stresses, tension stress, shear stress, and second order effects. The equations and material factors are retrieved from NS-EN 1995-1 and the glue laminated timber handbook from Moelven (CEN, 2010; Moelven, 2015). The referencing equations and sections from Eurocode and The Moelven Handbook are shown in *slanted writing*, while the numbering according to this thesis is shown in regular text.

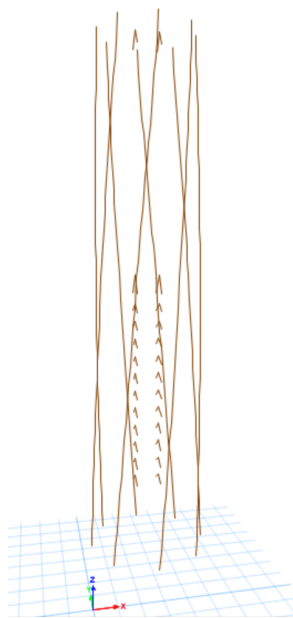


Figure C.1: Elements that were calculated

C.1 Calculations of the Glue Laminated Elements

Calculations have been computed for the rotating exterior columns and the truss system for the octagon twisted and tapered model. All are of glue laminated elements, of strength grade equal to GL32c, where the value 32 stands for the characteristic compressional strength of the material.

Using ETABS, the results from the governing ULS combinations were obtained. Each element was subdivided in ETABS into three meshed elements. The maximum moment, axial force, torsion and shear force was retrieved for each meshed element. These values were the maximum values along the entire length of the meshed element, and not only at the joints between the elements. Each meshed element has been dimensioned according to the applied forces, and the governing meshed segment determines the cross-section for the whole element. All together there were 720 meshed elements that were analyzed using Excel.

The rotating exterior columns functions as a support system for the glass curtain wall. Other than this, the columns are designed such that they do not carry a large amount of the governing loads. This leads to the elements being a secondary support system, due to the stiff concrete core and the composite columns. As a result of the desired architectonic expression of the exterior columns, the width was set to 280 mm. Leaner elements will aesthetically be unfavorable. The following cross-sectional dimensions were looked at (Moelven, 2015):

- $b \times h = 280 \times 225 \text{ mm}^2$
- $b \times h = 280 \times 270 \text{ mm}^2$
- $b \times h = 280 \times 360 \text{ mm}^2$

C.1.1 Material Property for GL32c

The design strength parameters was retrieved from Moelven AS, which is one of the main companies in Norway proucing glue laminated timber elements. The strength parameters in Table C.1 show the orthotropic material properties for glue laminated timber. When loaded parallel with the fibers, the strength and elastic properties are much larger than when forces are applied perpendicular or angled to the fibers. The parameters are retrieved from the Moelven's handbooks, *from Table 1-1* (Moelven, 2015).

Design strength parameter	Abbreviation	Value (MPa)
Bending strength	f_{md}	$19.48 \times k_h$
Tensional strength	f_{td}	$11.87 \times k_h$
Characteristic compressional strength	$f_{c,0,k}$	24.5
Compressional strength design	f_{cd}	$14.91 \times k_h$
Shear strength	f_{vd}	$2.13 \times k_h$
E-modulus for stability	$E_{0,05}$	10800

Table C.1: Strength parameters for GL32c

Table C.2 shows the parameters that were essential for further calculations. They were retrieved from NS-EN 1995-1-1 and Moelven's handbook (CEN, 2010; Moelven, 2015).

Design parameter	Reference	Value
Factor for loading period of loads	From Table 3.1 (CEN, 2010)	$k_{mod} = 0.7$
Material factor for massive wood elements	From Equation (2-8) (Moelven, 2015)	$\gamma_m = 1.25$
Correctional factor for height less than 600 mm	From Equation (3.2) (CEN, 2010)	$k_h = \min\{1.1 \text{ or } (600/h)^{0.1}\}$
Modification factor for stress for glue laminated timber	From Section 6.1.6(2) (CEN, 2010)	$k_m = 0.7$
Effective width due to cracks and moisture	From Section 4.1.1 (Moelven, 2015)	$b_{ef} = 0.8 \times b$

Table C.2: Design parameters for GL32c

C.1.2 Combined Tension and Bending Equation

The elements that were located in the uppermost part of the structures exterior underwent tensional forces. These elements were subjected to both bending about both axes and tension. Equation C.1 and Equation C.2 is calculated for each meshed element in tension, from NS-EN 1995-1-1, Equation (6.17) and Equation (6.18). The governing equation is the one where the largest bending moment is un-factored by k_m .

$$\frac{\sigma_{t,0,d}}{f_{t,0,d}} + \frac{\sigma_{m,y,d}}{f_{m,y,d}} + \frac{k_m \times \sigma_{m,z,d}}{f_{m,z,d}} \leq 1.0 \quad (\text{C.1})$$

$$\frac{\sigma_{t,0,d}}{f_{t,0,d}} + \frac{k_m \times \sigma_{m,y,d}}{f_{m,y,d}} + \frac{\sigma_{m,z,d}}{f_{m,z,d}} \leq 1.0 \quad (\text{C.2})$$

The value of k_m was set to 1.0, even though it is 0.7 for glue laminated timber. This was done since the results from ETABS showed that governing moment for each element was either in the major or minor direction, while the other then was close to zero. As a result, this was a simplified and conservative method to obtain the utilization degree of the tension loaded elements.

C.1.3 Buckling in Compression

For the elements that are subjected to compressional axial force, it is necessary to check whether the elements are prone to buckling. The critical buckling load was calculated for each story as expressed in Equation C.3, from Equation (4-16) from Moelven's handbook.

$$P_{cr} = \frac{\pi^2 \times E \times I}{(\beta \times L)^2} \quad (\text{C.3})$$

The effective length of the columns were calculated with $\beta = 0.7$, which corresponds to a column with fixed-fixed connections, shown in Figure 4-13 in Moelven's handbook (Moelven, 2015). This is the most conservative situation, and close to the one simulated in ETABS. The results showed that the critical buckling load was over five times the actual loading. Which states that buckling is not an issue.

C.1.4 Second Order Effects

For the columns in compression, first and second order effects were calculated for each element. The calculations determine the non-linear effects that should be included in the calculations. The second order moment was included along the minor axis by the expression given in Equation C.4, given in Equation (4-18) (Moelven, 2015).

$$M_2 = P \times (\delta_0 + \delta_P) = P \times \frac{L/500}{1 - (P/P_{cr})} \quad (\text{C.4})$$

Since the second order effect is a product of the axial loading and length of the columns, the moment was calculated for each meshed element. Each meshed elements length was multiplied with a factor of three to illustrate the actual length of each column. The second order effects had a factor of 10-100 times larger values than the actual bending moment retrieved from ETABS. This demonstrates that the columns can be seen as only axially loaded in the ETABS models.

C.1.5 Slenderness of the Columns

The slenderness is necessary to take into account for the columns that are loaded in compression. This is solved by determining a strength reduction factor, k_c , and adding this factor to the utilization check equations. Equation C.5 and Equation C.6 determine the slenderness of the cross section, *from Equations (6.21) and (6.22) in NS-En 1991-1-4*. For all the cross section alternatives the α_{rel} in Equation C.6 was larger than 0.3.

$$\lambda_y = \frac{\beta \times L}{i_y} \quad (\text{C.5})$$

$$\lambda_{rel} = \sqrt{\frac{P}{P_{cr}}} = \frac{\lambda_y}{\pi} \times \sqrt{\frac{f_{c,0,k}}{E_{0,05}}} \quad (\text{C.6})$$

$$k = 0.5(1 + 0.1 \times (\alpha_{rel} - 0.3) + \alpha_{rel}^2) \quad (\text{C.7})$$

$$k_c = \frac{1}{k + \sqrt{k^2 - \lambda_{rel}^2}} \text{ for } \lambda_{rel} > 0.3 \quad (\text{C.8})$$

The strength reduction due to slenderness, k_c , shown in Equation C.8 is determined by the cross section, *from Equation (6.22) (CEN, 2010)*. To be able to calculate k_c , it was necessary to calculate k , expressed in Equation C.7, *from Equation (6.21) (CEN, 2010)*.

C.1.6 Combined Compression and Bending Equation

For the elements that were subjected to both bending about both axes and compression, the utilization was checked by Equation C.9 and Equation C.10, *from NS-EN 1995-1-1 Eq.(6.23) and Eq.(6.24)*.

$$\frac{\sigma_{c,0,d}}{k_{c,y} \times f_{c,0,d}} + \frac{\sigma_{m,y,d}}{f_{m,y,d}} + \frac{k_c \times \sigma_{m,z,d}}{f_{m,z,d}} \leq 1.0 \quad (\text{C.9})$$

$$\frac{\sigma_{c,0,d}}{k_{c,z} \times f_{c,0,d}} + \frac{k_c \times \sigma_{m,y,d}}{f_{m,y,d}} + \frac{\sigma_{m,z,d}}{f_{m,z,d}} \leq 1.0 \quad (\text{C.10})$$

The second order effects, k_c , were added to the moment about the minor axis, making this the governing moment by a factor of 10-100 compared to the moment about the major axis.

C.1.7 Shear Equation

All elements were checked against the shear capacity by Equation C.11, from Equation (4.5) NS-EN 1995-1. The results showed that the shear was never governing for determining the cross section. The element with the largest shear force was subjected to 51.6 kN, This element had the cross-section; $b \times h = 280 \times 225$. Equation C.12 shows the design check for this element, equation from Equation (4-6) (Moelven, 2015).

$$\tau_d = \frac{3V}{2 \times b_{ef} \times h} \leq f_{vd} \quad (\text{C.11})$$

$$\tau_d = \frac{3 \times 51.6 \times 10^3}{2 \times 0.8 \times 280 \times 225} = 1.54 \leq f_{vd} = 2.13 \times 1.1 \quad (\text{C.12})$$

APPENDIX *D*

Results obtained in ETABS for the plain octagon model is shown in this appendix. The general layout of the model is shown in Figure D.1. From the results, and when comparing these to the other models, it is believed that the structure is modeled correctly. All the values for displacement, seismic drift and utilization are within acceptable regions. The value of the wind induced drift is not within the acceptable region.

D.1 Results from ETABS for Plain Octagon Model

D.1.1 Plan and 3D View of the Structure

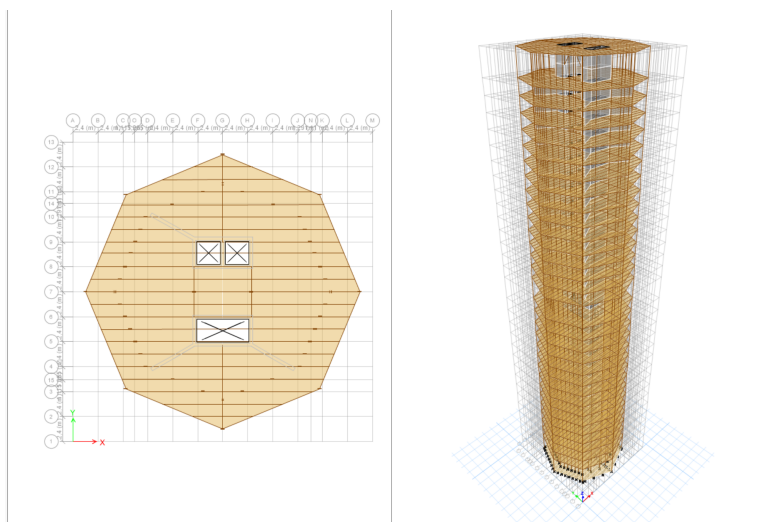


Figure D.1: Plan section and 3D view of octagon plain model

D.1.2 Utilization of Composite Columns

The model was created by re-analyzing the structure after utilization checks for the composite columns, as shown in Figure D.2 and Figure D.3. The model had an linear increase from the top in compressional forces for the composite columns. The soft stories had to have large cross section areas of the columns, due to the low amount of additional support at these floors. From the range of utilization shown in Figure D.2 and Figure D.3, it is clear that the utilization is within the applied range of 65-95% for almost all the columns.

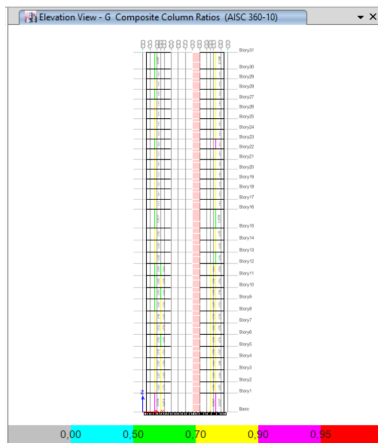


Figure D.2: Utilization degree for composite columns at elevation G for ULS wind loads

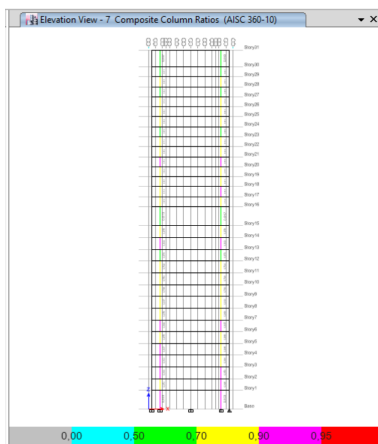


Figure D.3: Utilization degree for composite columns at elevation 7 for ULS wind loads

D.1.3 Displacements

The results in Figure D.4 and Figure D.5, show that the displacement is vertical and that the structure behaves as a cantilever structure. The displacement due to wind loads is equal to $\Delta_{wind} = 230.02 \text{ mm}$, which is within the requirement of $w_{max} = 244 \text{ mm}$. The results for the earthquake induced displacement is of $\Delta_{seis} = 107.25 \text{ mm}$, which is half of the wind induced.

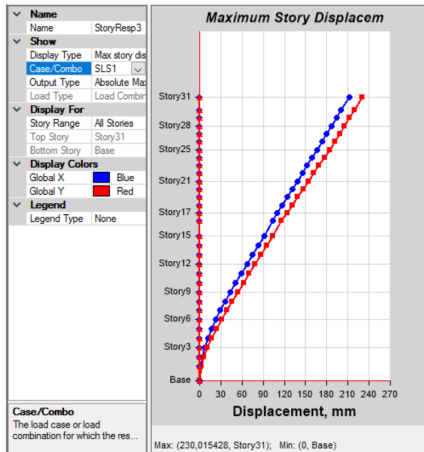


Figure D.4: Displacement due to serviceability wind loads

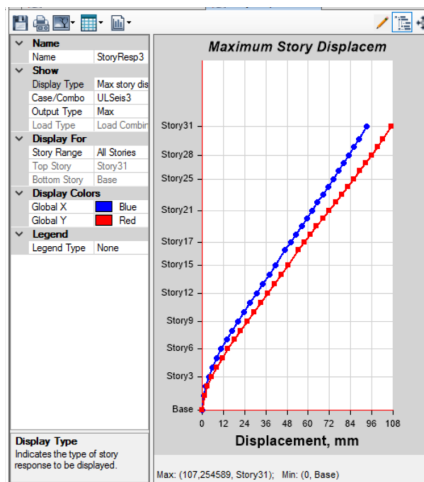


Figure D.5: Displacement due to serviceability seismic loads

D.1.4 Drift Ratio

For the drift ratio, the mid-height soft story, story 17, has the lowest stiffness and largest displacement. Shown in Figure D.6 and Figure D.7. This is logical since the story is of 6.5 meters without a large increase in stiffness contributions. Since the displacement limit from wind loads was set to $L/500$, this is equivalent to a 0.2% drift ratio per story in percent. Consequently, Figure D.6 shows that the drift ratio is not within this limit, the value shown needs to be multiplied with 100%. The seismic displacement is limited by a drift ratio equal to 0.3%, and this is satisfied as shown in Figure D.7.

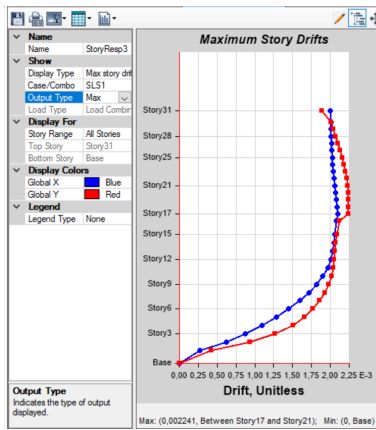


Figure D.6: Drift ratio due to serviceability wind loads

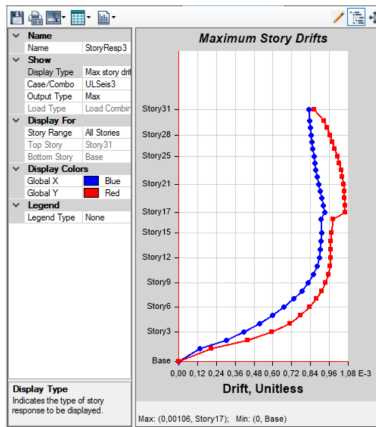


Figure D.7: Drift ratio due to serviceability seismic loads

D.1.5 Overturning Moments

The plotted graph for the overturning moment is shown in Figure D.8 and Figure D.9. From these figures, it is clear that the moment is linearly increasing with a decrease in height. The figures show that the overturning moment is equal to $2.0 \times 10^6 \text{ kNm}$ due to wind induced response, and $1.5 \times 10^6 \text{ kNm}$ due to seismic response of the structure.

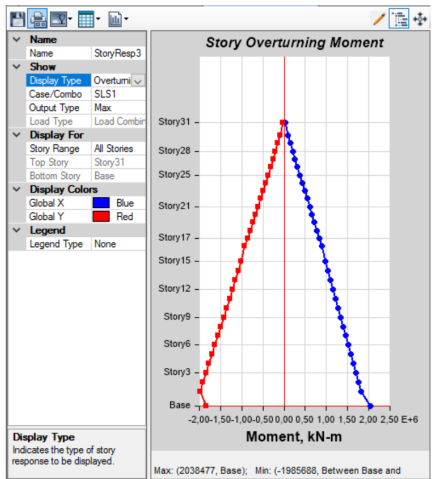


Figure D.8: Overturning moment due to serviceability wind loads

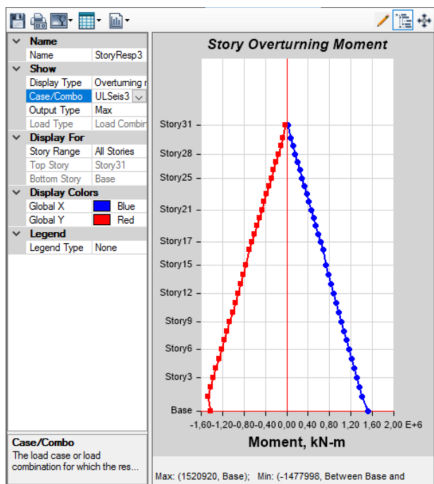


Figure D.9: Overturning moment due to serviceability seismic loads

D.1.6 Shell Stresses in Shear Walls

The stresses S11, shown in Figure D.10, are the stresses in x-direction. They illustrate the stress from the dead and live load as well as load-transfer for exterior columns. The stresses in z-direction, S22, shown in Figure D.11, are the stresses in the service core due to the governing wind load combination. This is varying with height, being maximum at the bottom with a value equal to -21.82 MPa , in compression. The maximum values of the stresses are within the given design requirement of $f_{cd} = 25.5 \text{ MPa}$.

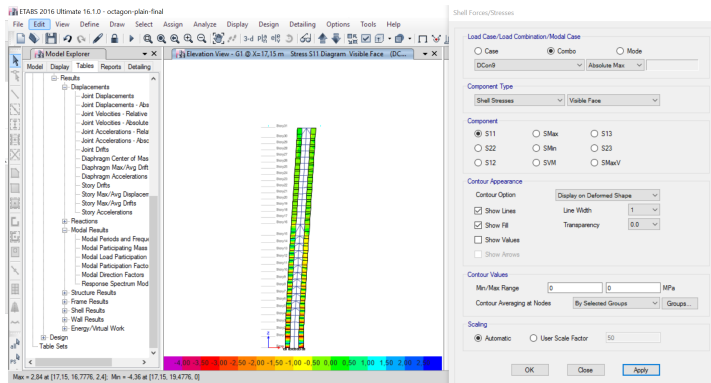


Figure D.10: Stress S11 at elevation X=17.15 m due to ULS wind loads

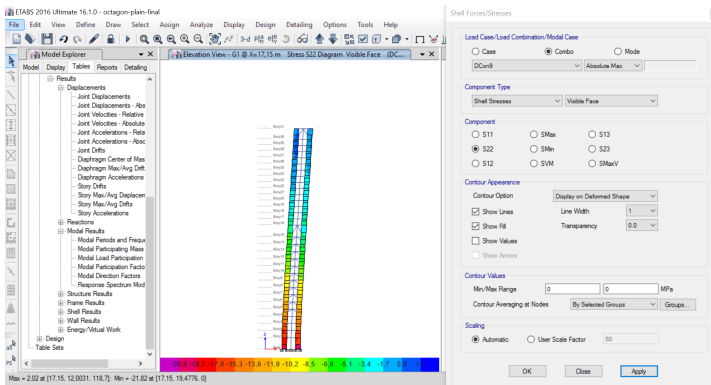


Figure D.11: Stress S22 at elevation X=17.15 m due to ULS wind loads

APPENDIX \mathcal{E}

Results obtained in ETABS for the octagon model that is twisted is shown in this appendix. The general layout of the model is shown in Figure E.1. From the results, and when comparing these to the other models, it is believed that the structure is modeled correctly. All the values for displacement, seismic drift and utilization are within acceptable regions.

E.1 Results from ETABS for Twisted Octagon Model

E.1.1 Plan and 3D View of the Structure

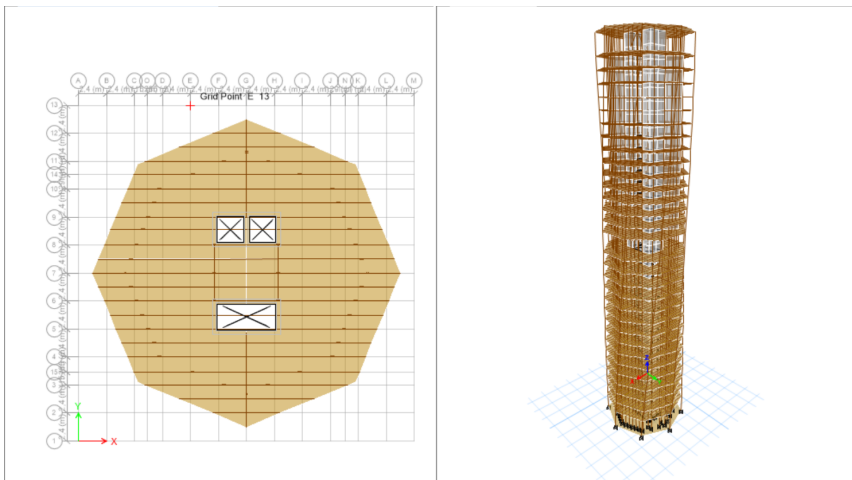


Figure E.1: Plan section and 3D view for octagon twisting model

E.1.2 Utilization of Composite Columns

The model was created by re-analyzing the structure after utilization checks for the composite columns, as shown in Figure E.2 and Figure E.3. The model was first analyzed with the required cross sections for the octagon plain model. From the results it was clear that the uppermost stories had a larger degree of utilization, while the columns in the middle section had a lower degree of utilization. The model had a linear increase from the top in compressional forces for the composite columns. The soft stories had to have large cross section areas of the columns, due to the low amount of additional support for these floors.

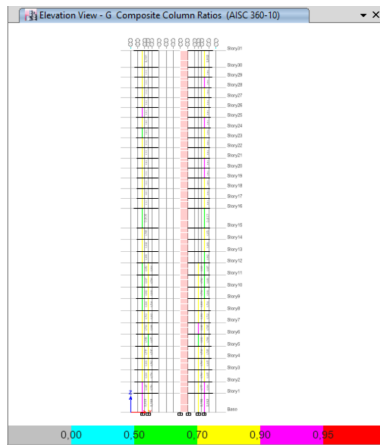


Figure E.2: Utilization degree for composite columns at elevation G for ULS wind loads

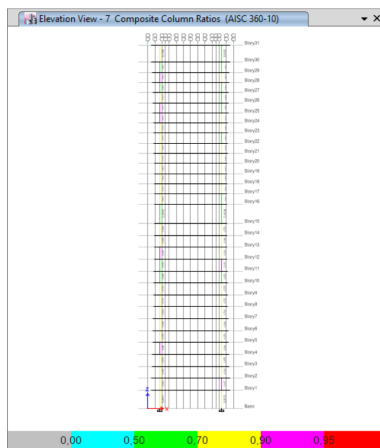


Figure E.3: Utilization degree for composite columns at elevation 7 for ULS wind loads

E.1.3 Displacements

The results in Figure E.4 and Figure E.5, show that the displacement is vertical and that the structure behaves as a cantilever structure. The displacement due to wind loads is equal to $\Delta_{wind} = 209.33 \text{ mm}$, which is within the requirement of $w_{max} = 244 \text{ mm}$. The displacement has decreased with 9 percent compared to the octagon plain model. The results for the earthquake induced displacement is of $\Delta_{seis} = 106.47 \text{ mm}$, which is half of the wind induced, and approximately equal to the value for the octagon plain model.

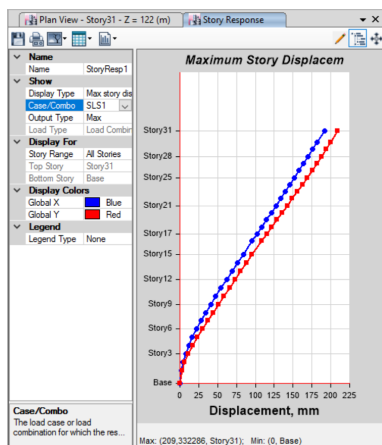


Figure E.4: Displacement due to serviceability wind loads

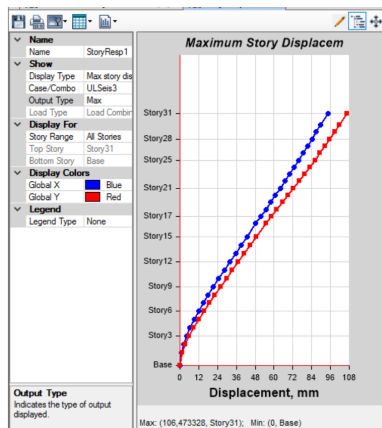


Figure E.5: Displacement due to serviceability seismic loads

E.1.4 Drift Ratio

For the drift ratio, the mid-height soft story, story 17, and up to 21, have the lowest stiffness and largest displacement, shown in Figure E.6 and Figure E.7. However, story 20 illustrates an abnormal low stiffness in x-direction and most likely the model has some errors. These errors were not found. Since the displacement limit for wind loads was set to $L/500$, this is equivalent to a 0.2% drift ratio in percent. Consequently, Figure E.6 shows that the drift ratio is not within this limit. The seismic displacement is limited by a drift ratio equal to 0.3%, and this is satisfied as shown in Figure E.7.

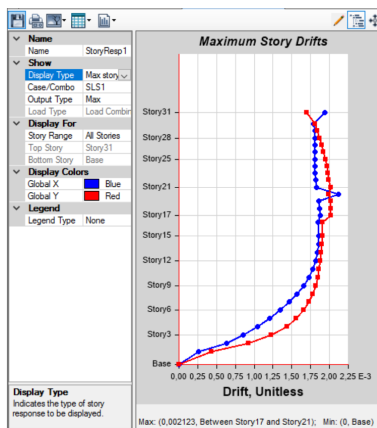


Figure E.6: Drift ratio due to serviceability wind loads

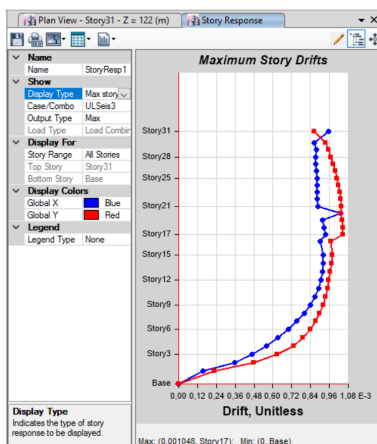


Figure E.7: Drift ratio due to serviceability seismic loads

E.1.5 Overturning Moments

The plotted graph for the overturning moment is shown in Figure E.8 and Figure E.9. From these figures, it is clear that the moment is linearly increasing with a decrease in height. The figures show that the overturning moment is equal to $2.1 \times 10^6 \text{ kNm}$ due to wind induced response, and $1.6 \times 10^6 \text{ kNm}$ due to seismic response of the structure. When comparing the results to the octagon plain model, it is clear that the overturning moment has increased with an insignificant amount.

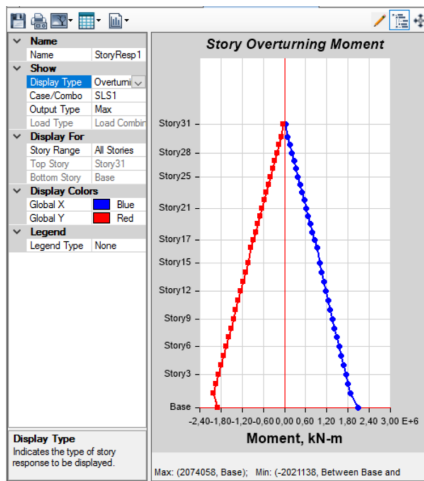


Figure E.8: Overturning moment due to serviceability wind loads

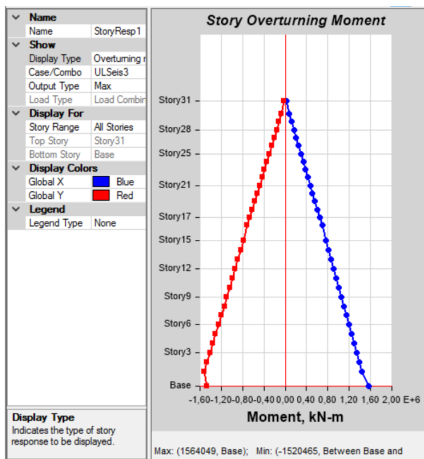


Figure E.9: Overturning moment due to serviceability seismic loads

E.1.6 Shell Stresses in Shear Walls

The stresses S11, shown in Figure E.10, are the stresses in x-direction. They illustrate the stress from the dead and live load as, well as load transfer for exterior columns. The stresses in z-direction, S22, shown in Figure E.11, are the stresses in the service core due to the governing wind load combination. This is varying with height, being maximum at the bottom with a value equal to $-25.08 MPa$, in compression. The maximum values of the stresses are barely within the given design requirement of $f_{cd} = 25.5 MPa$. When comparing the maximum value to the maximum stress in S22 for the octagon plain model, it is clear that the stresses in the service core have increased due to a decrease in the composite columns cross section area. The service core is thus applied with a large ratio of the total loading.

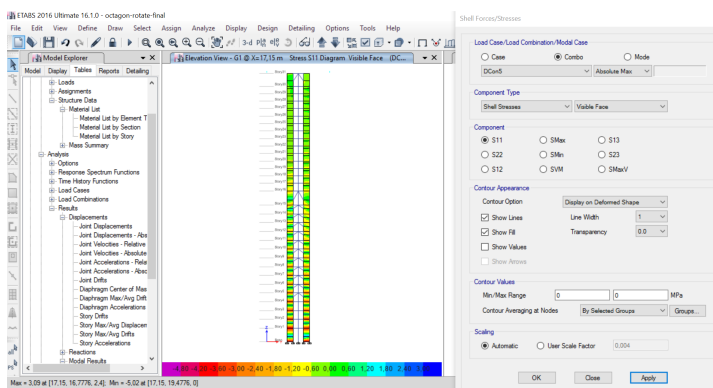


Figure E.10: Stress S11 in service core at elevation X=17,15 m due to ULS wind loads

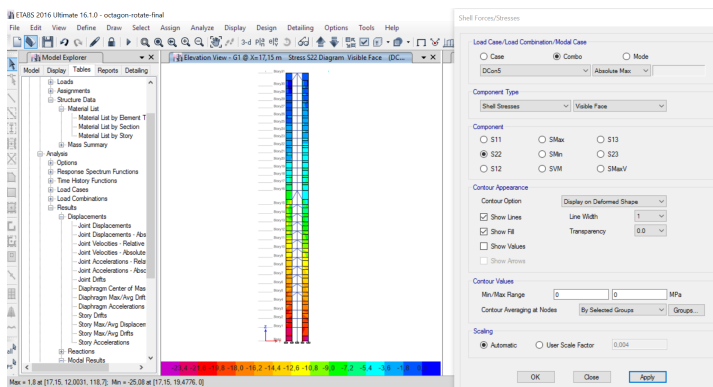


Figure E.11: Stress S22 in service core at elevation X=17,15 m due to ULS wind loads

APPENDIX \mathcal{F}

Results obtained in ETABS for the octagon model that is twisted and tapered is shown in this appendix. The general layout of the model is shown in Figure F.1. From the results, and when comparing these to the other models, it is believed that the structure is modeled correctly. All the values for displacement, drift ratio and utilization are within acceptable regions.

F.1 Results from ETABS for Twisted and Tapered Octagon Model

F.1.1 Plan and 3D View of the Structure

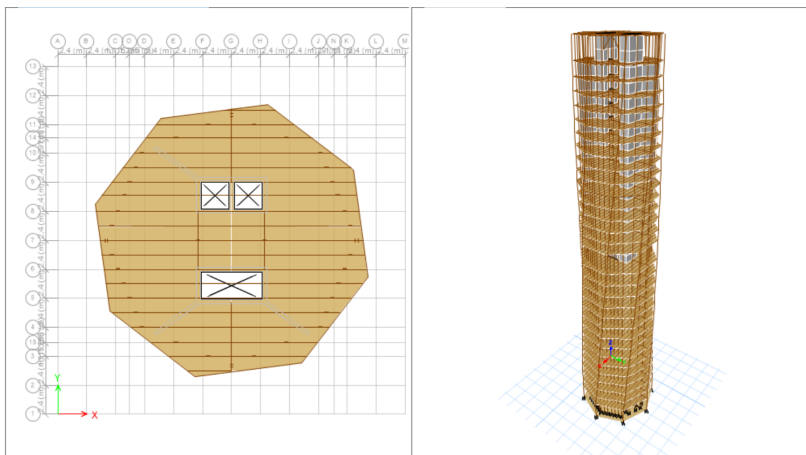


Figure F.1: Plan section and 3D view of octagon twisting and tapered model

F.1.2 Utilization of Composite Columns

The model was created by re-analyzing the structure after utilization checks for the composite columns, as shown in Figure F.2 and Figure F.2. The model was first analyzed with the cross sections from the octagon twisted model. From the results it was clear that the uppermost stories had a lower degree of utilization, due to tapering. The columns at the lower stories had a larger degree of utilization.

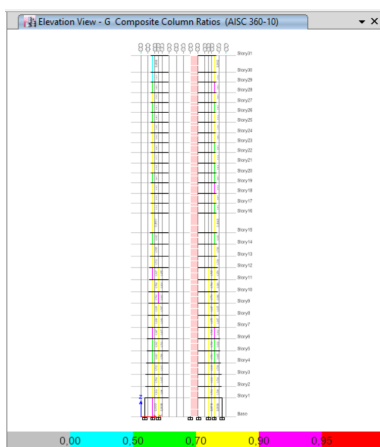


Figure F.2: utilization degree for composite columns at elevation G due to ULS wind loads

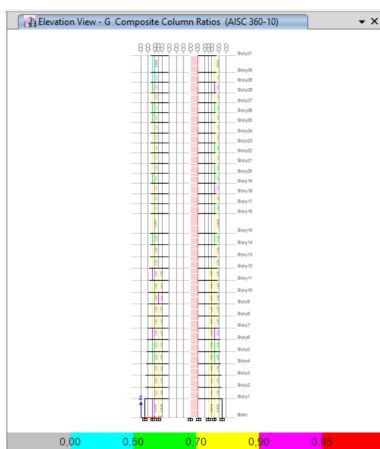


Figure F.3: utilization degree for composite columns at elevation G due to ULS wind loads

F.1.3 Displacements

The results in Figure F.4 and Figure F.5, show that the displacement is vertical and that the model behaves as a cantilever structure. The displacement due to wind loads is equal to $\Delta_{wind} = 184.32 \text{ mm}$, which is within the requirement of $w_{max} = 244 \text{ mm}$. The displacement has decreased with 12 percent compared to the octagon twisted model, and 20 percent compared to the octagon plain model. The results for the earthquake induced displacement is of $\Delta_{seis} = 94.57 \text{ mm}$, which is half of the wind induced. The seismic displacement has also decreased, with a percentage value equal to 11 percent compared to the octagon twisted model.

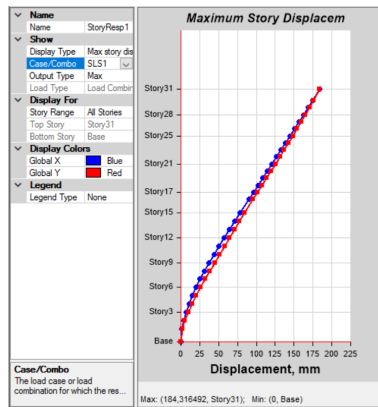


Figure F.4: Displacements due to serviceability wind loads

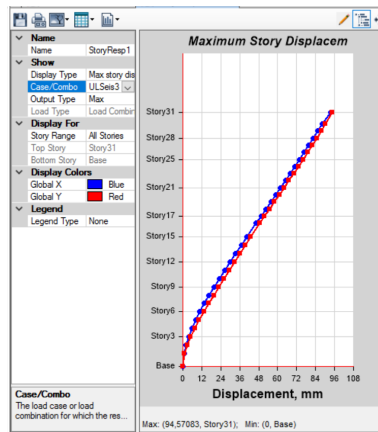


Figure F.5: Displacements due to serviceability seismic loads

F.1.4 Drift Ratio

For the drift ratio, the mid-height soft story, story 17, has the lowest stiffness and largest displacement, shown in Figure F.6 and Figure F.7. However, all the stories above story 17 have a drift ratio that is almost equal to story 17. This is a desired output for a drift ratio plot. Since the displacement limit for wind loads was set to $L/500$, this is equivalent to a 0.2% drift ratio per story in percent. Consequently, Figure F.6 shows that the drift ratio is just within this limit, the value shown needs to be multiplied with 100%. The other octagon models were not within this limit. The seismic displacement is limited by a drift ratio equal to 0.3%, and this is satisfied as shown in Figure F.7.

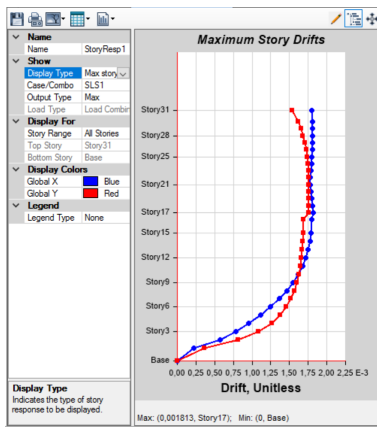


Figure F.6: Drift ratio due to serviceability wind loads

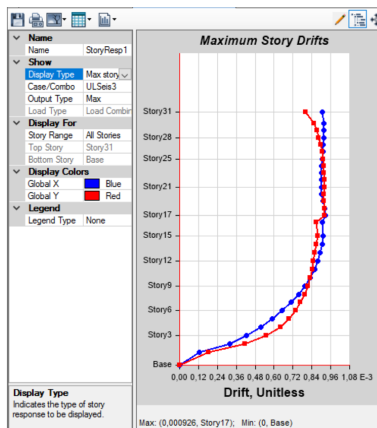


Figure F.7: Drift ratio due to serviceability seismic loads

F.1.5 Overturning Moments

The plotted graph for the overturning moment is shown in Figure F.8 and Figure F.9. From these figures, it is clear that the moment is linearly increasing with a decrease in height. The figures show that the overturning moment is equal to $1.83 \times 10^6 \text{ kNm}$ due to wind induced response, and it is reduced with 12 percent compared to the octagon twisted model. This shows that tapering has a large positive effect for the overturning moment. For seismic response of the structure, it is $1.4 \times 10^6 \text{ kNm}$. This is a decrease of 10 percent compared to the octagon twisted model.

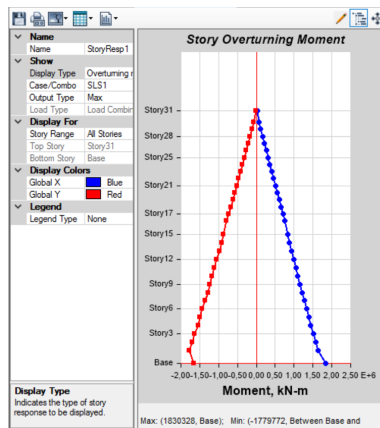


Figure F.8: Overturning moment due to serviceability wind loads

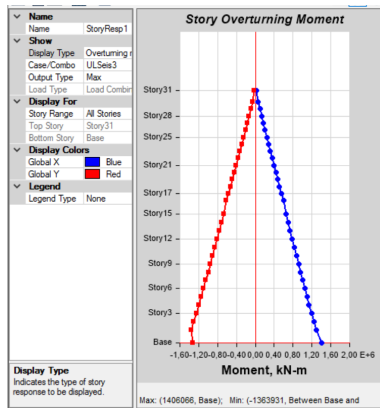


Figure F.9: Overturning moment due to serviceability seismic loads

F.1.6 Shell Stresses in Shear Walls

The stresses S11, shown in Figure F.10, are the stresses in x-direction. They illustrate the stress from the dead and live load as well as load transfer for exterior columns. The stresses in z-direction, S22, shown in Figure F.11, are the stresses in the service core due to the governing wind load combination. This is varying with height, being maximum at the bottom with a value of -20.35 MPa , in compression. The maximum values of the stresses are within the given design requirement of $f_{cd} = 25.5 \text{ MPa}$, and reduced compared to the octagon twisted model. Thus, even with lower cross section areas of the composite columns, the service core is not applied with additional loads.

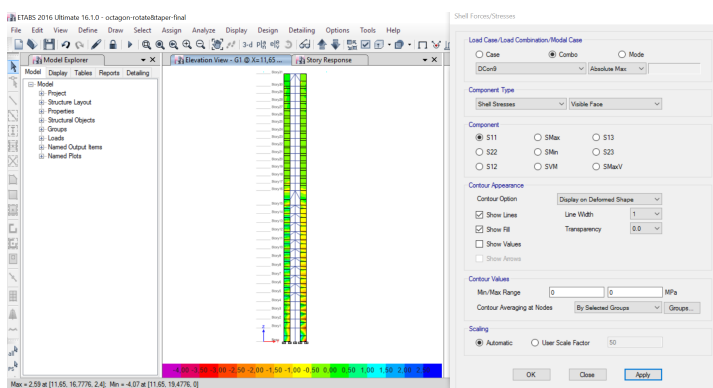


Figure F.10: Stress S11 at service core at elevation X=11.65 m due to ULS wind loads

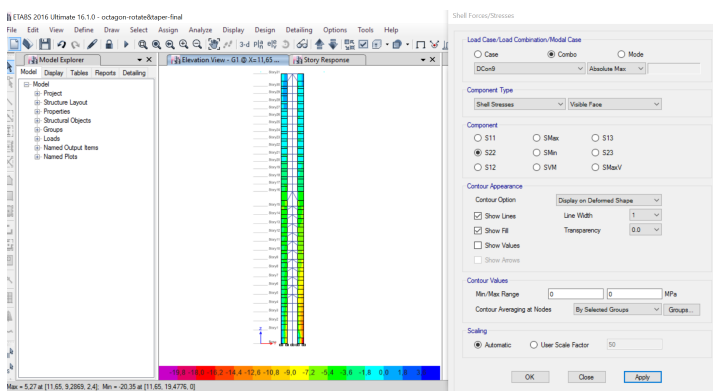


Figure F.11: Stress S22 at service core at elevation X=11.65 m due to ULS wind loads

APPENDIX *G*

Results obtained in ETABS for the plain hexagon model is shown in this appendix. The general layout of the model is shown in Figure G.1. The results in this appendix indicate that there are errors in the model, and illustrate the limitations with ETABS when operating with user-defined materials. Since the model was optimized to reach a range of 65-95 % utilization of the composite columns, all the results were inconclusive due to the low mass at the upper stories. The student tried to determine what was inefficient and the error with the model. However, the same model was used to create the hexagon twisted and hexagon twisted and tapered models, and these results are accurate and comparable to the octagon models. Thus, the error was not implemented into the other models.

G.1 Results from ETABS for Plain Hexagon Model

G.1.1 Plan and 3D View of the Structure

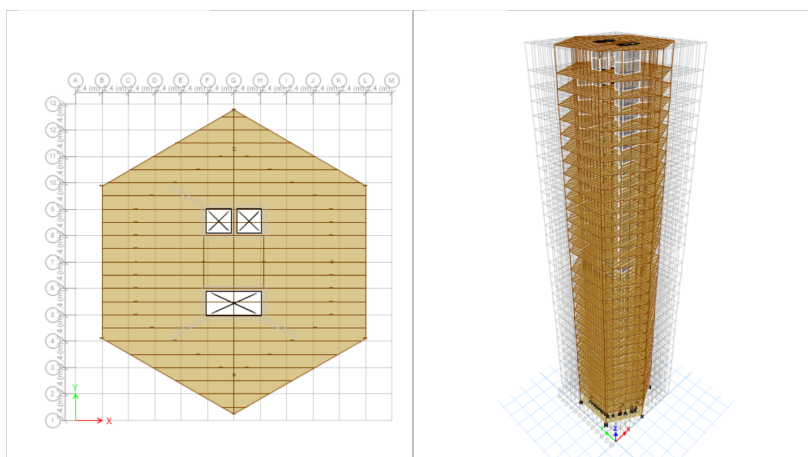


Figure G.1: Plan section and 3D view of hexagon plain

G.1.2 Utilization of Composite Columns

The model was created by re-analyzing the structure after utilization checks for the composite columns, as shown in Figure G.2 and Figure G.3. The model was first analyzed with the cross sections from the octagon plain model. From the results it was clear that the loads were not applied in the same pattern as for the octagon. Figure G.3 illustrates the low loading of the composite columns closes to the windward side. The columns that have an utilization degree less than 0.5, are of the smallest cross section, with HE100A steel cross section within a rectangle concrete section. The other columns in the model had cross sections that were close to the same as for the octagon model. Thus, the error is somewhere on the windward side close to elevation at midsection of the structure.

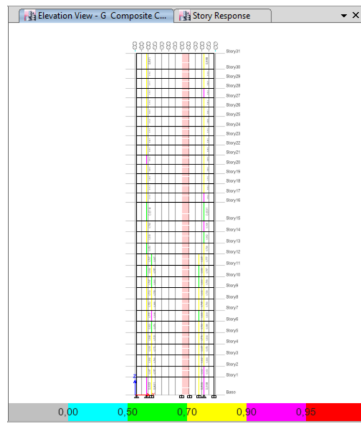


Figure G.2: Utilization degree for composite columns in elevation G due to ULS wind loads

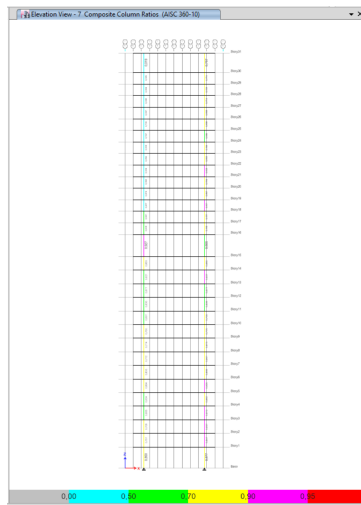


Figure G.3: Utilization degree for composite columns in elevation 7 due to ULS wind loads

G.1.3 Displacements

The results in Figure G.4 and Figure G.5, show that the displacement is vertical and that the structure behaves as a cantilever structure. The displacement due to wind loads is equal to $\Delta_{wind} = 205.17 \text{ mm}$, which is within the requirement of $w_{max} = 244 \text{ mm}$. The displacement is actually lower than that of the octagon plain model. The results for the earthquake induced displacement is of $\Delta_{seis} = 38695.05 \text{ mm}$, which is immense. The seismic displacement is a function of the frequency and mass, and due to the low stiffness for the upper stories, the displacement is large.

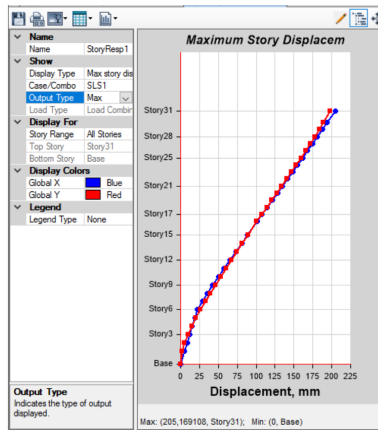


Figure G.4: Displacement due to serviceability wind loads

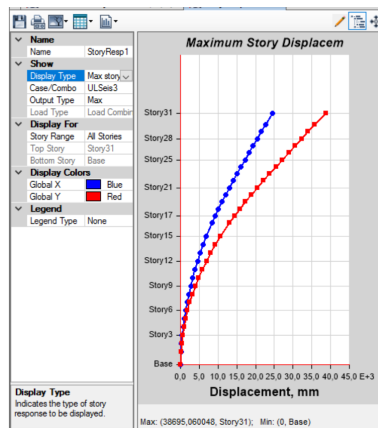


Figure G.5: Displacement due to serviceability seismic loads

G.1.4 Drift Ratio

For the drift ratio, the mid-height soft story, story 17, has the lowest stiffness and largest displacement under wind loads, shown in Figure F.6. For the earthquake induced displacement, the drift ratio is largest at the 21st story, shown and Figure F.7. For the drift ratio due to wind loading, the drift ratio is unusually large for the first story. The drift ratio from seismic loading illustrates the low degree of stiffness for the top ten stories. Comparing with the limiting value of 0.3%, only the lower fifteen stories are within this limit. This is also illustrated in the displacement curve under seismic loads, shown in Figure G.5, where the displacement is within requirements for the lower fifteen stories, but very large for the upper stories.

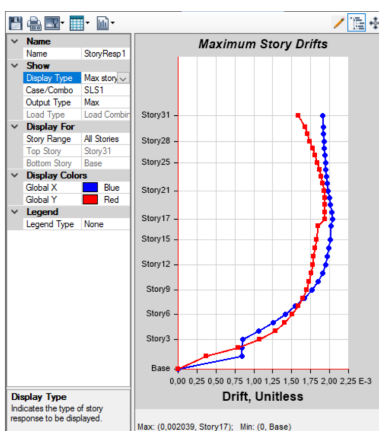


Figure G.6: Drift ratio due to serviceability wind loads

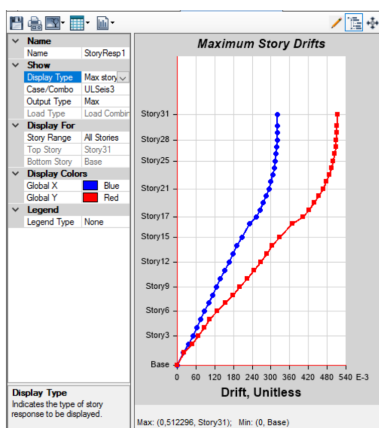


Figure G.7: Drift ratio due to serviceability seismic loads

G.1.5 Overturning Moments

The plotted graph for the overturning moment is shown in Figure G.8 and Figure G.9. For these figures, it is clear that the moment is linearly increasing with a decrease in height, as for the other models. The figures show that the overturning moment is equal to $2.05 \times 10^6 \text{ kNm}$ due to wind induced response. For seismic response of the structure, it is $1.56 \times 10^6 \text{ kNm}$. These values are comparable to those from the octagon plain model, showing that additional loading is not the reason for the large values of displacement and drift under seismic loads.

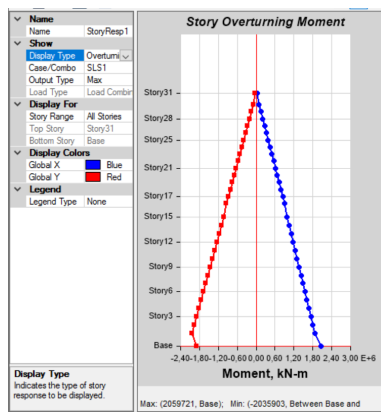


Figure G.8: Overturning moment due to serviceability wind loads

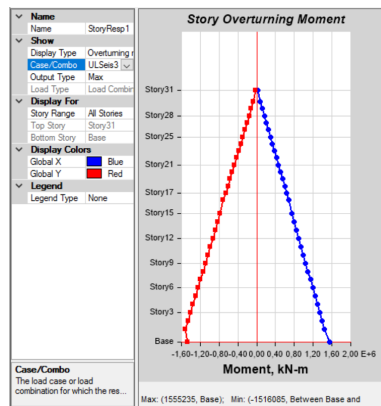


Figure G.9: Overturning moment due to serviceability seismic loads

G.1.6 Shell Stresses in Shear Walls

The stresses S11, shown in Figure G.10, are the stresses in x-direction. They illustrate the stress from the dead and live load as well as load transfer for exterior columns. The stresses in z-direction, S22, shown in Figure G.11, are the stresses in the service core due to the governing wind load combination. This is varying with height, being maximum at the bottom with a value equal to -28.47 MPa , in compression. The maximum values of the stresses are not within the given design requirement of $f_{cd} = 25.5 \text{ MPa}$. Thus, the service core is loaded over the threshold due to the lean composite columns.

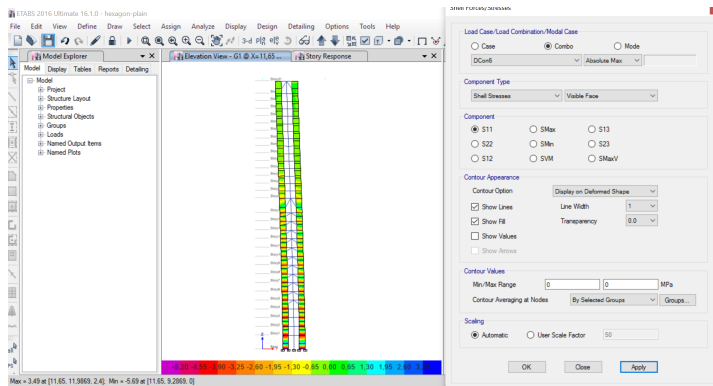


Figure G.10: Stress S11 in service core at elevation X=11.65 m due to ULS wind loads

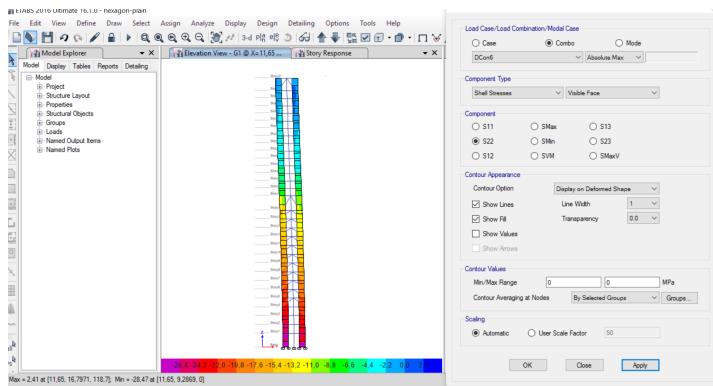


Figure G.11: Stress S22 in service core at elevation X=11.65 m due to ULS wind loads

APPENDIX *H*

Results obtained in ETABS for the hexagon twisted model is shown in this appendix. The general layout of the model is shown in Figure H.1. From the results, and when comparing these to the hexagon plain model, it is clear that the errors in the hexagon plain model have not been transferred to the hexagon twisted model. All the values for displacement, seismic drift and utilization are within acceptable regions.

H.1 Results from ETABS for Twisted Hexagon Model

H.1.1 Plan and 3D View of the Structure

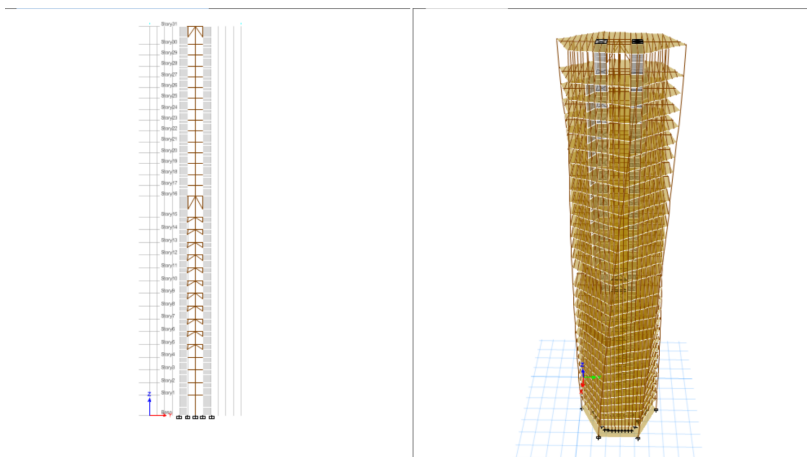


Figure H.1: Elevation view and 3D view of hexagon twisting model

H.1.2 Utilization of Composite Columns

The model was created by re-analyzing the structure after utilization checks for the composite columns, as shown in Figure H.2 and Figure H.3. The model was first analyzed with the cross sections from the hexagon plain model. From the results it is clear that the errors and the lean composite columns for elevation 7, had to be changed into composite columns of equivalent thickness as for the hexagon twisted model.

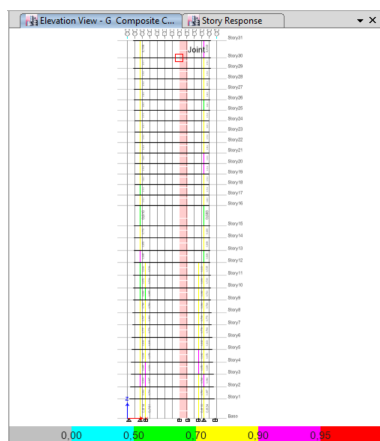


Figure H.2: Utilization degree at elevation G due to ULS wind loads

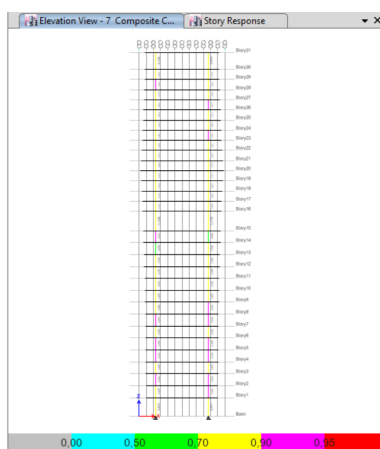


Figure H.3: Utilization degree at elevation 7 due to ULS wind loads

H.1.3 Displacements

The results in Figure H.4 and Figure H.5, show that the displacement is vertical and that the structure behaves as a cantilever structure. The displacement due to wind loads is equal to $\Delta_{wind} = 226.16 \text{ mm}$, which is within the requirement of $w_{max} = 244 \text{ mm}$. The displacement has increased compared to the hexagon plain model, but this model cannot be seen as applicable due to the large displacements under seismic loading. The displacement is however also larger than the octagon twisted model, by 7.5 percent. The results for the earthquake induced displacement is $\Delta_{seis} = 112.65 \text{ mm}$, which is half of the wind induced. The seismic displacement is now within the specified thresholds, it is also almost as small as the displacements for the octagon twisted model.

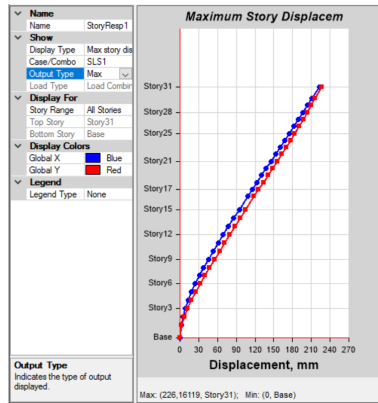


Figure H.4: Displacement due to serviceability wind loads

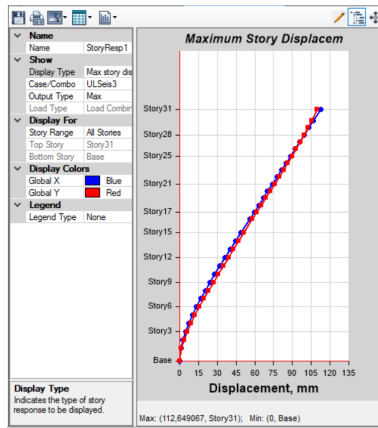


Figure H.5: Displacement due to serviceability seismic loads

H.1.4 Drift Ratio

For the drift ratio, the mid-height soft story, story 17, has the lowest stiffness and largest displacement, shown in Figure H.6 and Figure H.7. However, all the stories above story 17 have a drift ratio that is almost equal to story 17. This is a desired output for a drift ratio plot. However, Figure H.6 shows unusually large drift for the lowest stories in x-direction. Since the displacement limit from wind loads was set to $L/500$, this is equivalent to a 0.2% drift ratio in percent. Consequently, Figure H.6 shows that the drift ratio is not within this limit, the value shown needs to be multiplied with 100%. The seismic displacement is limited by a drift ratio equal to 0.3%, and this is satisfied as shown in Figure F.7.

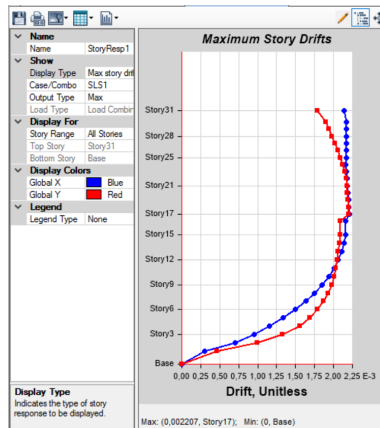


Figure H.6: Drift ratio due to serviceability wind loads

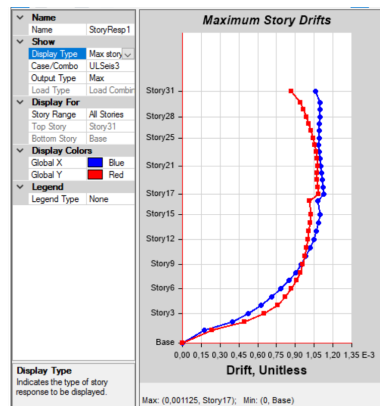


Figure H.7: Drift ratio due to serviceability seismic loads

H.1.5 Overturning Moment

The plotted graph for the overturning moment is shown in Figure H.8 and Figure H.9. For these figures, it is clear that the moment is linearly increasing with a decrease in height. The figures show that the overturning moment is equal to $2.08 \times 10^6 \text{ kNm}$ due to wind induced response. For seismic response of the structure, it is $1.56 \times 10^6 \text{ kNm}$. These values are comparable to what was achieved for the octagon twisted structure.

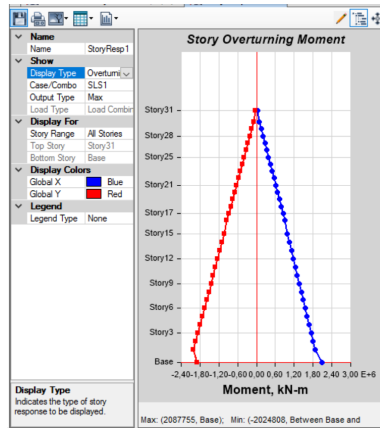


Figure H.8: Overturning moment due to serviceability wind loads

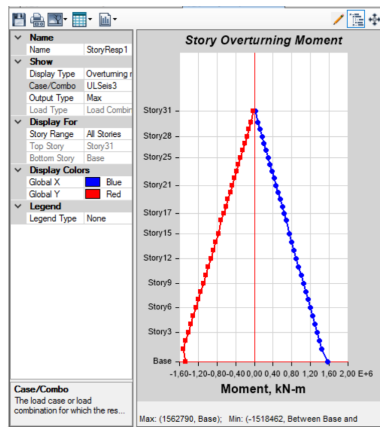


Figure H.9: Overturning moment due to serviceability seismic loads

H.1.6 Shell Stresses in Shear Walls

The stresses S11, shown in Figure H.10, are the stresses in x-direction. They illustrate the stress from the dead and live load as well as load transfer for exterior columns. The stresses in z-direction, S22, shown in Figure H.11, are the stresses in the service core due to the governing wind load combination. These are varying with the height, being maximum at the bottom with a value equal to $-21.97 MPa$, in compression. The maximum values of the stresses are within the given design requirement of $f_{cd} = 25.5 MPa$.

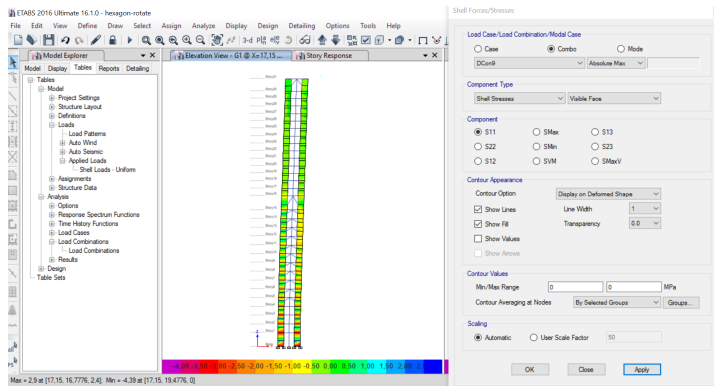


Figure H.10: Stress S11 at elevation X=17.15 m due to ULS wind loads

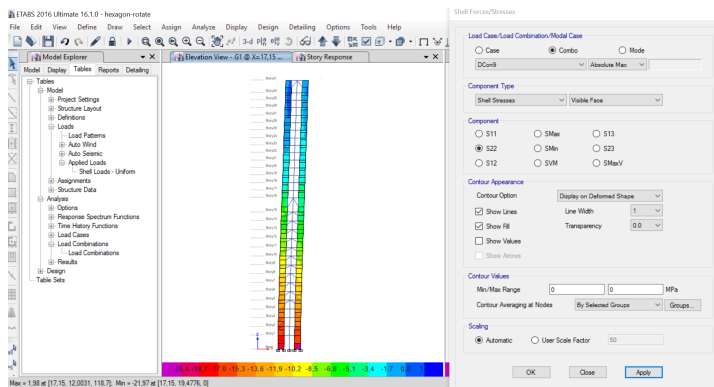


Figure H.11: Stress S22 at elevation X=17.15 m due to ULS wind loads

APPENDIX I

Results obtained in ETABS for the hexagon twisted and tapered model is shown in this appendix. The general layout of the model is shown in Figure 8.2. From the results, and when comparing these to the other hexagon plain model, it is believed that the structure is modeled correctly. All the values for displacement, seismic drift and utilization are within acceptable regions. It is worth mentioning that there may be some error in this model since the analysis took a considerable longer time to run, than the others. This error was not found.

I.1 Results from ETABS for Twisted and Tapered Hexagon Model

I.1.1 Plan and 3D View of the Structure

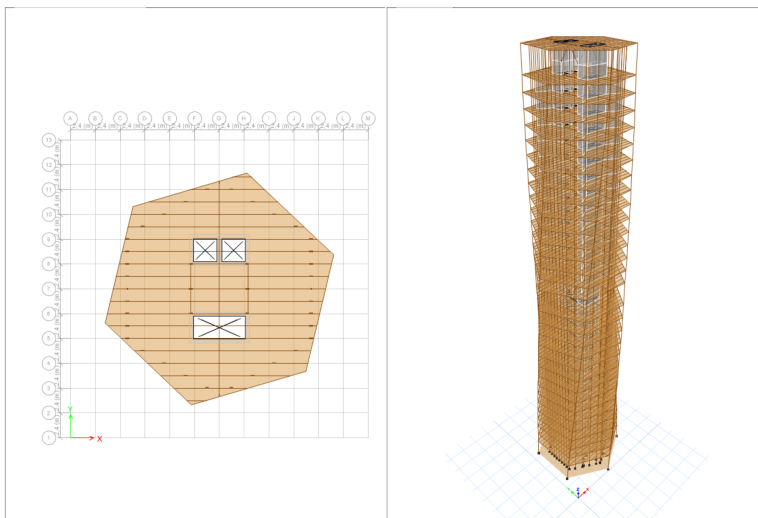


Figure I.1: Plan section and 3D view of hexagonal twisting and tapered

I.1.2 Utilization of Composite Columns

The model was created by re-analyzing the structure after utilization checks for the composite columns, as shown in Figure I.2 and Figure I.3. The model was first analyzed with the cross sections from the hexagon twisted model. From the results it was clear that the upper stories required less support form the composite columns, while the lower stories required larger cross sections than the results from the hexagon twisted model.

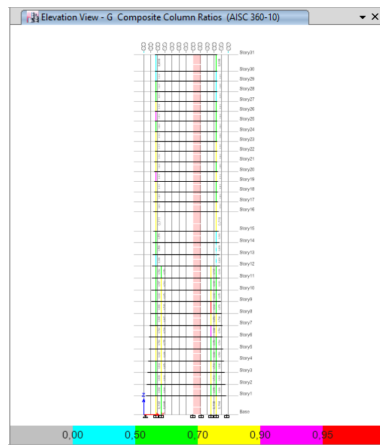


Figure I.2: Utilization degree at elevation G for ULS wind loads

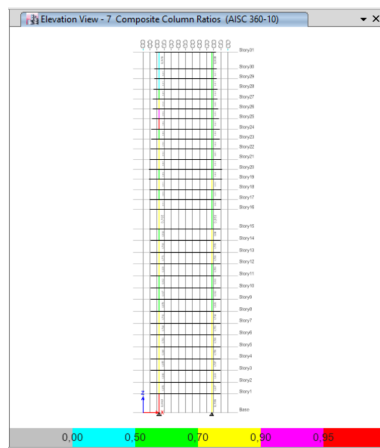


Figure I.3: Utilization degree at elevation 7 for ULS wind loads

I.1.3 Displacements

The results for the displacements are shown in Figure I.4 and Figure I.5. The displacement due to wind loads is equal to $\Delta_{wind} = 196.83 \text{ mm}$, which is within the requirement of $w_{max} = 244 \text{ mm}$. The displacement has decreased compared to the hexagon twisted model, with 13 percent. The displacement is however larger than the octagon twisted and tapered model, by 6.4 percent. The results for the earthquake induced displacement is $\Delta_{seis} = 97.83 \text{ mm}$, which is half of the wind induced displacement. The seismic displacement has been reduced with 13 percent compared to the hexagon twisted model. The displacement is however slightly larger than the octagon twisted and tapered model, by 3.3 percent.

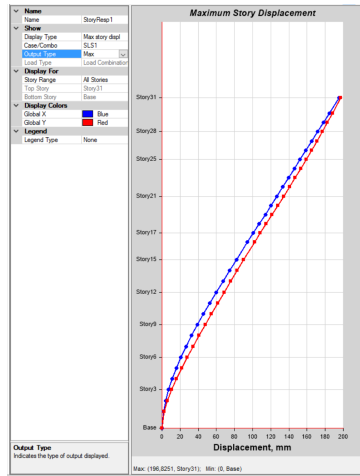


Figure I.4: Displacement due to serviceability wind loads

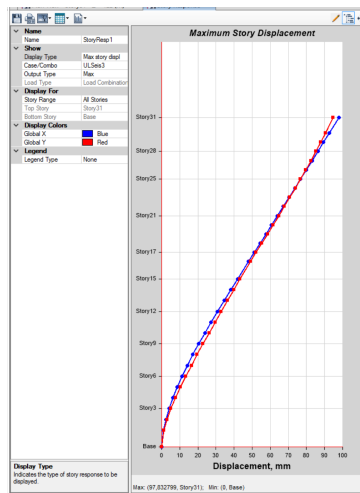


Figure I.5: Displacement due to serviceability seismic loads

I.1.4 Drift Ratio

For the drift ratio, it is the 19th story that has lowest stiffness and largest displacement, shown in Figure I.6 and Figure I.7. The drift ratio is especially large in global y-direction, illustrating a possible error in this story. However, all the stories above story 17 have a drift ratio that is almost equal to story 17. This is a desired output for a drift ratio plot. Since the displacement limit for wind loads was set to $L/500$, this is equivalent to a 0.2% drift ratio in percent. Consequently, Figure I.6 shows that the drift ratio is not within this limit. The seismic displacement is limited by a drift ratio equal to 0.3%, and this is satisfied as shown in Figure I.7.

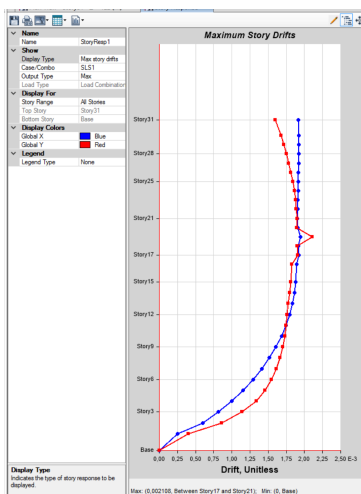


Figure I.6: Drift ratio due to serviceability wind loads

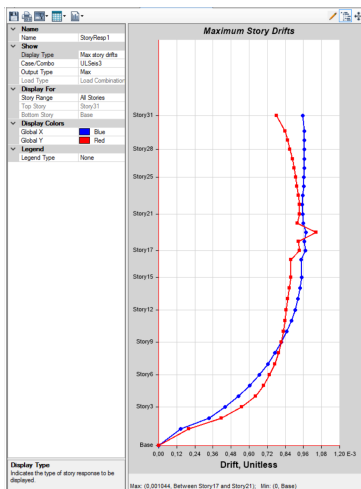


Figure I.7: Drift ratio due to serviceability seismic loads

I.1.5 Overturning Moments

The plotted graph for the overturning moment is shown in Figure I.8 and Figure I.9. From these figures, it is clear that the moment is linearly increasing with a decrease in height. The figures show that the overturning moment is equal to $1.83 \times 10^6 \text{ kNm}$, form wind induced response. This is a decrease of 12 percent compared to the hexagon twisted model. This illustrates the benefits of adding tapering to the structure. For seismic response of the structure, it is $1.40 \times 10^6 \text{ kNm}$. The seismic overturning moment has decreased with 11 percent compared to the octagon twisted model.

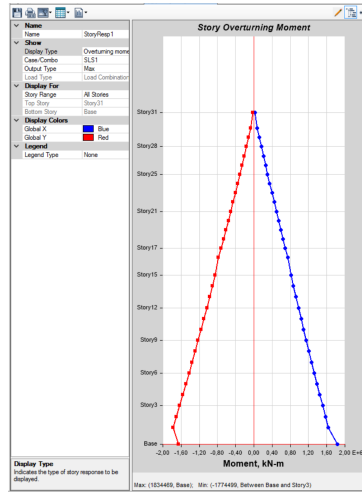


Figure I.8: Overturning moment due to serviceability wind loads

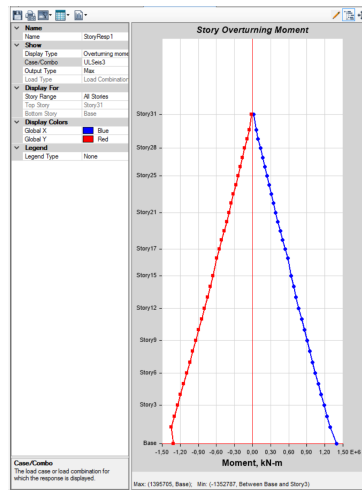


Figure I.9: Overturning moment due to serviceability seismic loads

I.1.6 Shell Stresses in Shear Walls

The stresses S11, shown in Figure I.10, are the stresses in x-direction. They illustrate the stress from the dead and live load as well as load transfer for exterior columns. The stresses in z-direction, S22, shown in Figure I.11, are the stresses in the service core due to the governing wind load combination. This is varying with height, being maximum at the bottom with a value equal to -19.95 MPa , in compression. The maximum values of the stresses are within the given design requirement of $f_{cd} = 25.5 \text{ MPa}$.

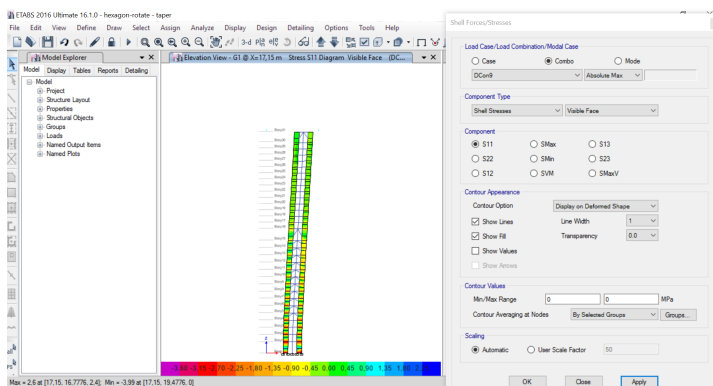


Figure I.10: Stress S11 at elevation X=17.15 m due to ULS wind loads

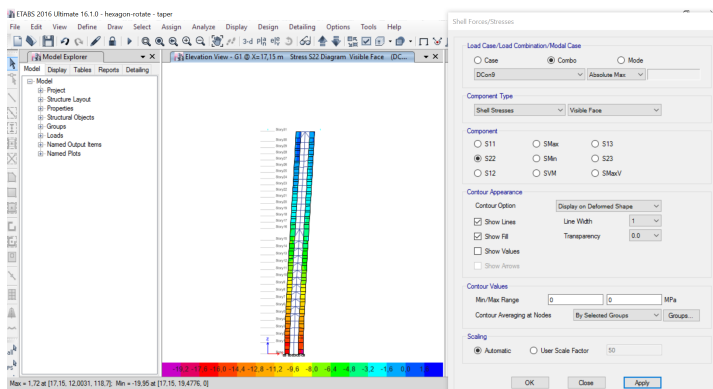


Figure I.11: Stress S22 at elevation X=17.15 m due to ULS wind loads